Volume 9, No. 6
October, 1961

THE SOVIET JOURNAL OF

ATOMIC ENERGY

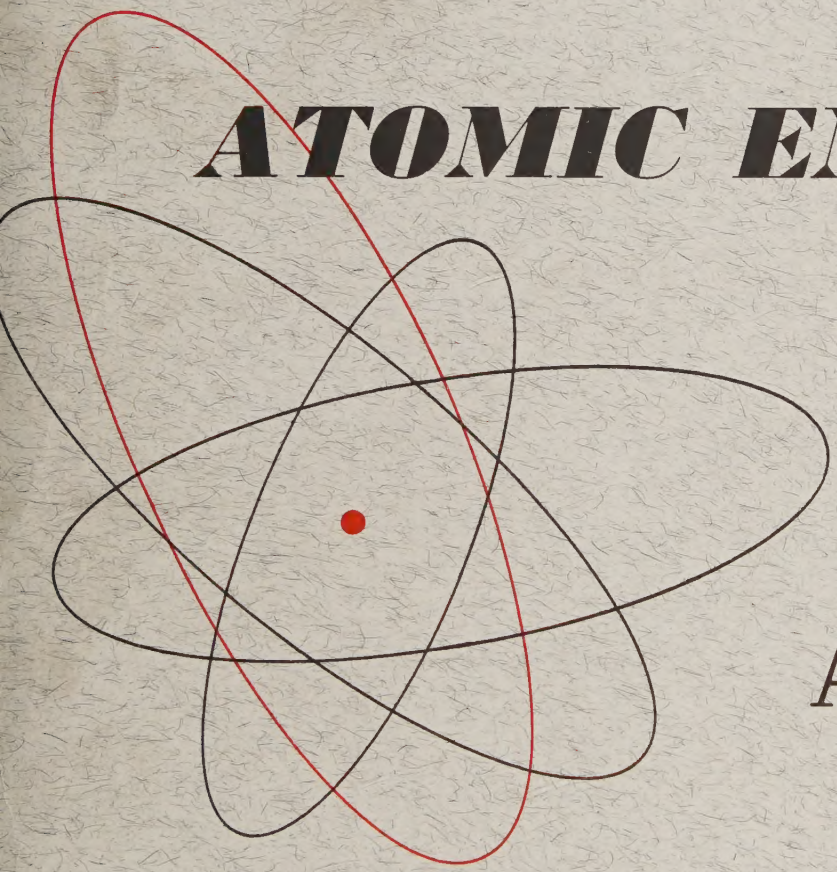

Атомная энергия

TRANSLATED FROM RUSSIAN

CONSULTANTS BUREAU

МЕТАЛЛУРГИЯ ПОЛУПРОВОДНИКОВ

THE METALLURGY OF SEMICONDUCTORS

by Yu. M. Shashkov

Translated from Russian

(Original published by the State Scientific-Technical Press for Literature on Ferrous and Non-Ferrous Metallurgy, Moscow)

In this up-to-date survey of semiconductor metallurgy, the two main semiconductor materials – germanium and silicon – and their physical and chemical properties are discussed. A detailed review of chemical methods of purifying these elements is followed by a description of metallurgical methods of purification. Partition coefficients are given for many impurities and apparatus used in purification is surveyed.

Methods of growing single crystals are treated in an excellent chapter, with the method related to the type of defect to be expected in the finished crystal. Of particular interest is a discussion of alloying and doping.

The last section of the volume deals with heat treatment and diffusion of impurities, production of rectifiers and transistors, and methods of etching crystals and finished devices.

Technologists concerned with industrial processes of established value, as well as graduate students, will find this book of great value. The 293 references provide a good selective guide to the existing literature on the subject.

PARTIAL CONTENTS

208 pages **$9.50**

CONSULTANTS BUREAU ENTERPRISES, INC.
227 W. 17 ST., NEW YORK 11, N. Y.

THE SOVIET JOURNAL OF

ATOMIC ENERGY

A translation of ATOMNAYA ÉNERGIYA,
a publication of the Academy of Sciences of the USSR

(Russian Original Dated December, 1960)

Vol. 9, No. 6 October, 1961

CONTENTS

Annual subscription $ 75.00
Single issue 20.00
Single article 12.50

CONTENTS (continued)

NOTE

The Table of Contents lists all material that appears in Atomnaya Énergiya. Those items that originated in the English language are not included in the translation and are shown enclosed in brackets. Whenever possible, the English-language source containing the omitted reports will be given.

Consultants Bureau Enterprises, Inc.

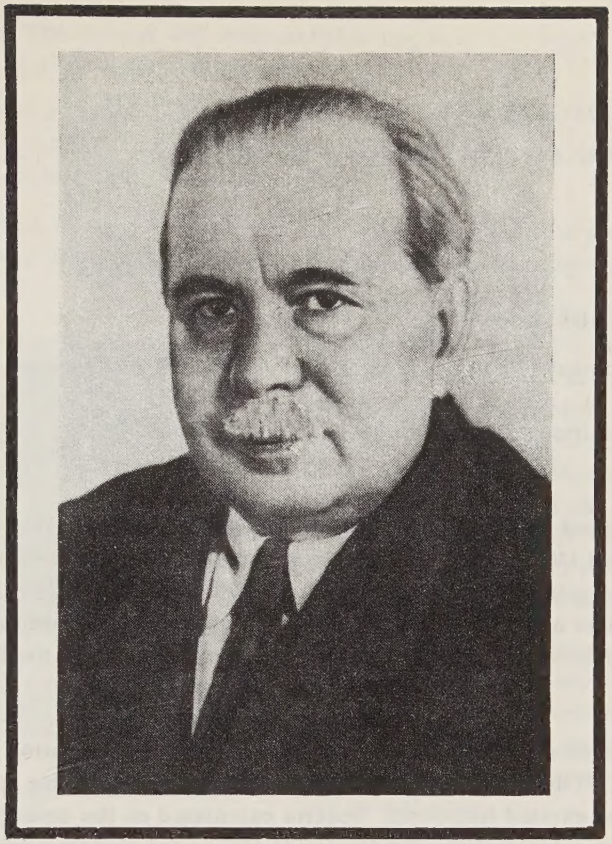

DMITRII VASIL'EVICH EFREMOV

Professor Dmitrii Vasil'evich Efremov, member of the CPSU, died on November 27, 1960 in his 61st year, after a long and serious illness.

D. V. Efremov was born in Leningrad in 1900. After graduating from the Leningrad Polytechnical Institute, D. V. Efremov worked at the 'Elektrosila' factory and rose from an ordinary engineer to become the chief engineer.

During the last 14 years, D. V. Efremov was the Deputy Minister and then Minister of Electrical Industry of the USSR, First Deputy Minister of Electrical Power Stations and Electrical Industry, Deputy Chairman of the Bureau for Electrical Power, Chemical and Forestry Industry of the Council of Ministers of the USSR, and Deputy Director of the Atomic Energy Utilization Directorate of the Council of Ministers of the USSR.

D. V. Efremov directed the construction of major Soviet turbogenerators and many electrical machines, as well as special nuclear particle accelerators.

D. V. Efremov, a scientist and communist, was a great patriot and continued his work right up to the last days of his life.

During the 19th congress of the Party, he was elected as a candidate for the Central Committee CPSU.

For his distinguished services to his country, D. V. Efremov was awarded three orders of Lenin, three Labor Red Banner orders, a 'Mark of Distinction' order, and other medals. He was awarded the Lenin and Stalin prizes.

D. V. Efremov was a pleasant and considerate person and was very concerned with the welfare of his colleagues.

The memory of Dmitrii Vasil'evich Efremov will always remain in our hearts.

Pravda, November 29, 1960

A group of colleagues

NEUTRON SPECTRA EMITTED IN THE FISSION OF U^{235} AT 0, 45, AND 90° TO THE DIRECTION OF MOTION OF THE FRAGMENTS

Yu. A. Vasilev, Yu. S. Zamyatnin, E. I. Sirotinin, and É. F. Fomushkin

Translated from Atomnaya Énergiya, Vol. 9, No. 6, pp. 449-454, December, 1960
Original article submitted February 29, 1960

Neutron spectra emitted at 0, 45, and 90° to the direction of motion of the fragments in the fission of U^{235} by 14.3 Mev neutrons have been measured. The angular distribution of the fission neutrons was found to be $N(0°) : N(45°) : N(90°) = (3.23 \pm 0.12) : (1.75 \pm 0.07) : 1.00$. The experimental data are compared with spectra calculated on the assumption of an isotropic Maxwellian neutron distribution in the center-of-mass system of the fragment.

Introduction

Measurements of fission neutron spectra [1, 2] and the angular distribution relative to the direction of motion of the fragments [3, 4] have shown that the main mechanism responsible for the production of fission neutrons is evaporation from the excited fragments. Spectra calculated on the assumption that the neutrons are evaporated isotropically and have a Maxwellian distribution in the center-of-mass system of the fragment [1, 5] are in good agreement with experiment, in spite of the simplifications introduced into the theory. However, the values of W (the average kinetic energy per nucleon in the fragments) which are in the best agreement with the experimental data on neutron spectra are always lower than the directly measured values [6, 7]. This leads to some doubt as to the correctness of the assumptions made in the theory.

Complete information on the mechanism of production of fission neutrons can be obtained from studies of the spectrum and angular distribution of the neutrons in the center-of-mass system of the fragment for various cases of fission. However, it is relatively difficult to obtain such data from the spectra of fission neutrons obtained in the laboratory system of coordinates, since it is necessary to allow for the velocity distribution of the fragments, their excitation energy distribution [8], and finally, the averaging of the spectra over all angles relative to the direction of motion of the fragments. It is very difficult to set up an experiment in which all these effects would be excluded, and hence in the first approximation, it is expedient to measure neutron spectra emitted at some definite angles θ to the direction of motion of the fragments. This excludes the necessity of averaging the spectra over the various angles, and thus considerably simplifies the transition from the laboratory to the center-of-mass system.

In the present work, we have determined the spectra of neutrons emitted in the fission of U^{235} by 14.3 Mev neutrons at 0, 45, and 90° relative to the direction of motion of the fragments. The angular distribution of the neutrons was thus obtained at the same time.

Measurements and Results

The spectra and the angular distribution of the neutrons were measured by the time-of-flight method. The flight-path was 75 cm and the resolving time $7 \cdot 10^{-9}$ sec. A detailed description of the method and apparatus is given in [9].

The particular feature of the experiment was that the source of the fission neutrons was a multilayer fission chamber with fragment collimation (Fig. 1).

The direction of motion of the fragments in this chamber was defined by collimators made from nickel ribbons 0.1 mm thick. Each collimator cell was in the form of a rectangular parallelepiped with a base of

2 × 2 mm and a height of 4 mm. The average and most probable fragment exit angles were roughly 14°. This collimation enabled us to record up to 1.2% of the fissile events.

The U^{235} films were deposited on either side of aluminum discs 0.5 mm thick. The diameter of the films was 80 mm and their thickness about 6 mg/cm^2. The total weight of the U^{235} was 3.5 g, and 0.75% of the fissile events occurring in the uranium were recorded during the experiments.

The chamber was filled with a mixture of argon and carbon dioxide (10%) to a pressure of 760 mm Hg. With the high-voltage electrodes at about 1000 volts, the rise-time of pulses from the chamber was approximately 0.1μsec.

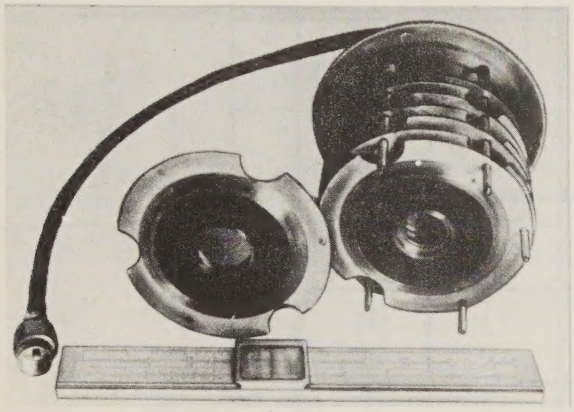

Fig. 1. Fission chamber with the fragment collimation system.

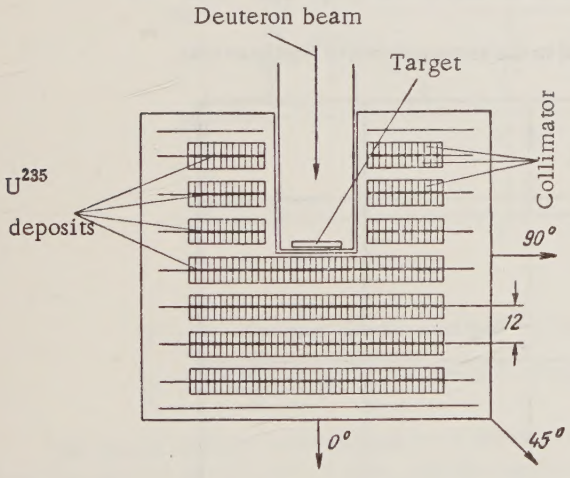

Fig. 2. Position of the fission chamber relative to the target of the accelerator tube. The arrows show the directions to the neutron detector.

The position of the chamber relative to the target of the accelerator tube is shown in Fig. 2. The measurements were carried out at 0, 45, and 90° in the neutron energy interval 0.4-5 Mev. About 2.5 × 10^3 fission neutrons were recorded at each angle. The background was of the order of 10 to 15% and increased with increasing angle. At the limits of the interval, i.e., at θ = 90°, the background reached 45%. Statistical errors did not exceed 10-15%, except for the energy range 0.4-0.6 Mev, where they reached 25% at 90°.

Figure 3 shows the neutron spectra emitted in the fission of U^{235} at 0, 45, and 90°. Figure 4 shows a comparison between the estimated integral spectrum obtained on the basis of the present results with the measured spectrum given in [9]. The two sets of results agree to within experimental error.

The neutron spectra emitted by the fragments were determined from the experimental data by subtracting the neutron spectra evaporated prior to fission. This was done with the aid of the results given in [9]. It was assumed that the angular distribution of the neutrons evaporated prior to fission is isotropic. The spectra obtained after this subtraction are shown in Fig. 5.

The angular distribution of the fission neutrons (cf. Table) was determined by numerical integration of the spectra shown in Figs. 3 and 5 with respect to the energy.

The present data were also used to estimate the angular distribution of fission γ-rays with energies $E_\gamma > 0.3$ Mev. Assuming that the γ spectrum is independent of the angle of emission of the γ rays relative to the direction of motion of the fragments, it was found that $n_\gamma(0°) : n_\gamma(45°) : n_\gamma(90°) = (1.31 \pm 0.07) : (1.22 \pm 0.06) : 1.00$.

Discussion of Results

As was to be expected, the present results indicate considerable differences between neutron spectra (in the laboratory system) emitted at different angles θ to the direction of motion of the fragments. There is a considerable anisotropy in the angular distribution of the neutrons: $b_{14} = N(0°)/N(90°) = 3.23 \pm 0.12$. The result $b'_{14} = 4.03 \pm 0.23$, which was obtained after subtraction of the neutrons evaporated prior to fission, agrees to within experimental error with the corresponding quantity $b_T = 4.35 \pm 0.19$ obtained for the fission of U^{235} by thermal neutrons [3]. The somewhat lower value obtained for b'_{14} as compared with b_T may be explained by an increase in the average energy of neutrons evaporated from the fragments [9]. The agreement between the values obtained for b'_{14} and b_T confirms the value obtained in [9] for the fraction of neutrons evaporated prior to fission.

Since the form of the neutron spectra at different angles θ and the magnitude of the anisotropy are very dependent on the neutron spectrum in the center-of-mass system of the fragment, we have tried to deduce information on this spectrum from the results of our experiments. With this aim in view, we have carried out calculations using various assumptions about the neutron spectrum in the center-of-mass system of the fragment. In these calculations we

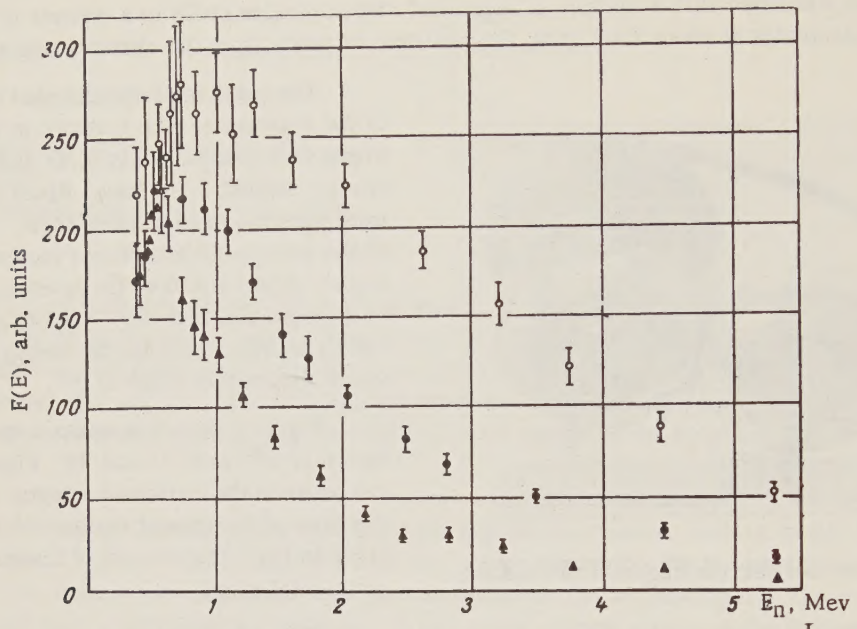

Fig. 3. Neutron spectra in the fission of U^{235} by 14.3 Mev neutrons at 0° (○), 45° (●), and 90° (▲) relative to the direction of motion of the fragments. The errors are statistical and all spectra are reduced to the same number of fissile events.

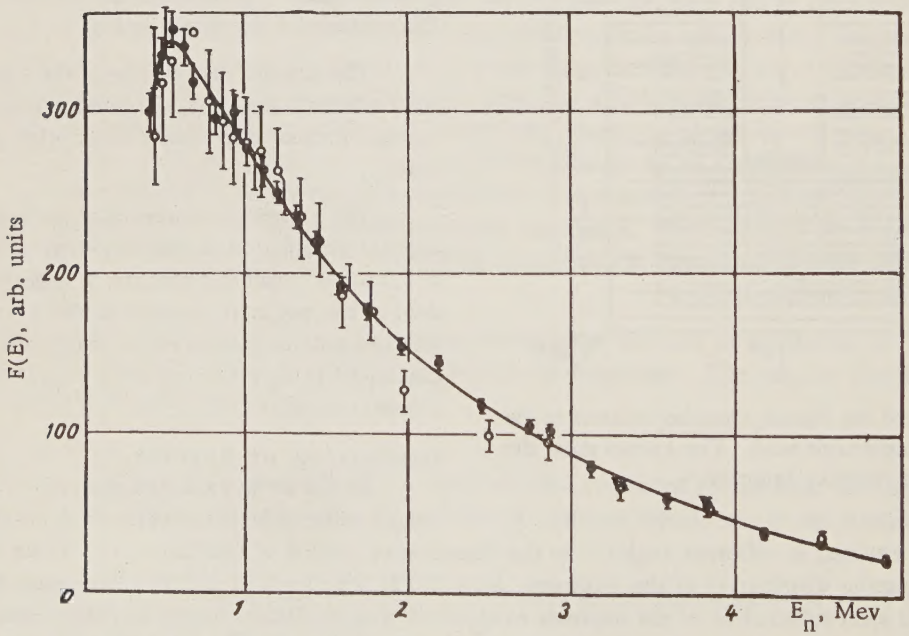

Fig. 4. Comparison of the estimated integral spectra based on the present results (○) with the spectrum reported in [9] (continuous curve and ●). The errors are statistical.

took into account the fragment mass distribution, the dependence of the total kinetic energy of the fragments on R_A, i.e., the fragment mass ratio [7], the dependence of ν on the fragment mass [10], and also the angular distribution of fragments passing through the collimator. In all cases an isotropic neutron emission in the center-of-mass system of the fragment was assumed.

Angular Distribution of the Fission Neutrons of U^{235}

	Measured		Calculated			
	all neutrons	neutrons from fragments	T = 1 Mev	T = 0.6 Mev	T = 0.2 Mev	spectrum from [12]
N (0°)	3,23±0,12	4,03±0,23	1,75	3,82	42,40	4,30
N (45°)	1,75±0,07	1,89±0,12	1,51	2,88	17,10	2,42
N (90°)	1,00	1,00	1,00	1,00	1,00	1,00

Note. The calculated angular distributions of the neutrons emitted by fragments were obtained on the assumption of a Maxwellian neutron distribution in the center mass system of the fragment.

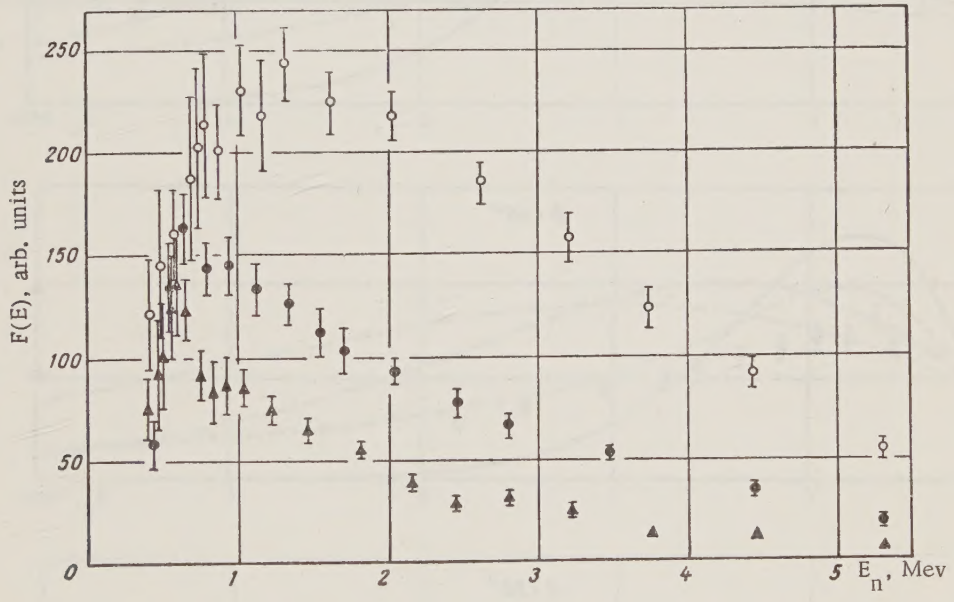

Fig. 5. Neutron spectra emitted by the fission fragments of U^{235} at 0° (○), 45° (●), and 90° (▲) to the direction of motion of the fragments. The errors are statistical.

The results of these calculations for a Maxwellian spectrum in the center-of-mass system, corresponding to temperatures of 0.2, 0.6, and 1.0 Mev, and the spectrum obtained in [11] for Cf^{252}, are compared with experimental data in Fig. 6. As can be seen, the experimental results agree neither with the calculations nor with the spectrum given in [11].

Calculations are being carried out at the present time which will take into account the temperature distribution as described in [12]. According to our estimates, this should increase the fraction of low- and high-energy neutrons in the spectrum, and should, at any rate, considerably reduce the discrepancy between theory and experiment. The discrepancy between the calculated and experimental angular distributions (cf. Table) may possibly be due to an anisotropic emission of neutrons in the center-of-mass system of the fragment [13]. If it is assumed that the preferred emission of neutrons in the backward and forward directions is symmetric with respect to the angle of 90° [12, 14], then corrections for the anisotropy would change the form of the spectrum in the same direction as the temperature distribution.

It should be noted that the apparent discontinuity at about 0.6 Mev for $\theta = 90°$ should not be treated too seriously, because of the inadequate accuracy in this region. However, if this peak does in fact occur, then it might be explained by the emission of a small number of neutrons from the waist of the dividing nucleus.

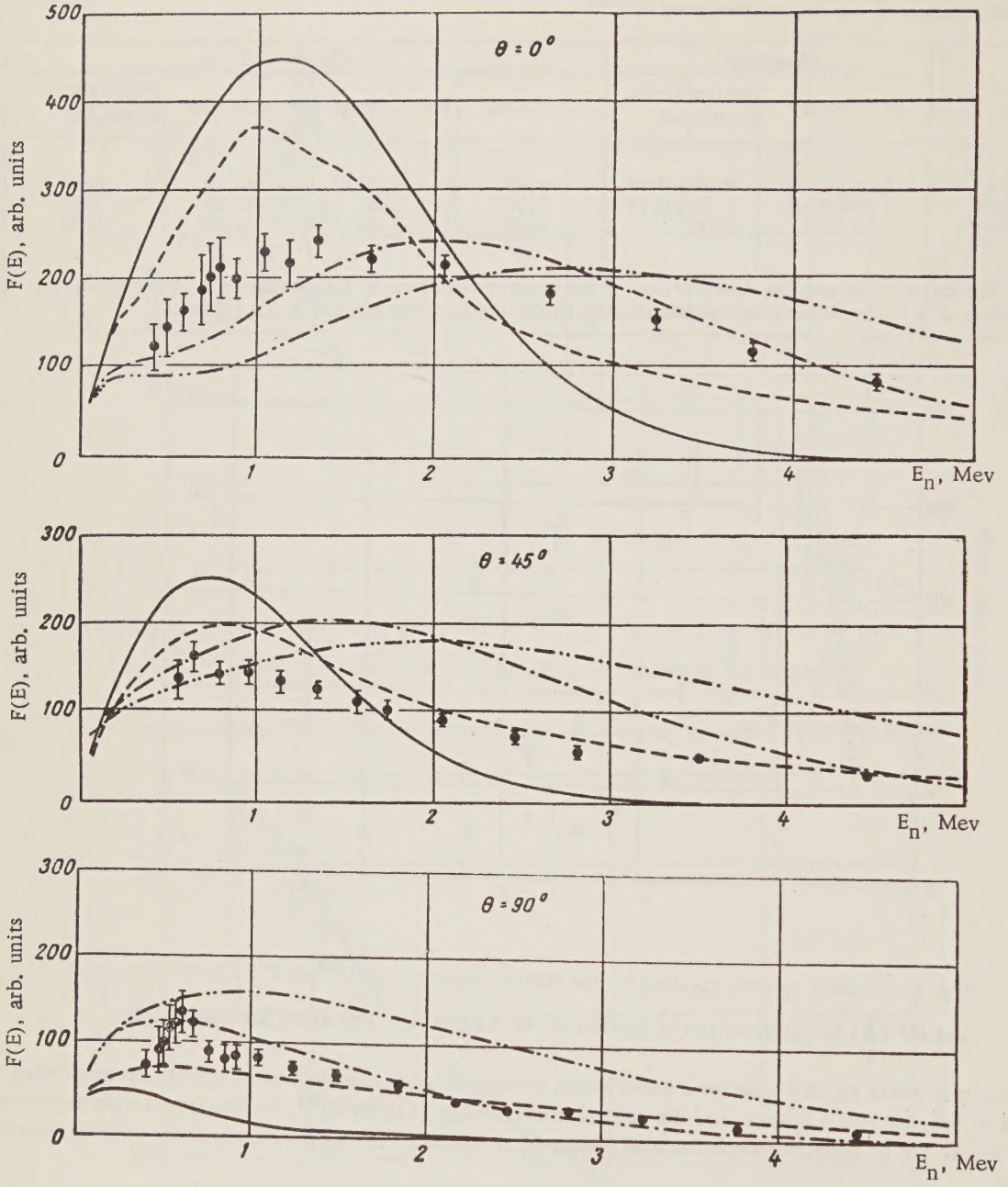

Fig. 6. Comparison of experimental results (⊕) with neutron spectra calculated on the assumption of a Maxwellian distribution of neutrons in the center-of-mass system of the fragment with T = 0.2 Mev (————), 0.6 Mev (— · —), 1.0 Mev (— · · —) with the spectrum obtained in [11] (— — —). All the spectra are normalized at $\theta = 0°$.

In conclusion the authors wish to thank P. V. Toropov for assistance in the preparation of the electronics; Yu. Ya. Glazunov, A. N. Maslov, N. I. Nemudrov, V. A. Parshin, and V. S. Khorkhordin for taking part in the measurements; and V. A. Komarov, M. P. Novikov, G. A. Peretokin, and L. A. Chernov for writing the computer program.

LITERATURE CITED

1. B. Watt, Phys. Rev. 87, 1037 (1952).
2. B. G. Erozolimskii, Atomnaya Énergiya, Supplement No. 1, p. 74 (Atomizdat, Moscow 1957).*
3. J. Fraser, Phys. Rev. 88, 536 (1952).
4. R. Wilson, Phys. Rev. 72, 189 (1947); R. Ramanna and P. Rama Rao, Communication No. 1663 submitted by India to the 2nd International Conference on the Peaceful Uses of Atomic Energy (Geneva, 1958).
5. B. G. Erozolimskii, Atomnaya Énergiya, Supplement No. 1, p. 74 (Atomizdat, Moscow 1957).*
6. D. Brunton and G. Hanna, Canad. J. Research 28A, 190 (1952); R. Leachman, Phys. Rev. 87, 444 (1952).
7. W. Stein, Phys. Rev. 108, 94 (1957).
8. R. Leachman, Phys. Rev. 101, 1005 (1956); R. Leachman and S. Kazek, Phys. Rev. 105, 1511 (1957).
9. Yu. A. Vasil'ev et al., Zh. éksperim. i teor. fiz. 38, 671 (1960).
10. S. Whetstone, Phys. Rev. 114, 581 (1959); V. F. Apalin et al., Atomnaya Énergiya 8, No. 1, 15 (1960).*
11. H. Bowman and S. Thompson, Communication No. 652 submitted by the USA to the 2nd International Conference on the Peaceful Uses of Atomic Energy (Geneva 1958).
12. J. Terrell, Phys. Rev. 113, 527 (1959).
13. D. Hill and J. Wheeler, Usp. fiz. Nauk 52, Nos. 1 and 2 (1954).
14. V. M. Strutinskii, Nuclear Reactions at Low and Intermediate Energies, a collection of papers [in Russian] p. 522 (Academy of Sciences Press, Moscow, 1958).

*Original Russian pagination. See C. B. translation.

COHERENT ELECTRON RADIATION IN A SYNCHROTRON

Yu. M. Ado and V. V. Elyan

Translated from Atomnaya Énergiya, Vol. 9, No. 6, pp. 455-460,
December, 1960
Original article submitted May 28, 1960

The coherent radiation of electrons in a synchrotron was investigated experimentally for a wavelength of 10 cm, corresponding to the 50th harmonic of the electron frequency of revolution for various electron distributions inside the separatrix. In most cases, the theory of coherent radiation of electrons is confirmed. A disparity with the theory is observed for almost uniform electron distributions. The radiation was used for measurements of the electron phase oscillations and adiabatic damping of the phase oscillation amplitudes. The experiment was carried out on the synchrotron at the Physics Institute, Academy of Sciences, USSR at 280 Mev with an initial betratron acceleration.

Introduction

In the case of circular motion of an electron, electromagnetic waves are radiated with frequencies that are multiples of the frequency of revolution [1]. In the region of wavelengths comparable with the dimensions of the bunch, the radiation is coherent and depends on the character of the electron distribution around the orbit [2-6]. This is taken into account by the introduction of a form factor F_{nm} in the formula for the coherent radiation intensity

$$W_{nm} = w_{nm} N^2 F_{nm}, \tag{1}$$

where w_{nm} is the intensity of the radiation of an individual electron undergoing phase oscillations with a frequency Ω; N is the number of accelerated electrons; n is the number of the harmonic; m = 0, 1, 2, 3, . . . characterizes the side frequencies close to the nth harmonic.

The form factor F_{nm} has been calculated for several shapes of the stationary distribution of the electrons for the phase oscillation amplitudes $f(\Phi)$ [5]:
for

$$f(\Phi) = \frac{\Phi}{2\Phi_0} \sqrt{(2\Phi_0)^2 - \Phi^2}, \tag{2}$$

$$F_{n0} = \frac{\sin^2(2n\Phi_0)}{(2n\Phi_0)^2}; \tag{2'}$$

for

$$f(\Phi) = \delta(\Phi - \Phi_0), \tag{3}$$

$$F_{n0} = J_0^2(n\Phi_0); \tag{3'}$$

for

$$f(\Phi) = \frac{\pi\Phi}{2\Phi_0^2} e^{-\frac{\pi}{4}\left(\frac{\Phi}{\Phi_0}\right)^2}, \tag{4}$$

$$F_{n0} = e^{-2\frac{n^2\Phi_0^2}{\pi}}, \tag{4'}$$

where Φ_0 is the mean amplitude of the phase oscillations in the bunch.

If $m \neq 0$, then $F_{nm} = 0$ for all three cases of the stationary distribution.

The acceleration of electrons in the synchrotron is accompanied by the damping of the phase oscillations. The coherent radiation intensity then changes in accordance with the laws described by the form factors (2'), (3'), and (4'), depending on the character of the electron distribution over Φ. In cases (2') and (3'), this change is of an oscillatory character. This property was first observed on the synchrotron at the Physics Institute, Academy of Sciences, USSR at 5 Mev in a study of the coherent radiation for the 16th and 24th harmonics and was used for the measurement of adiabatic pinching of the bunch [6].

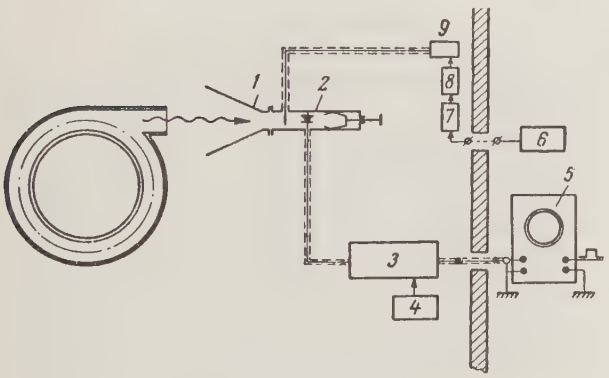

Fig. 1. Block diagram of the equipment.

For a nonstationary phase oscillation amplitude distribution of the electrons, it is not necessary that $F_{nm} = 0$ for $m \neq 0$ [5]. Moreover, the radiation signal turns out to be amplitude-modulated by the phase oscillations frequency. In this case, the frequency of the electron phase oscillations can be measured experimentally.

Equipment

The radiation was brought out of the synchrotron chamber through a lateral tube of 8 cm diam. A superheterodyne receiver was used to pick up the radiation. The layout of the equipment is shown schematically in Fig. 1. A born antenna 1 and mixer 2 were placed right next to the accelerator. A klystron (K-11) oscillator 9, intermediate-frequency amplifier 3, and stabilized power supplies 4 and 8 were placed at a distance of about 3 m from the accelerator magnetic to avoid effects from the varying magnetic field on the operation of the circuit. The intermediate-frequency amplifier was six-stage tuned amplifier with a 0.5 Mc passband and amplification factor of $\sim 5 \times 10^5$. The intermediate frequency was chosen as 25 Mc. After detection, the signal was fed to an OK-17M oscillograph 5 equipped with a photographic attachment. The oscillograph sweep was triggered by a pulse synchornized with the magnetic field of the accelerator. The oscillograph sweep was calibrated by time marks. The equipment allowed the receiver to be retuned over a range of ~10 Mc, which was limited by the region of klystron oscillation. The klystron signal frequency was changed by the varying of the voltage on the reflector by means of two selsyns 6 and 7.

Experimental Results

Oscillographs were taken for various distributions of the electrons in the separatrix.

In the synchotron with betatron starting, the distribution could be changed by shifting the time of switching on the high-frequency accelerating voltage with respect to the optimum time. The experimentally obtained dependence of the relative number of particles N trapped in synchrotron operation on the instance for switching on the accelerating field is shown in Fig. 2. The optimum time for switching on the accelerating field corresponds to N =100. On segments I and III, the electrons fall inside the separatrix on phase trajectories close to each other. Therefore, the character of the electron phase oscillation amplitude distribution is close to a δ function. For region II, a more even filling of the separatrix and a Φ distribution of the electrons close to (2) are characteristic. The amount of trapped electrons on segment I depends on the accelerating field voltage. Hence when this amount is measured, the frequency should be chosen from the greatest value of N on segment I.

Figure 3 shows typical oscillograms of the radiation obtained when the accelerating field was switched on at segment II. As seen from the oscillograms, there was no radiation during the betatron operation of the accelerator as long as the electron energy was $E \lesssim 4$ Mev; it appeared only after formation of the bunch. At $E > 180$ Mev, the radiation intensity decreases sharply and signal drops below the level of the equipment noise. The shape of the radiation pulse depends on the conditions of trapping in synchrotron operation, i.e., on the amplitude and frequency of the accelerating field, its rise time, and the time at which the field is switched on. Under some conditions, the radiation appears to be partially amplitude-modulated. In the oscillogram of Fig. 3b, the region with this type of modulation is indicated by an arrow.

Figure 4 shows oscillograms of this region taken with a fast sweep for three values of the accelerating voltage amplitude U. The modulation frequency ratio measured from the oscillograms

$$F_1 : F_2 : F_3 = 0.85 : 1 : 1.15$$

is in good agreement with the theoretically calculated ratio of the phase oscillation frequencies:

$$F_1 : F_2 : F_3 = \sqrt{U_1 \sin \varphi_{s1}} : \sqrt{U_2 \sin \varphi_{s2}} : \sqrt{U_3 \sin \varphi_{s3}} = 0{,}84 : 1 : 1{,}10,$$

where φ_s is the equilibrium phase.

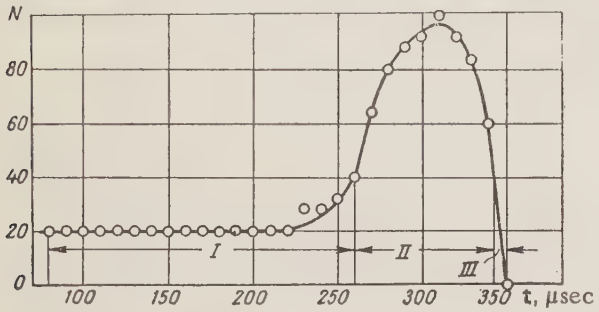

Fig. 2. Experimental dependence of the number of particles N trapped in synchrotron conditions of acceleration on the time at which the high-frequency accelerating voltage is switched on. The time is counted from the instant at which the magnetic field passes through zero.

Data for the Phase Oscillation Frequency Measurements

U, volts	$\sin \varphi_s$	F, kc	α^0_{max}	ψ^0_{max}
800	0,77	52±5	92±9	100±10
1000	0,87	63±6	115±11	120±12
1200	0,91	84±6	127±12	130±13

This shows that such amplitude modulation is due to the phase oscillations of the particles distributed under nonstationary conditions in accordance with the amplitudes of these oscillations.

The table lists the frequencies of the phase oscillations F, the maximum amplitudes of the phase oscillations α_{max}, obtained from the known relation between F and α_{max} [7], and the maximum size of the separatrix ψ_{max} determined from the oscillograms of Fig. 4.

In the calculations we used the values E = 80 Mev, magnetic field exponent 0.65, frequency of revolution of the electrons 58 Mc.

From a comparison of α_{max} and ψ_{max}, it is seen that the contribution to the modulation comes from the electrons grouped close to the separatrix.

The radiation is of an oscillatory character only under specific conditions of bunch formation in the transitional operation, when the amplitude distribution of the phase oscillations is close to a δ function. For example, when the accelerating field is switched on at times corresponding to segment I in Fig. 2, the radiation depends on the energy in the way shown in Fig. 5. Shortly after the beginning of synchrotron operation, however, the radiation becomes either quite irregular (noise) (see, for example, Fig. 3a) or partially regular (Fig. 3c). Depending on the frequency of the accelerating field, the regularity can begin to be disturbed at different electron energies from E = 8 Mev (Fig. 5a) to E = 60 Mev (Fig. 5b). This effect is obviously connected with the redistribution of the electrons in the separatrix during the acceleration process.

Slow oscillations of the radiation intensity (see Fig. 5) are due to the adiabatic damping of the phase oscillations; similar oscillations have been observed in [6].

Figure 6 shows curves of the phase oscillation amplitude damping calculated by the method of adiabatic invariance [7] and the experimental results obtained on the basis of the analysis of the oscillograms (see Fig. 5).

While the experimental points are in very good agreement with the calculated curves for Φ_0 i $\lesssim 140°$, they are not in agreement with the curves for $140° \lesssim \Phi_0$ i $\lesssim 180°$. This means that the capture of electrons in synchrotron operation on segment I of Fig. 2 takes place on phase trajectories with amplitudes less than 140°.

We also measured the bandwidth of the frequencies of the 50th harmonic. It turned out that, for radiation with a signal of oscillatory form (see Fig. 5), the bandwidth of the harmonic frequencies does not exceed 0.5 Mc. This

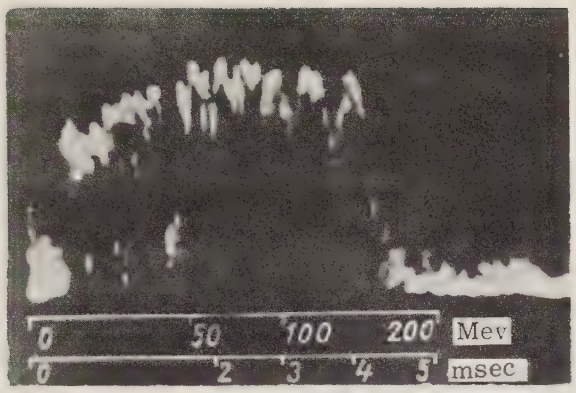

a

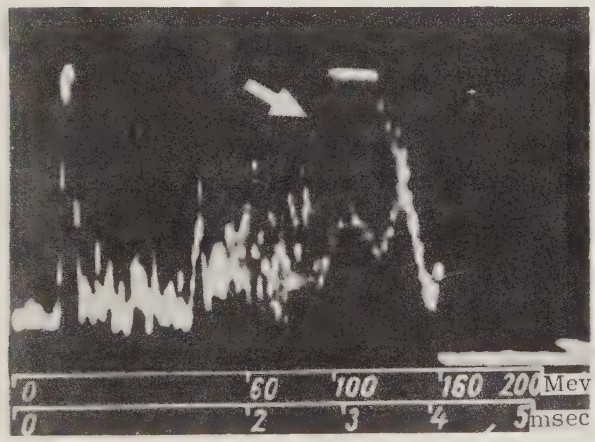

b

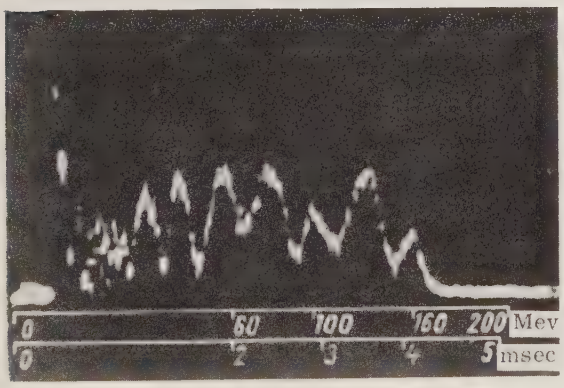

c

Fig. 3. Oscillograms of coherent radiation.

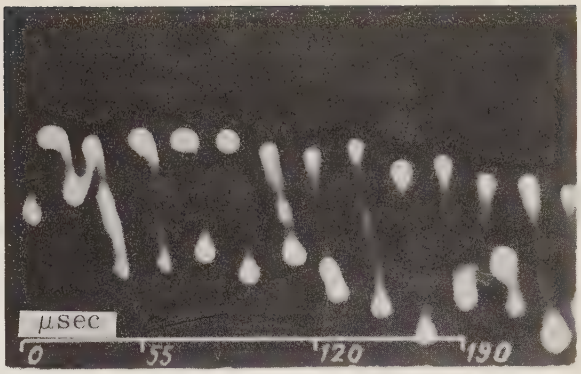

a

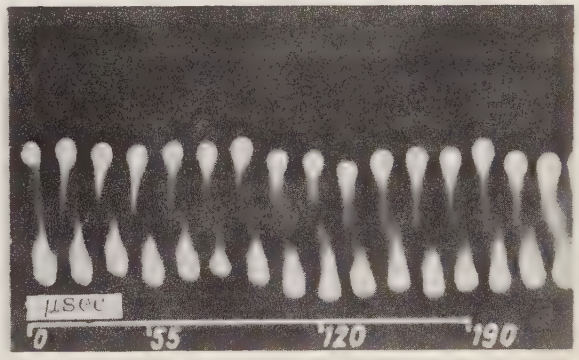

b

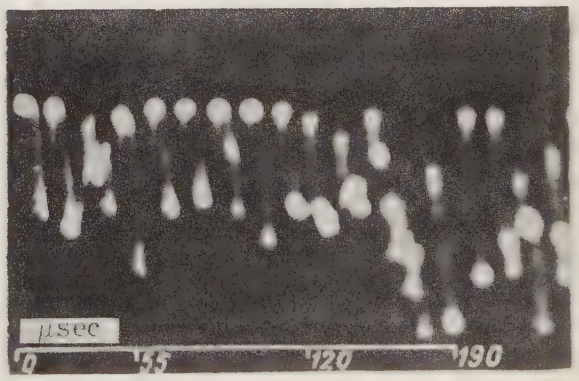

c

Fig. 4. Oscillograms of the intensity of coherent radiation amplitude-modulated by the phase oscillation frequency. A) U = 300 volts; b) U = 1000 volts; c) U = 1200 volts.

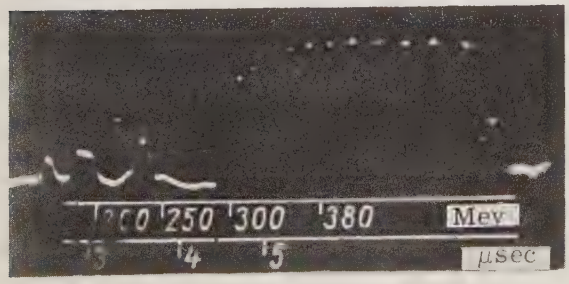

a

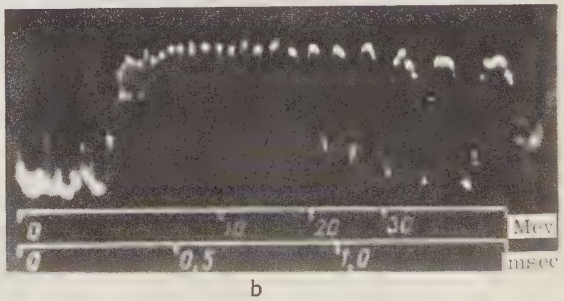

b

Fig. 5. Modulation of the radiation intensity by slow oscillations.

confirms the theoretical conclusion that for distributions of type (3) the side frequencies of the radiation vanish, i.e., $F_{nm} = 0$ for $m \neq 0$.

The noise character of the radiation (see Fig. 3) is accompanied by a broad frequency band (Fig. 7), i.e., in this case $F_{nm} \neq 0$ for $m \neq 0$. This has not been explained theoretically thus far. We believe that the phenomenon of broad frequency bands near the harmonics of the radiation of the electron bunch with a distribution of type (2) can be properly explained qualitatively by the unavoidable fluctuations in the phase oscillation amplitude distribution of the electrons, which are not taken into account by the theory.

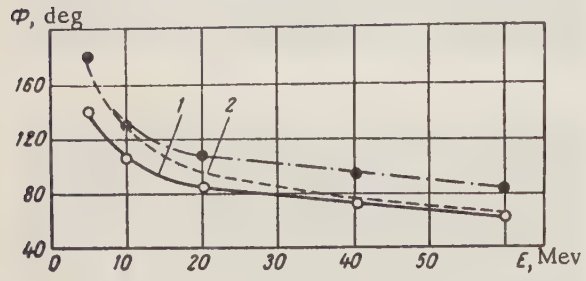

Fig. 6. Adiabatic damping of phase oscillations. 1 and 2) Theoretical curves; ○ and ●) experimental results for $\Phi_{0i} = 140°$ and $\Phi_{0i} = 180°$, respectively.

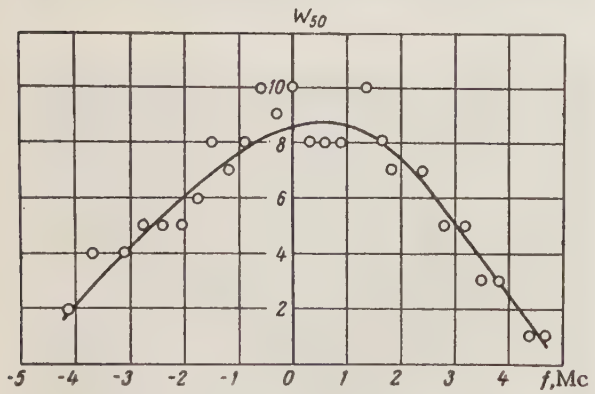

Fig. 7. Relative distribution of the radiation intensity in the band of the 50th harmonic for optimum switching on of the accelerating field.

The sharp decrease in the radiation intensity at electron energies above 180 Mev is explained by the fact that up to this time the phase oscillation amplitude distribution of the electrons is close to Gaussian (4). The value of F_{n0}(4') then becomes incomparably smaller than (2') and (3'). The formation of a distribution of type (4) is confirmed by other experiments made at the synchrotron of the Physics Institute, Academy of Sciences, USSR at 280 Mev [8].

CONCLUSIONS

1. By means of coherent radiation of electrons one can readily record the beginning of the formation of the electron bunch in a synchrotron with betatron starting.

2. For a nonstationary distribution of electrons in the separatrix, the radiation can be used for the measurement of the phase oscillation frequency.

3. The use of coherent radiation from the 50th harmonic for the study of phase oscillation damping is possible only for phase oscillation amplitude distributions of the δ-function type. For other types of distributions, lower harmonics should be used.

4. The theory of coherent radiation of electrons in the synchrotron is in agreement with experimental only in special cases. To generalize the theoretical conclusions, it is necessary to consider the effect of the fluctuations in the electron distribution on the coherentness.

In conclusion, the authors thank Prof. P. A. Cherenkov, Prof. M. S. Rabinovich, Prof. A. M. Prkhorov, and L. V. Iogansen for valuable discussions.

LITERATURE CITED

1. D. D. Ivanenko and A. A. Sokolov, Classical Field Theory [in Russian] (Moscow, State Technical Press, 1949).
2. E. McMillan, Phys. Rev. 68, 144 (1945).
3. L. Schiff, Rev. Scient. Instrum. 17, 6 (1946).
4. M. L. Levin, Zhur. Tekh. Fiz. 17, 1159 (1947).
5. L. V. Iogansen and M. S. Rabinovich, Zhur. Éksp. i Teor. Fiz. 35, 4 1013 (1958).
6. A. M. Prokhorov, Radiotekhnika i Élektronika 1, 1, 71 (1956).
7. M. S. Rabinovich, Tr. Fizicheskogo Instituta AN SSSR 10, 23 (1958).
8. K. A. Belovintsev and B. N. Yablokov, Pribory i Tekhnika Éksperimenta 2, 12 (1959).

HEAT EXCHANGE DURING THE FLOW OF MERCURY AND WATER IN A TIGHTLY PACKED ROD PILE

V. I. Subbotin, P. A. Ushakov, B. N. Gabrianovich,

and A. B. Zhukov

Translated from Atomnaya Énergiya, Vol. 9, No. 6, pp. 461-469,
December, 1960
Original article submitted August 28, 1959

The results of an experimental investigation of heat transfer in mercury and water in tightly packed rods are presented. The problems of thermal simulation of the rods are considered, the results of measuring the temperature field of the heat-exchange surface are given, and the experimental apparatus, procedure, and processing of the data are described. For a given group of tightly packed rods a procedure is suggested for making an approximate thermal calculation.

It is customary in calculating heat transfer to liquids with Pr > 0.6 in complex channels to recommend the equations derived for circular tubes, for instance the equation of M. A. Mikheev [1]:

$$Nu_f = 0{,}021 Re_f^{0,8} Pr_f^{0,43} (Pr_f/Pr_w)^{0,25}, \quad (1)$$

the equation of Colburn [2]:

$$Nu = 0{,}023 Re^{0,8} Pr^{1/3}, \quad (2)$$

and others. The hydraulic diameter d_h is taken accordingly as the reference dimension. These recommendations are endorsed by a number of authors [3-6]. Recently, however, the results of investigations have been published showing that the use of d_h as the defining dimension does automatically imply allowance for the peculiarities of heat transfer in rod piles subjected to an arbitrary flow pattern [7, 8]. Weisman [8] showed on the basis of a generalization of several papers that the influence of the spacing in a triangular latticework of rods can be taken into account by introducing into Eq. (2) the following variable coefficient in place of the factor 0.023:

$$K = 0{,}026x - 0{,}006, \quad (3)$$

where $x = s/2R_2$ is the relative rod spacing and is equal to 1.1-1.5; $Re > 25 \cdot 10^3$.

It is unfeasible to extrapolate the relation (3) in the hope of obtaining reliable data for closely packed piles with x = 1, since the heat exchange in closely packed piles depends on the construction and thermal conductivity of the rods, even more strongly than in piles with x > 1, due to the acute asymmetry of the cells.

The published data on heat transfer of piles in axial flow of a liquid metal ($Pr \ll 1$) is almost completely restricted to the papers [9, 10]. The results of these papers, evidently, can be used for approximate heat exchanger calculations. It should be noted that in general no data have been published on tightly packed piles.

Problems in the Thermal Simulation of Tightly Packed Rods

Consider a pile with a large number of heat-generating rods. In this case the influence of edge effects on heat exchange and the hydrodyanmics of the central pile cells cannot be taken into account. We shall adopt the following assumptions: 1) The physical parameters of the system are constant; 2) the liquid is incompressible; 3) heat is liberated uniformly throughout the volume of the rods; 4) ideal thermal contact is maintained between the heat-gene-

part of the rod and the protective casing; 5) the longitudinal cross convection of heat in the rods is small; 6) the temperature and velocity distributions are steady-state.

As a result of analysis of the differential energy equations, the equation of motion, and appropriate boundary conditions on the basis of similarity theory a system of dimensionless parameters is obtainable, characterizing the heat-exchange process in the pile cell:

$$Nu = f\left(\frac{l}{d_h}, \xi_1, \frac{\lambda_1}{\lambda_2}, \frac{\lambda_2}{\lambda_3}, Re, Pr\right);$$
$$T_w = f\left(\frac{l}{d_h}, \varphi, \xi_1, \frac{\lambda_1}{\lambda_2}, \frac{\lambda_2}{\lambda_3}, Re, Pr\right); \quad (4)$$

$$\frac{t_w - \bar{t}_f}{\bar{q}R_2}\lambda_3 = \frac{d_h}{NuR_2} + T_w, \quad (5)$$

where l is the pile length (m); $\xi = R_1/R_2$ is the dimensionless radius (R_1, R_2 are the inside and outside radii of the tube or rod casing, respectively, in m); λ_1, λ_2, λ_3 are the heat conductivities of the heat-generating rod, rod casing (or tube), and liquid, respectively (kcal/m · hr · °C); $T_w = \frac{t_w - \bar{t}_w}{\bar{q}R_2}\lambda_3$ is a dimensionless temperature parameter (t_w is the wall temperature, °C; $\bar{q}$ the heat flow density, kcal/m² · hr); t_f is the temperature of the heat carrier (°C); $d_h = 4F/P$ is the equivalent hydraulic diameter of the pile cell, m (P is wetted perimeter of the pile cell, m; F the active cross section of the cell).

In the channels of the pile there is no axial symmetry, so that the temperature of the heat carrier and heat-exchange surface is governed not only by the properties and flow conditions of the heat carrier, but also by the parameters of the heat-generating rods (ξ_1, λ_1/λ_2, λ_2/λ_3).

In many instances it proves difficult to realize exact simulation of the rod, so that one must resort to approximate simulation. Consider the two limiting cases: $\lambda_1 \gg \lambda_2$ and $\lambda_1 \ll \lambda_2$. The conditions t = const or q = const will apply to the inner surface of the rod in correspondence with these two cases.

Let us examine the conditions for approximate simulation in the case when $\lambda_1 \simeq \lambda_2$. The heat-exchange process in the cell is uniquely determined by the geometry, flow conditions, properties of the heat carrier, and the boundary conditions, which in dimensionless form may be written

$$f\left(\frac{l}{d_h}, \varphi, Re, Pr, T_w, \frac{q - \bar{q}}{\bar{q}}\right) = 0.$$

The connection between the parameters T_w and $\frac{q - \bar{q}}{\bar{q}}$ can be found by solving the problem of heat conduction for the heat-generating rod and casing. If we write T_w in Fourier series form

$$T_w = \sum_{k=1}^{\infty} A_{6k} \cos 6k\varphi, \quad (6)$$

the distribution of heat flow will have the form

$$\frac{q - \bar{q}}{\bar{q}} = -\sum_{k=1}^{\infty} B_{6k} \cos 6k\varphi = -\sum_{k=1}^{\infty} 6k\, C_{6k} A_{6k} \cos 6k\varphi; \quad (7)$$

$$C_{6k} = \frac{\lambda_2}{\lambda_3}\frac{m - \xi_1^{12k}}{m + \xi_1^{12k}}; \; m = \frac{1 + \lambda_1/\lambda_2}{1 - \lambda_1/\lambda_2}. \quad (8)$$

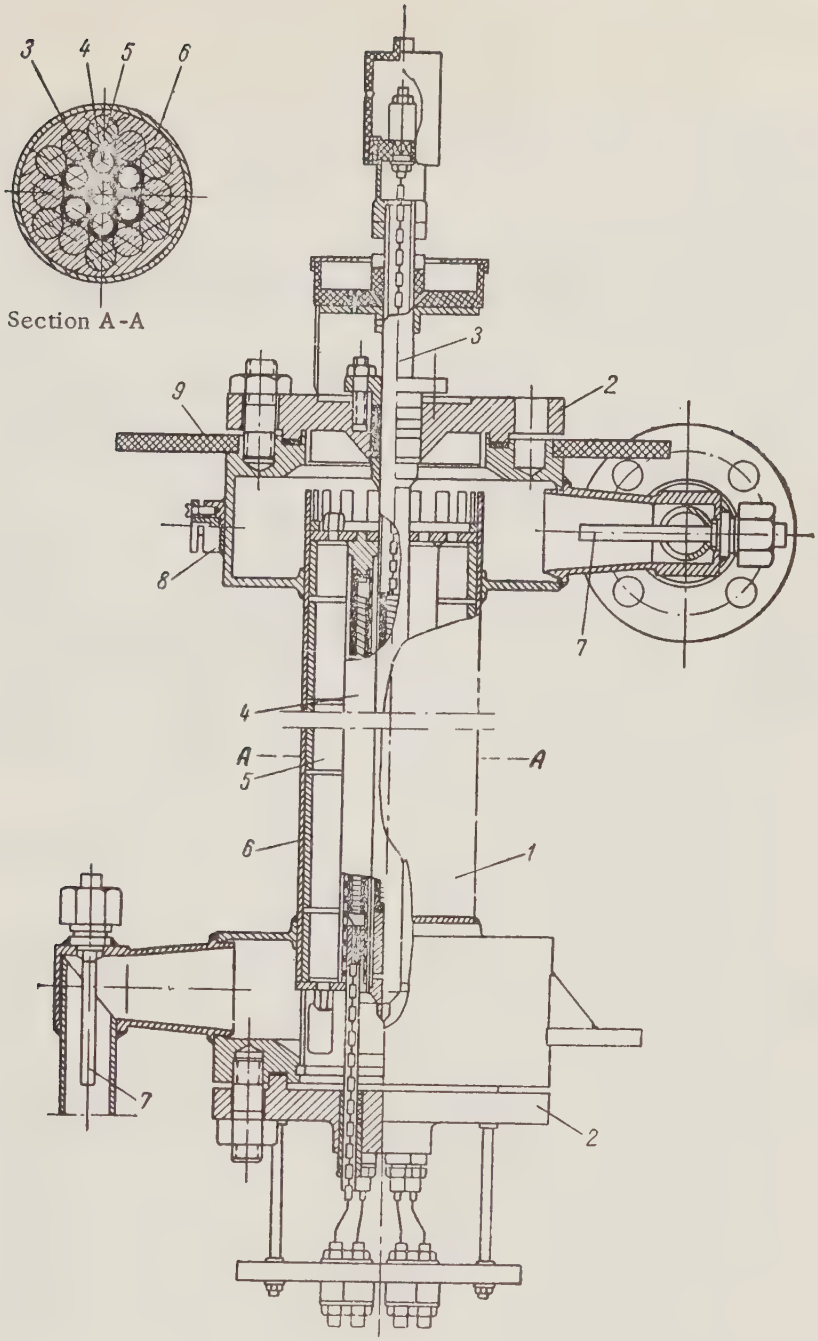

Fig. 1. Experimental heat exchanger: 1) Case; 2) flanges; 3) central tube; 4) side tubes; 5) rod displacers; 6) contour displacer; 7) thermocouple case; 8) packing nuts for thermocouples to measure temperature of the mercury in the cells; 9) thermocouple panel.

In the first approximation in the expansions (6) and (7),we stop with the fundamental harmonic (k = 1). Then we can write

$$Nu \approx f\left(\frac{l}{d_h},\ Re,\ Pr,\ C_6\right); \tag{9}$$

$$T_w \approx f\left(\frac{l}{d_h},\ \varphi,\ Re,\ Pr,\ C_6\right). \tag{10}$$

The resultant system of similarity criteria for approximate simulation was used by the authors to generalize the experimental results.

Experimental Apparatus

The transfer of heat to mercury was studied on a stainless steel (type 1Kh18N9T) loop. The mercury was circulated by a centrifugal pump. The mass flow of mercury was regulated by a throttle device and was measured preliminarily by a graduated Venturi tube.

The construction of the experimental heat exchanger is shown in Fig. 1. The dimensions of the heat-exchanger assemblies are the following (in millimeters): $R_2 = 8.8^{-0.025}$; $R_1 = 6.8^{+0.025}$; $l = 500^{\pm 0.5}$; $l_0 = 430^{\pm 2}$; $d_h = 1.81$.

The heat exchanger consists of a cylindrical case, inside which a pile of seven tubes and 12 rods are mounted. The tubes are heated by nichrome electric heaters. The central tube is inserted through packing, making it possible to turn it at any angle without disrupting the operation of the apparatus.

Twelve nichrome-constant thermocouples, 0.08 mm diameter, are attached to the surface of the central tube. The thermocouples are placed in a stainless steel capillary with a diameter of 0.5 mm. The thermocouple junctions are calked onto the surface of the tube. The capillaries have been fitted into longitudinal recesses and covered by a layer of metal, deposited by means of an ÉM-Z-A metallizer, after which the surface of the tube was carefully cleaned. (The method of making and inserting the thermocouples is described in detail in [11]).

The temperature of the heat carrier at the inlet and outlet of the heat exchanger is measured by thermocouples. Moreover, the temperature of the heat carrier in the individual pile cells at the outlet from the packet is measured by thermocouples in capillary covers.

The tests with mercury and with distilled water were conducted one after the other using the same heat exchanger. The apparatus for studying heat transfer to water was also made of stainless steel.

Experimental Procedure and Processing of the Data

In our tests we measured the temperature field of the surface of the central tube with the heat carrier flowing at different velocities. The temperature of the medium at the inlet and the heat flow were held constant. The tube was turned from $\varphi = 0$ to $\varphi = 360°$.

For various distances from the entrance, the dependence of the temperature drop from wall to liquid on the reduced angle was determined. For this purpose the data obtained for different central cells were averaged, and the angle φ, equal to 0-360°, was transformed to the reduced angles θ, equal to 0-30°. In calculating the temperature drops, the mean temperature of the heat carrier in the central cells and in a given cross section was assumed to be the temperature of the liquid. A correction for the depth of insertion of the thermocouples was introduced on the assumption that the heat flow distribution over the perimeter of the tube was cosinusoidal. The depth of insertion of the thermocouples was ~ 0.2 mm. The average temperature drops over the perimeter were found by graphical integration of the relation $\vartheta = f(\varphi)$, where ϑ is the local temperature drop of the wall to liquid (°C).

In the tests with mercury and water, we used the same central tube I. Control tests with water were conducted with a new central tube II.

The heat-transfer coefficients, averaged over the tube perimeter, were calculated as

$$\bar{\alpha}_I = \frac{\bar{q}}{\bar{\vartheta}}, \tag{11}$$

There exists another method for finding the mean heat-transfer coefficient:

$$\bar{\alpha}_{II} = \frac{1}{F}\int_F \frac{q}{\vartheta}\,dF. \tag{12}$$

But the mean value of the temperature of the heat-exchange surface can be found only in terms of $\bar{\alpha}_I$:

$$t_w = \frac{1}{F}\int_F t_w dF = \bar{t}_f + \frac{q}{\bar{\alpha}_I}.$$

Also investigated in the case of mercury was the heat exchange with a fixed position of the central tube. On the basis of these data we also calculated the mean heat-transfer coefficients on the assumption that the temperature distribution over the tube perimeter was cosinusoidal.

In special tests we checked the influence of the unheated case on the temperature conditions of the central tube. It was found that heating of the case does not alter the heat exchange in the central cells. This serves as a basis for extending the data obtained to piles with a large number of rods.

The heat flow distribution over the tube perimeter was calculated from Eqs. (6) and (7).

In processing the experimental data, we took the mean temperature of the heat carrier in the central cells as the reference temperature in the similarity criteria. The values of the water and mercury parameters were borrowed from [12, 13].

Results and Generalization of the Experimental Data

The limits of variation of the fundamental quantities are given in Table 1. A typical distribution of temperature drops is shown in Fig. 2. Such distributions were obtained with mercury flow velocities (w) equal to 1.14, 0.86, 0.67, and 0.22 m/sec and with water flow velocities of 5.91, 5.80, 5.77, 4.10, 2.22, 2.17, and 1.54 m/sec. The various points in Fig. 2 stand for the reading of thermocouples located diametrically opposite one another. The slight divergence in readings of these thermocouples can be attributed to a small irregularity in heat flow and slight distortion of the cell geometry due to allowances in the tube dimensions. It is also evident from Fig. 2 that the temperature of the tube surface changes considerably over the perimeter. A similar picture was noted in the water experiments.

TABLE 1

Limites of Variation of the Fundamental Quantities

Quantity	Value	
	for mercury	for water
w, m/sec	0,22—1,14	1,54—5,91
t_f, °C	24	33; 41—44
q, kcal/m^2 · hr	$27{,}2\cdot10^3$	$27{,}2\cdot10^3$
λ_2/λ_3	1,8	24
Pr	0,022—0,025	3,9—4,9
Re	3800—18600	4640—16450
Pe	80—470	—

The temperature distribution law for mercury flowing in the pile is very nearly cosinusoidal. In the case of water, more clearly pronounced temperature maxima are seen along the lines tangent to the tubes. The temperature distributions, averaged over the cells, are shown in dimensionless form in Fig. 3. With increasing velocity, the irregularity of the temperature distribution over the perimeter should decrease due to the deeper penetration of turbulence into the narrow parts of the cells. However, in the investigated velocity range this effect was only slight. The influence of length was also insignificant.

The value of T_W (λ_2/λ_3) averaged over velocity and length can be described by the following approximate relations: for mercury

$$T_w \frac{\lambda_2}{\lambda_3} \approx 0{,}18\cos 6\varphi, \tag{13}$$

for water

$$T_w \frac{\lambda_2}{\lambda_3} \approx 0{,}121\cos 6\varphi + 0{,}019\cos 12\varphi + 0{,}040\cos 18\varphi + 0{,}016\cos 24\varphi. \tag{14}$$

Figure 4 illustrates the nature of the heat flow distribution over the perimeter of the central tube. The close packing is characterized by the fact that radial heat flow along the lines tangent to the rods is completely absent. The values of the heat flow at $\theta = 0°$, calculated on the basis of our experiments, are very nearly zero. This is definite indication that the results obtained are valid. The heat flow distribution over the perimeter of the central tube can be described approximately by the following relations: for mercury

$$q/\bar{q} \approx 1 - \cos 6\varphi, \tag{15}$$

for water

$$q/\bar{q} \approx 1 - 0{,}67\cos 6\varphi - 0{,}20\cos 12\varphi - 0{,}07\cos 18\varphi - 0{,}04\cos 24\varphi. \quad (16)$$

In general, the heat flow distributions obtained for mercury and water and basically no different from one another.

Figure 5 shows the temperature distribution over the length of the pile. It is evident that the heat carrier temperature in the central cells is appreciably different from the mean temperature over the pile cross section.

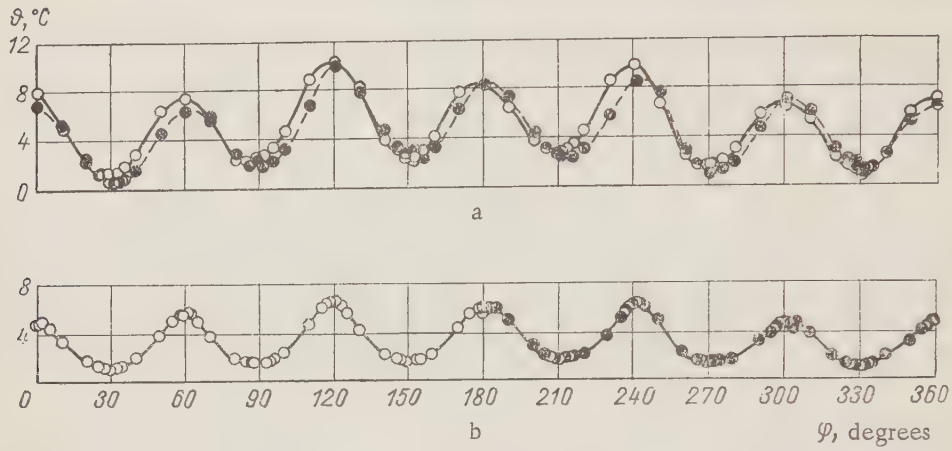

Fig. 2. Typical distributions of temperature drops over the tube perimeter: a) Mercury, w = 1.14 m/sec; b) water, w = 4.10 m/sec.

TABLE 2

Mean Heat-Transfer Coefficients and Nu Numbers, Obtained for Mercury and Water [a]

Mercury (Pr=0,022—0,025)				Water (Pr=3,9—4,9)			
limits of tube rotation, deg.	Pe	$\bar{\alpha}_I$, kcal/m²·hr·°C	Nu	limits of tube rotation, deg.	Re	$\bar{\alpha}_I$, kcal/m²·hr·°C	Nu
0—360	86	2860	0,71	30—210	4650	4910	16,1
No turn	128	3280	0,82	0—120	6240	7000	23,1 [b]
» »	158	3540	0,89	30—210	5990	5990	19,8
» »	182	3800	0,96	0—360	5520	5500	18,5
» »	204	3850	0,98	30—210	11970	9190	30,4
» »	225	4050	1,03	0—210	16300	11680	38,6
0—360	270	4480	1,14	0—90	16450	14850	49,4 [b]
0—360	350	4800	1,23	0—360	15100	11150	37,4
No turn	398	4730	1,22	—	—	—	—
» »	435	5000	1,29	—	—	—	—
0—360	470	5160	1,32	—	—	—	—

[a] See Fig. 2 for the angle of rotation notation. Tube I was used in all cases except those marked by b.

[b] Tube II was used.

The mean values of the heat-transfer coefficients over the perimeter α_I and Nu numbers for the stabilized interval are given in Table 2. The dependence of Nu on Pe for mercury is shown in Fig. 6. As a result of the relatively large pile lengths the mean values of the heat transfer coefficients over the length and perimeter differ from the stabilized values by no more than 5%.

The results obtained for water are compared in Fig. 7 with data calculated from Eq. (1).* This comparison is arbitrary with Re = (4-10) · 10^3, since Eq. (1) is recommended only for Re > 10^4. The values of Nu calculated from Eq. (1) differ from the experimental values approximately by a factor of two.

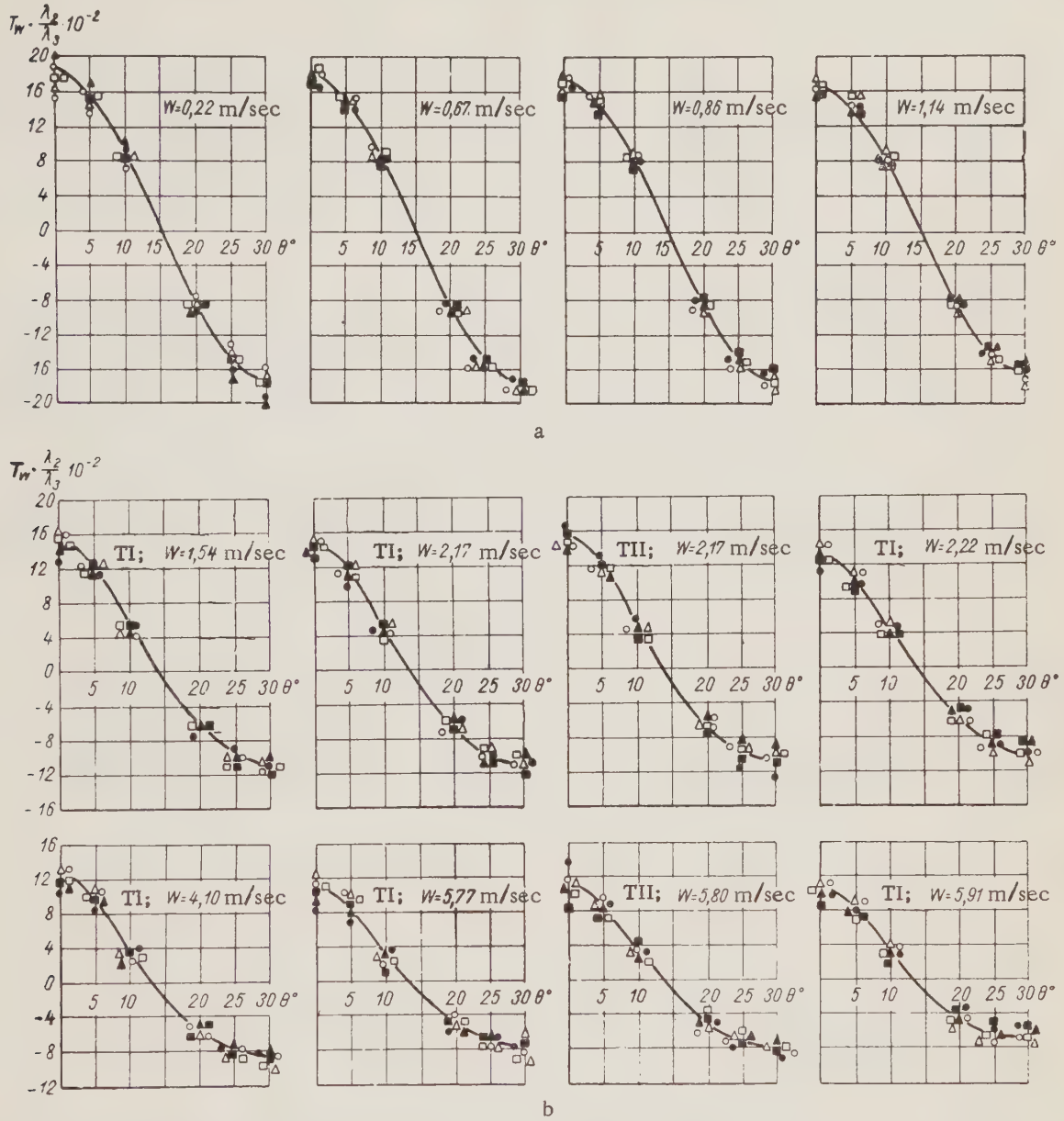

Fig. 3. Dependence of the parameter T_W λ_2/λ_3 on the reduced angle θ: a) Mercury; b) water. ▲) l_1 = = 64 mm; ■) l_2 = 124 mm; ●) l_3 = 184 mm; △) l_4 = 244 mm; □) l_5 = 304 mm; ○) l_6 = 364 mm.

The errors in measuring the temperature drops ϑ did not exceed ±(0.2-0.3)°C. The error due to geometry, heat losses at the ends, and power measurements amounted to ~ ±4%. Then for $\bar{\vartheta} \simeq 4$°C, the limiting relative errors in measuring the mean heat-transfer coefficient and maximum temperature drop from wall to liquid are

$$\frac{\delta\alpha}{\alpha} \approx \pm 12\% \quad \text{and} \quad \frac{\delta(t_w^{\max} - t_f)}{\bar{\vartheta}} \approx \pm 23\%.$$

*In our experiments the correction factor $(Pr_f/Pr_W)^{0.25}$ barely differed from unity.

In processing the results, most of the random errors were eliminated. It may therefore be expected that the systematic error $\delta(t_w^{max}-t_f)/\bar{\vartheta}$ is less than ± 23%.

Conclusions and Recommendations

The following procedure is recommended for an approximate thermal analysis of heat-liberating rods and tight packing in the pile. The procedure is applicable for Re from 3000 to 20,000.

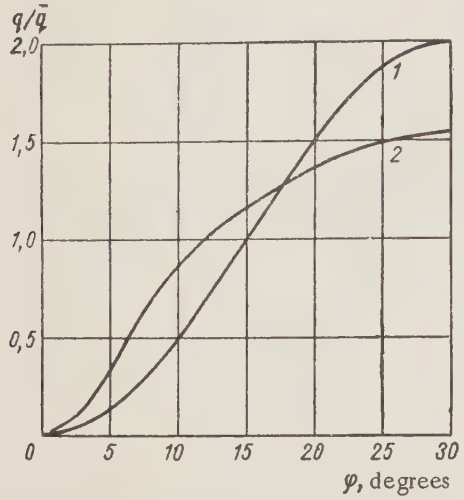

Fig. 4. Heat flow distribution over tube perimeter: 1) Mercury; 2) Water.

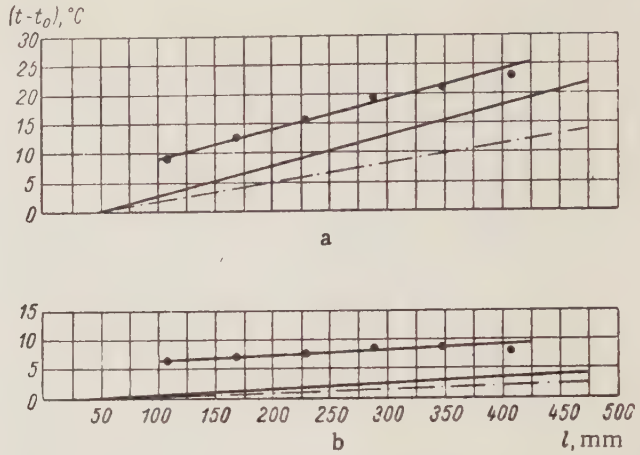

Fig. 5. Temperature distribution over length: a) Mercury, w = 0.67 m/sec; b) water, w = 1.54 m/sec. —·—·—·—·) mean temperature of heat carrier over pile cross section; ———) temperature of heat carrier in central cells, —●—●—●—) mean temperature of tube wall over perimeter.

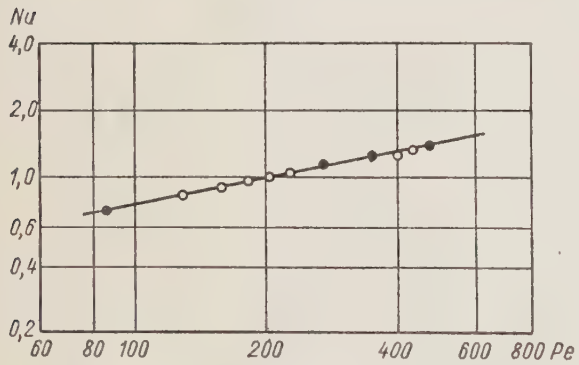

Fig. 6. Experimental dependence Nu = f(Pe) for mercury: O) Tests without rotation of the central tube; ●) tests with rotation of the central tube.

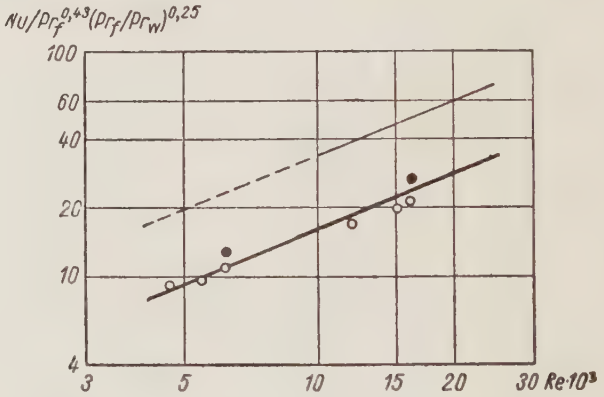

Fig. 7. Experimental data, obtained for water: O) tube I; ●) tube II; – – – –) curve constructed according to Eq. (1).

The rod parameters should satisfy the approximate simulation conditions (8)-(10):

$$C_6' \approx C_6 \approx 10 \quad \text{for} \quad Pr = 0{,}02 - 0{,}03;$$
$$C_6' \approx C_6 \approx 130 \quad \text{for} \quad Pr = 4 - 5$$

(primes indicate natural parameters).

The heat flow distribution over the rod perimeter is described approximately by the relations (15) for values of Pr from 0.02 to 0.03 and (16) for values of Pr from 4 to 5.

The mean temperature of the rod surface over the perimeter is calculated with the help of the relations

$$Nu = f(Pe) \quad \text{and} \quad \frac{Nu}{Pr_f^{0,43}\,(Pr_f/Pr_w)^{0,25}} = f(Re),$$

which are given in Figs. 6 and 7.

Knowing the heat flow distribution $q/\bar{q}$ and mean temperature t_w, it is easy to determine the local temperature of the heat-exchange surface by applying the solution of the heat conductivity problem (6)-(8).

In tightly packed piles,the dead zones in the vicinity of the rod tangent can cause an irregular deposit of oxides and other impurities of the heat carrier on the heat-exchange surface, which leads not only to an increase in the mean temperature of the surface,but also to an increase in temperature nonuniformity over the perimeter of the rod. The results can therefore be extended only to those cases in which allowance is made for the possibility of contamination of the heat exchange surface.

The authors express their gratitude to A. I. Leipunskii for his lively interest in the paper and for valuable comments.

Also taking part in the work were A. A. Sholokhov and V. E. Minashin.

LITERATURE CITED

1. M. A. Mikheev, Coll.: Heat Transfer and Thermal Simulation [in Russian] (Izd-vo AN SSSR, Moscow, 1959) p. 122.
2. A. Colburn, Trans. Amer. Inst. Chem. Engrs. 29, 174 (1933).
3. M. A. Mikheev and A. S. Sinel'nikov, Transactions of the Scientific Research Institutes. Collection of Papers from the Engineering Physics Department [in Russian] (1931), Vol. 1, No. 433.
4. A. Ya. Inayatov and M. A. Mikheev, Teploénergetika 3, 48 (1957).
5. I. V. Kipriyanov, Collection of Papers from the Central Committee for Heavy Industry: Heat Transfer and Aerodynamics [in Russian] (1952) Book 22.
6. A. N. Shcherban and O. A. Kremnev, Investigation of Heat Transfer Coefficients in Mining Models [in Russian] (Izd-vo AN Ukr SSR, 1951).
7. P. Miller, J. Byrnes, and D. Benforado, J.A.I. Ch. E. No. 2, 226 (1956).
8. J. Weisman, Nucl. Sci. and Engng. 6, No. 1, 78 (1959).
9. R. Brooks and A. Rosenblatt, Mech. Engng, 75, No. 5, 363 (1953).
10. Liquid Metal Heat Exchangers (Sodium and Sodium-Calcium Alloy) (from English, edited by A. E. Sheindlin) [Russian translation] (IL, Moscow, 1958).
11. V. E. Minashin et al., Coll.: Problems of Heat Exchange [in Russian] (Izd-vo AN SSSR, Moscow, 1959) p. 193.
12. M. A. Mikheev, Principles of Heat Transfer [in Russian] (Gosenergoizdat, Moscow-Leningrad, 1956) p. 368.
13. N. A. Nikol'skii et al., Coll.: Problems of Heat Exchange [in Russian] (Izd-vo AN SSSR, Moscow, 1959) p. 39.

THE EFFECT OF A PARTIALLY INSERTED ABSORBING CONTROL ROD ON THE NEUTRON FLUX DENSITY DISTRIBUTION

J. Čermák and L. Trlifaj

Institute of Nuclear Studies, Czechoslovak Academy of Sciences, Prague

Translated from Atomnaya Énergiya, Vol. 9, No. 6, pp. 470-476, December, 1960
Original article submitted March 4, 1960

This paper presents a method of calculating the effectiveness of a partially inserted absorbing, cylindrical control rod in a reactor without a reflector. The method makes it possible to give a comparatively simple estimate of the distortion of the neutron flux density near the control rod. The calculations are made using the one group equation $\Delta\varphi + B^2\varphi = 0$, with special boundary conditions on the surface of the rod. As an example of the use of the method, the values of B^2 and the corresponding flux distributions φ have been calculated for several positions of the rod in the reactor.

The effect of a control rod is determined by the amount of reactivity which it counteracts, and depends not only on the control rod properties, but on its position in the reactor.

To get the basic ideas, it is sufficient to look at the simple diagram, shown in Fig. 1.

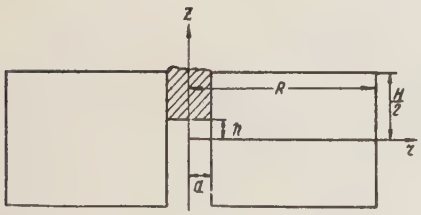

Fig. 1. Longitudinal section of reactor.

In a cylindrical homogeneous reactor of height H and radius R, there is a cylindrical cavity of radius a in which a control rod of the same radius moves. The control rod is inserted to a depth h ($-H/2 \leq h \leq H/2$). The rest of the region, which is not occupied by the control rod, may be empty, or filled with the same material as occurs in the homogeneous reactor.

The simplest physical picture of such a reactor configuration is obtained from the one group approximation. The neutron flux density, $\varphi = \varphi(r, z)$, and the value of the geometric buckling B^2, are given by the equation

$$\Delta\varphi + B^2\varphi = 0, \tag{1}$$

while the conditions at the external extrapolated boundary are

$$\varphi(R,\ z) = \varphi\left(r,\ \pm\frac{H}{2}\right) = 0, \tag{2}$$

and on the surface of the cavity (r = a), the condition holds that

$$\frac{\partial\varphi}{\partial n} = K\varphi, \tag{3}$$

The values of R and H/2 are the extrapolated values of these quantities. The derivative on the left side of equation (3) is taken along the external normal. The quantity K is a linear operator which depends upon what is inside the cavity (r = a). This cavity may be empty, filled with an absorber such as a control rod, or filled with the same material as the rest of the reactor.

It is difficult to give an exact picture of the operator K, since in any practical case some simple approximate value has to be resorted to. Equation (3) holds at the boundary between two media. For an infinite cylindrical cavity,

or a completely absorbing control rod in an infinite medium, Eq. (3) can be expressed by the extrapolation length λ, which depends on the radius of the control rod, and has a different value, depending upon whether we are dealing with an absorbing control rod or a cavity. There are different approximate formulas [1] for calculating λ. One way is to consider that the cavity is surrounded by a completely absorbing wall. Then Eq. (3) can be written in the form

$$\frac{\partial \varphi}{\partial n} = K\varphi = -\frac{1}{\lambda}\varphi. \tag{4}$$

If the cavity were filled with the same material as the reactor, then we would write (for $R \gg a$),

$$K\varphi = \frac{1}{2}\left(\frac{2{,}405}{R}\right)a\varphi. \tag{4a}$$

When part of the cavity is filled by an absorbing control rod (inserted to depth h) and the other part of the cavity is empty, the approximate expression of Eq. (4) may be used for K. Then

$$K\varphi = \begin{cases} -\delta\varphi & \text{for } -\frac{H}{2} \leqslant z \leqslant h; \\ -\gamma\varphi & \text{for } h < z \leqslant \frac{H}{2}; \end{cases} \tag{5}$$

where δ and γ are the reciprocals of the extrapolation lengths for the cavity and the absorbing control rod, respectively. If the empty cavity were filled with the same material as the reactor, then instead of the constant δ, we would use the constant from Eq. (4a). The function $K\varphi$ must be continuous at the boundary between regions in which we can, with sufficient accuracy, use the asymptotic relation (4). However, it is to be expected that the error will not be too great if the asymptotic expression (4) is also used in the transition regions in the vicinity of the point z = h. It should be emphasized that discontinuous boundary conditions of this sort are used, for example, in the theory of heat conduction.

From the solution of Eq. (1), with the boundary conditions (2) and (3), it is necessary to determine the minimum eigenvalue of B^2 corresponding with the neutron flux density distribution $\varphi(r, z)$. Expand the function $\varphi(r, z)$ in the interval $-H/2 \leq z \leq H/2$ in Fourier's series

$$\varphi(r,\ z) = \sum_{k=1}^{\infty} \varphi_k(r)\, g_k(z) \tag{6}$$

of the complete orthogonal system of functions

$$g_k(z) = \begin{cases} \cos \alpha_k z & \text{for } k \text{ odd}; \\ \sin \alpha_k z & \text{for } k \text{ even} \end{cases} \qquad \left(\alpha_k = \frac{k\pi}{H}\right). \tag{7}$$

The cylindrical functions are determined by the following equation

$$Z_k(r,\ B^2) = J_0\left(\sqrt{B^2 - \alpha_k^2}\, r\right) Y_0\left(\sqrt{B^2 - \alpha_k^2}\, R\right) - Y_0\left(\sqrt{B^2 - \alpha_k^2}\, r\right) J_0\left(\sqrt{B^2 - \alpha_k^2}\, R\right),$$

setting

$$\varphi_k(r) = \varphi_k \frac{Z_k(r,\ B^2)}{Z_k(a,\ B^2)},$$

where $\varphi_k = \varphi_k(a)$ represents the as yet unknown constant coefficients for values of k = 1, 2, ... Then for a given value of B^2 and given values of the coefficients φ_k, the function (6) will satisfy conditions (2).

It remains to satisfy condition (3), which is an operational equation in the space of the function $\varphi(a, z)$ determined on the surface of the region. If we represent the operator K on the basis of Eq. (7), then condition (3) will be equivalent to the system of linear equations

$$-\frac{H}{2}\frac{Z_k'(a,\ B^2)}{Z_k(a,\ B^2)}\varphi_k = \sum_{l=1}^{\infty} K_{kl}\varphi_l \quad (k = 1, 2, \ldots), \tag{8}$$

where $Z_k'(a, B^2) = \frac{\partial}{\partial r} Z_k(r, B^2)|_{r=a}$, and K_{kl} are matrix elements of the operator K as determined by (7).

Thus the problem is reduced to the solution of the infinite system of equations (8), which determines the eigenvalue B^2 and the corresponding eigenvector φ_k.

We now use the approximate expression for the operator K as given in equation (5). For the elements of K, we obtain the following expression

$$-K_{kl} = \delta \int_{-\frac{H}{2}}^{h} dz g_k(z) g_l(z) + \gamma \int_{h}^{\frac{H}{2}} dz g_k(z) g_l(z). \tag{9}$$

The minimum eigenvalue of B^2 according to Eqs. (8) and (9) is determined from the equations

$$Z_1'(a, B^2) = \gamma Z_1(a, B^2) \qquad \left(h = -\frac{H}{2}\right) \tag{10}$$

and

$$Z_1'(a, B^2) = \delta Z_1(a, B^2) \qquad \left(h = \frac{H}{2}\right). \tag{11}$$

Equation (10) holds in case of a completely inserted absorbing control rod, and Eq. (11) holds for an empty region. The flux density distribution in both cases is given exactly to an arbitrary constant multiplier, by the function $Z_1(r, B^2) \cos \alpha_1 Z$.

The determination of the eigenvalue and the corresponding eigenvector from the infinite system of equations (8) is almost as difficult as the solution of the original problem. In practical cases, however, the following method of solution is possible. Set $\varphi_k = 0$ for $k > N$, and replace Eq. (8) by the finite system of homogeneous equations

$$\frac{H}{2} \frac{Z_k'}{Z_k} \varphi_k = \sum_{l=1}^{N} K_{kl} \varphi_l \qquad (k = 1, 2, \ldots, N). \tag{12}$$

This finite system determines an approximate value of B^2 and the corresponding values of the Fourier coefficients φ_k (where $1 \leq k \leq N$), from which Eq. (6) gives the approximate distribution of the neutron flux density.

The problem is considerably simplified by the fact that the value of B^2 lies somewhere within the interval $B^2_{min} < B^2 < B^2_{max}$, the end points of which are determined by Eqs. (10) and (11).

TABLE 1

Geometric Buckling B^2 and Eigenvector φ_K for a Control Rod Inserted to Half Depth (h = 0)

N	$B^2 \cdot 10^3$	φ_1	φ_2	φ_3	φ_4	φ_5	φ_6	φ_7	φ_8	φ_9	φ_{10}	φ_{11}
4	0,2078	1	—0,865	—0,308	—0,0933	—	—	—	—	—	—	—
5	0,2061	1	—0,844	—0,216	—0,231	—0,184	—	—	—	—	—	—
6	0,2061	1	—0,838	—0,209	—0,224	—0,160	—0,0374	—	—	—	—	—
7	0,2054	1	—0,824	—0,173	—0,242	—0,121	—0,120	—0,118	—	—	—	—
8	0,2054	1	—0,822	—0,171	—0,240	—0,118	—0,117	—0,105	—0,0209	—	—	—
9	0,2049	1	—0,814	—0,152	—0,245	—0,0996	—0,132	—0,0835	—0,0767	—0,0851	—	—
10	0,2049	1	—0,812	—0,151	—0,245	—0,0983	—0,131	—0,0813	—0,0747	—0,0771	—0,0139	—
11	0,2047	1	—0,806	—0,139	—0,247	—0,0876	—0,137	—0,0700	—0,0866	—0,0628	—0,0547	0,0656

The solution of a finite number of equations has been carried out for a reactor of radius R = 215 cm and height 415 cm with a cavity of radius a = 2.5 cm and the reciprocal extrapolation lengths $\delta = 1.726 \cdot 10^{-4}$ cm^{-1}, $\gamma = 1.1629$ cm^{-1} for three values of h; namely, h = H/4, h = 0, and h = -H/4, i.e., with the control rod inserted one quarter,

one half, and three quarters of the length of the active zone. For a reactor without reflector, having these same dimensions, the buckling is

$$B^2 = \left(\frac{\pi}{H}\right)^2 + \left(\frac{2{,}405}{R}\right)^2 = 0{,}1824 \cdot 10^{-3} \text{ cm.}$$

Since the radius of the cavity, a, is small, and the value of δ is very near zero, the value of B^2 from Eq. (10) is practically equal to the value of B^2 for a bare reactor without a cavity; i.e., $B^2_{min} \simeq 0.1824 \cdot 10^{-3}$ cm^{-2}. The value of B^2_{max} from Eq. (11), corresponding to a completely inserted control rod is $0.2244 \cdot 10^{-3}$ cm^{-2}.

Now it can be shown that of the functions $Z'_k(a, B^2)/Z_k(a, B^2)$, only the first (k = 1) depends upon B^2 in an essential fashion, and the rest are almost independent. Consequently, if in formula (12) we leave out the first equation, and solve the system of the remaining N-1 equations by any numerical method for any value of B^2 in the interval $B^2(B^2_{min} < B^2 < B^2_{max})$ and $\varphi_1 = 1$, we will get an approximate value of the eigenvector φ_k of the finite system (12). After substituting the φ_k into the equations of the system, we can calculate the corresponding eigenvalue of B^2, starting from which the values of φ_k and B^2 can be improved by further iteraction of the solution. For calculations of this sort it is convenient to have a table prepared ahead of time for the ratio $Z'_k(a, B^2)/Z_k(a, B^2)$ as a function of B^2 in the interval $[B^2_{min}, B^2_{max}]$.

Table 1 gives the values of B^2 and the corresponding eigenvectors obtained by the solution of a finite number of equations for the case h = 0. It is clear from the values given that with this method of calculation, B^2 converges fairly rapidly with increasing N. The flux density distribution $\varphi(a, z)$ on the surface of the cavity is given for four values of N in Fig. 2 a and b. The calculational results for control rods inserted one quarter and three quarters of the depth (h = ± H/4) are given in Tables 2 and 3. The curves of the flux density distribution $\varphi(a, z)$ on the surface of

TABLE 2

Geometric Buckling B^2 and Eigenvector φ_K for a Control Rod Inserted to One Fourth Depth (h = H/4)

N	$B^2 \cdot 10^3$	φ_1	φ_2	φ_3	φ_4	φ_5	φ_6	φ_7	φ_8	φ_9	φ_{10}
4	0,1889	1	—0,278	0,180	0,0395	—	—	—	—	—	—
6	0,1881	1	—0,249	0,184	0,0869	0,0127	0,0775	—	—	—	—
8	0,1871	1	—0,198	0,218	0,0793	—0,0108	0,0274	—0,114	0,0126	—	—
10	0,1868	1	—0,187	0,218	0,0842	—0,0200	0,0221	—0,121	—0,0117	—0,0176	—0,0378

TABLE 3

Gometric Buckling B^2 and Eigenvector φ_K for a Control Rod Inserted to Three Fourths Depth (h = -H/4)

N	$B^2 \cdot 10^3$	φ_1	φ_2	φ_3	φ_4	φ_5	φ_6	φ_7	φ_8	φ_9	φ_{10}
4	0,2231	1	—0,430	—0,465	0,380	—	—	—	—	—	—
6	0,2224	1	—0,639	—0,722	0,642	0,448	—0,220	—	—	—	—
8	0,2222	1	—0,661	—0,758	0,677	0,483	—0,251	—0,0983	—0,0538	—	—
10	0,2221	1	—0,687	—0,769	0,670	0,443	—0,179	—0,00443	—0,155	—0,165	0,105

the cavity for these conditions are given in Figures 3 and 4. It is clear from the curves that the distortion of the neutron flux along the z axis can be quite large as compared with the original cosine distribution on the surface of the control rod.

Since the function $Z_k(r, B^2)/Z_k(a, B^2)$ rapidly approaches zero with increasing r for k > 1, and the more rapidly the greater the value of k, the higher harmonic terms in series (6) diminish relatively quickly. At a certain distance from the cavity, the distribution along the height is practically determined by the first harmonic, the cosine. This condition is illustrated in Fig. 5 (h = 0, N = 4).

Figure 6 shows the geometric buckling B^2 as a function of the depth of insertion of the control rod, hr.

The present method makes it relatively simple to determine the effectiveness of an absorbing cylindrical control rod in a reactor without reflector as a function of the depth of insertion. In the process of calculation, the approximate flux density distribution near the control rod is calculated simultaneously along with the effectiveness.

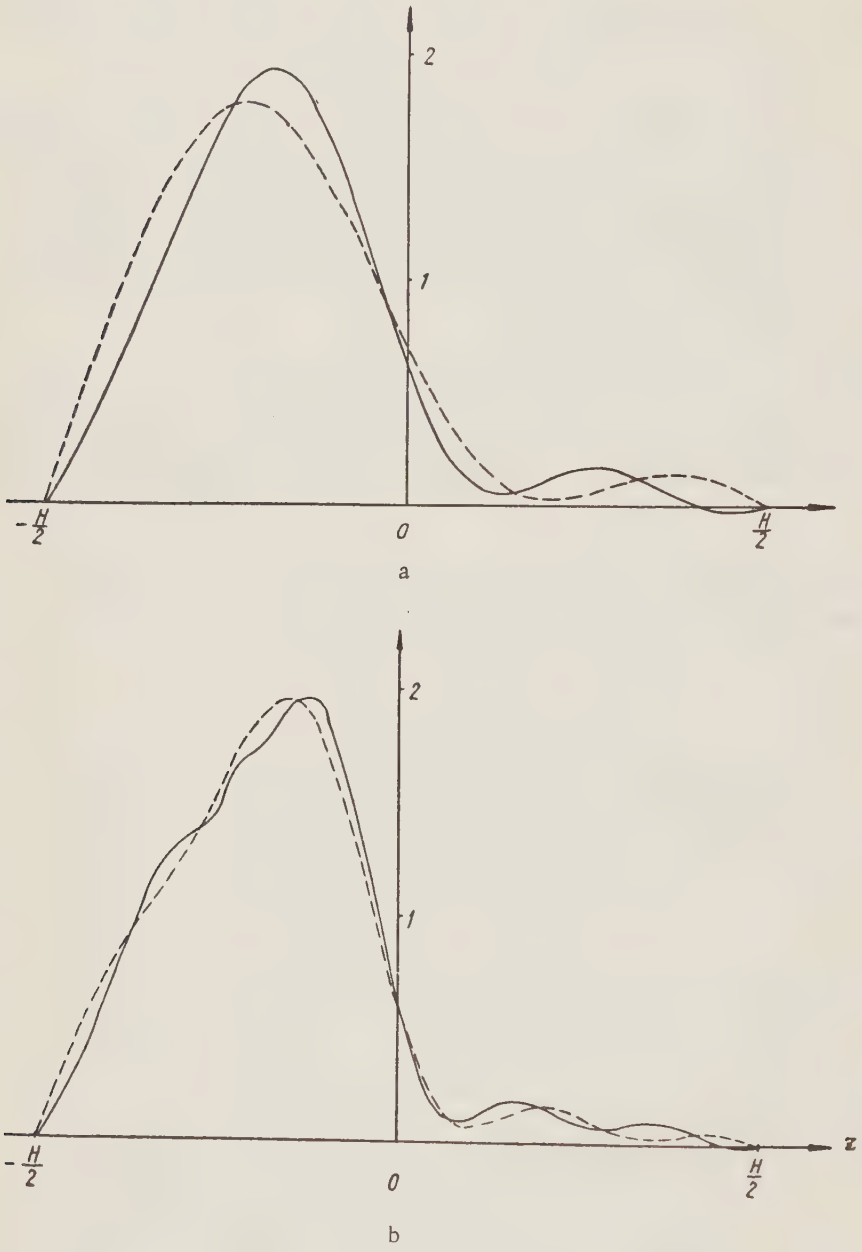

Fig. 2. Flux density distribution on the surface of the cavity (h = 0): a) ——— N = 6; — — — — N = 4; b) ——— N = 10, — — — — N = 8.

The one group approximation is used in this paper. A generalization of the method to the two group case would not present any fundamental difficulties, but one would have to contend with the difficulties which are peculiar to the two group approximation, such as determining the proper boundary conditions for the fact neutron group at the control rod surface.

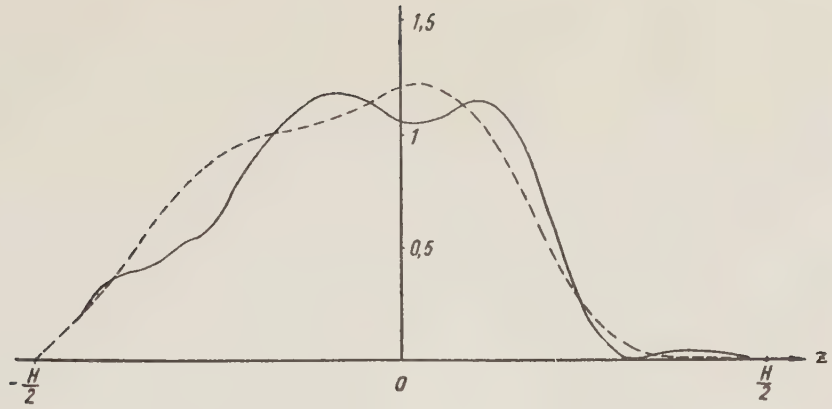

Fig. 3. Flux density distribution on the surface of the cavity (h = H/4): ——————) N = 10; — — — — —) N = 6.

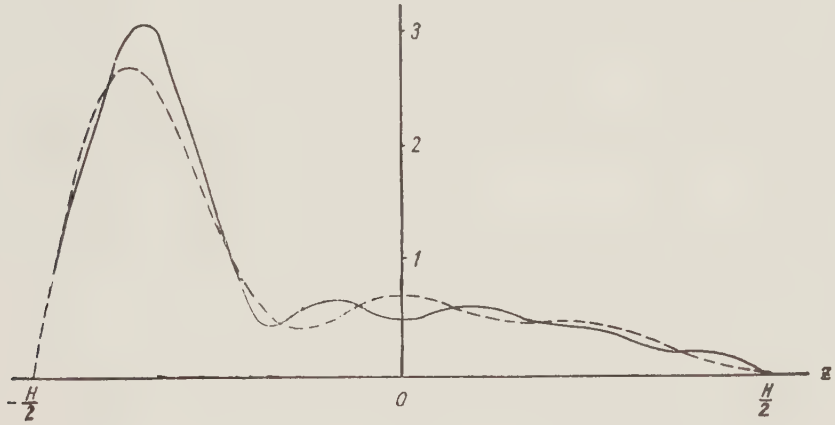

Fig. 4. Flux density distribution on the surface of the cavity (h = -H/4): ——————) N = 10; — — — — —) N = 6.

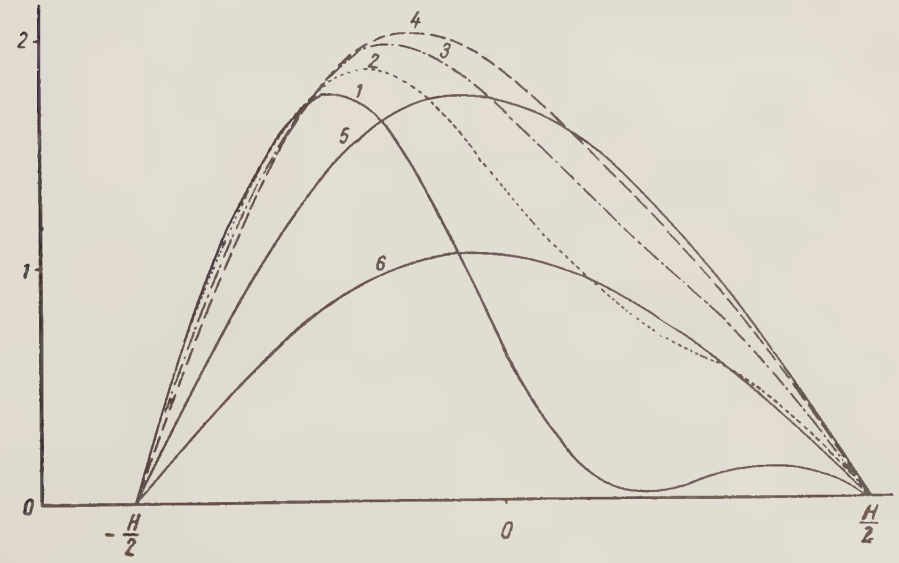

Fig. 5. Flux density distribution at different distances from the cavity, with the control rod inserted to half depth (h = 0). Distance from the cavity (in centimeters): 1) 2.5; 2) 10; 3) 20; 4) 30; 5) 100; 6) 150.

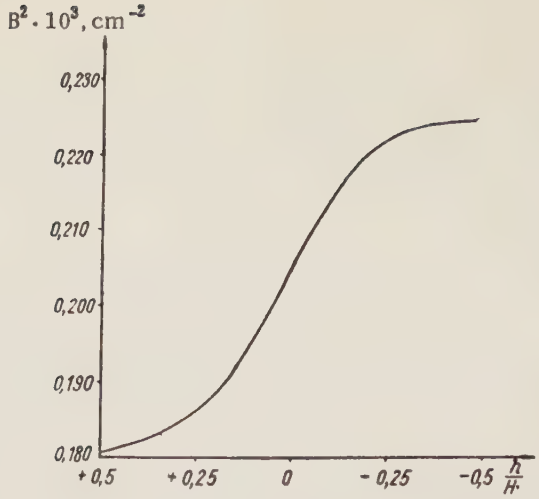

Fig. 6. Geometric buckling as a function of depth of insertion of control rod.

The results of the calculation of control rod effectiveness, which we have arrived at in the present paper, are to be compared with the calculations given in reference [2]. Although these results do not lend themselves to direct comparison, the curve shown in Fig. 6 is in complete qualitative agreement with the curves of reference [2].

We wish to thank R. Zezula, I. Svatosh, and M. Prazhskaya for carrying out the numerical calculations. Particularly great initiative was shown by R. Zezula, who also calculated the tables of the function $Z_k'(a, B^2)/Z_k(a, B^2)$ on the electronic BÉSM setup in the Calculational Center of the Academy of Sciences of the USSR.

LITERATURE CITED

1. B. Davison, Proc. Phys. Soc. 64A, 881 (1951).
2. Reactor Physics Constants, ANL-5800, 1958, p. 189.

INVESTIGATION OF THE ISOTOPIC COMPOSITION OF URANIUM IN RARE-EARTH MINERALS

Yu. A. Surkov, A. A. Vorobtev, V. A. Korolev,

and V. D. Vilenskii

Translated from Atomnaya Énergiya, Vol. 9, No. 6, pp. 477-482,
December, 1960
Original article submitted February 24, 1960

The isotopic composition of the uranium of rare-earth minerals (orthite, xenotime, and gadolinite) was investigated for the detection of possible traces of Cm^{247} in nature, by means of an ionization chamber with a multichannel analyzer of the pulse amplitudes. The results of the measurements are discussed. A method is given for the accurate calculation of distortions of the spectrum of α particles in ionization chambers with electron collimation. It is shown that during the investigation of samples of low intensity (0.2-1 mg of uranium), the relative content of U^{235}/U^{238} isotopes can be measured by an α-spectrometric method with an error up to ~ 1%.

Introduction

An investigation of Cm^{247} obtained in a reactor by irradiation of plutonium [1] made it possible to determine the lower limit of the half life of α decay, equal to $4 \cdot 10^7$ years. The absence in Cm^{247} of types of decay, other than spontaneous fission ($T_f > 6 \cdot 10^8$ years), indicates that it may exist in nature. The discovery of the highly anomalous content of U^{235} in magnetite by the authors of [2] is also in favor of this.

In its geochemical properties, curium is an analog of the rare-earth elements and, if it does exist in nature, would most probably be found in ancient rare-earth minerals.

A rough assessment of the amount of Cm^{247} which can exist in nature at the moment of formation of minerals indicates that its direct determination in rare-earth minerals is only possible if its half life is not less than $\sim 2 \cdot 10^8$ years. But if Cm^{247} existed in nature and decayed during geological time, then, being converted to U^{235} by the following degradation

$$Cm^{247} \xrightarrow{\alpha} Pu^{243} \underset{5\,hr}{\xrightarrow{\beta^-}} Am^{243} \xrightarrow[8600\ yr]{\alpha} Np^{239} \xrightarrow[2,3\ day]{\beta^-} Pu^{239} \xrightarrow[24\,400\ yr]{\alpha} U^{235} \xrightarrow[7,1\cdot 10^8\ yr]{\alpha},$$

it must have changed the isotopic composition of uranium (U^{235}/U^{238} ratio), the change being particularly appreciable in the case of rare-earth minerals having a slight uranium content.

In the present work an investigation was made of the isotopic composition of uranium in ancient rare-earth minerals, xenotime, orthite, and gadolinite, the age of which is ~ 2 billion years, i.e., about the same as the geologic age of the earth. Samples of these minerals were obtained from the Mineralogical Museum, Academy of Sciences of the USSR. The uranium content in xenotime, orthite, and gadolinite was 0.8, 0.1, and 0.06%, respectively.

Radiochemical Separation of Uranium from Minerals

For the α-spectrometric investigation, uranium was separated from the minerals by the following method. After the acid decomposition of the investigated minerals (HCl for orthite and gadolinite, and H_2SO_4 for xenotime), the solutions obtained were evaporated to dryness, nitric acid being added. Nitric acid and magnesium nitrate were then added to the residue until the concentration was 0.5 N and 2.5 M, respectively (a small amount of iron nitrate was also added to the solution obtained from xenotime, to combine the phosphate and sulfate ions). The uranium was then extracted with three equal amounts of ether. The ethereal layer was separated and evaporated to dryness in the presence of dilute hydrochloric acid. The residue was dissolved in 8N hydrochloric acid. After traces of iron had been removed by extraction with amyl acetate, the hydrochloric acid solution was passed through a chromatographic

column filled with Dowex-1 anionite; the latter was washed with 8N hydrochloric acid, while the uranium was eluted with 0.5 N hydrochloric acid. The solution obtained was evaporated to dryness and chromatographic purification was repeated. The purified uranium was precipitated electrolytically on stainless steel discs (diameter 70 mm) by a method described in detail in [3]. The hydrochloric acid solution of uranium was evaporated almost to dryness, and the residue was dissolved in a 1% solution of ammonium oxalate. This solution was then acidified with 6N nitric acid. Electrolysis was carried out at a temperature of 80°C and a cathode current density of 100-150 ma/cm^2. During electrolysis, several drops of 6N nitric acid were added periodically to the solution. After 15 min the solution was made alkaline with several drops of 6N ammonia, and electrolysis was continued an additional 10 min. The solution was mixed during the whole period of electrolysis. Under these conditions, uranium was 80-90% precipitated.

The preparations obtained by this method were perfectly suitable for α-spectrometric measurements.

Measurement Method

The relative content of U^{235} and U^{238} isotopes in the minerals was determined by the α activity of these isotopes. Since the amount of uranium in the samples investigated was small (0.25-1 mg), an apparatus with maximum possible illuminating power – a pulse-counting ion chamber with a grid – was used. Figure 1 (dashed curve) shows the α spectrum of the uranium isotopes, obtained in such a chamber. But the U^{235} content cannot be determined exactly by means of this method because of the considerable "tail" from the U^{234}. This tail is due to the absorption in the layer of the source of part of the energy of the α particles escaping parallel to the electrodes. The quality of the spectrum can be improved by using a mechanical collimator. In the first place, however, existing collimators do not allow sufficient improvement of the quality of the spectrum and, secondly, markedly reduce the counting rate. The use of electron collimation gives much better results. Various methods of introducing electron collimation are described in [4-6]. They are all based on the use of the relation between the pulse height at the high-voltage electrode and the angle of emergence of the α particle (height method of collimation) or the time lag of the pulse at the collecting electrode with respect to the pulse at the high-voltage electrode (time method of collimation). Use of both methods gives a substantial improvement in the quality of the spectrum with a relatively small decrease in the counting rate. In Fig. 1 the spectrum obtained by means of time collimation is represented by the solid curve. The counting rate here was 100% less. From a comparison of the spectra, it is evident that as a result of the use of collimation the quality of the spectrum is considerably improved, but that during this process the relative intensity of the lines is distorted, which is a shortcoming of electron collimation. It is found, however, that this distortion can be taken into account with high accuracy. To calculate the corresponding correction, we will examine in greater detail the time method of collimation, used in the present work.

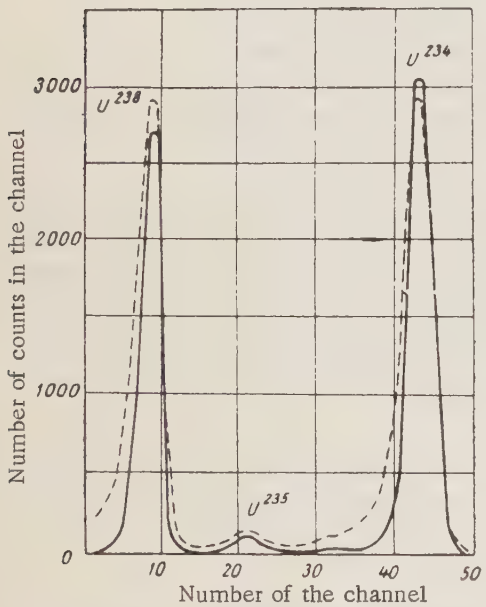

Fig. 1. Alpha spectrum of a natural mixture of uranium isotopes, obtained during measurements with (solid curve) and without (dotted curve) collimation.

Figure 2 shows the diagrammatic layout of the ionization chamber. The α-particle source is located on the high-voltage electrode. The emitted α particle ionizes the gas with which the chamber is filled (A + 0.5% CH_4). Under the effect of the applied electric field the electrons begin to move toward the grid, which leads to the immediate appearance of a pulse at the high-voltage electrode, irrespective of the direction of escape of the α particles. A pulse appears at the collecting electrode only after the electrons nearest the grid have reached the latter. The time lag t_{lag} is evidently independent of the orientation of the track and can be expressed by the formula

$$t_{lag} = \frac{d - R\cos\varphi}{w}, \qquad (1)$$

where R is the α-particle path, w is the rate of drift of the electrons; d is the distance between the high-voltage electrode and the grid; φ is the angle between the direction of emergence of the α particle and the perpendicular to the surface of the electrodes.

It can be shown that the distribution of the number of pulses with respect to the time lag must be uniform (with isotopic distribution of the α particles), as is shown in Fig. 3 for two groups of α particles of different energies. The α particles emerging perpendicularly to the surface of the electrodes correspond to pulses with minimum lag.

The method of time collimation is based on the fact that only those pulses for which t_{lag} is less than a certain value of t' are recorded. The pulses from α particles emerging at low angles are not recorded. The degree of collimation can be varied at will by varying the value t'.

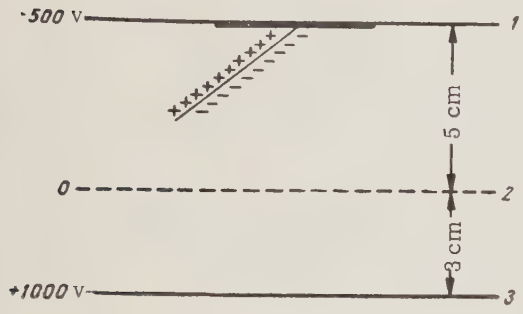

Fig. 2. Diagrammatic layout of the ionization chamber: 1) high-voltage electrode; 2) grid; 3) collecting electrode.

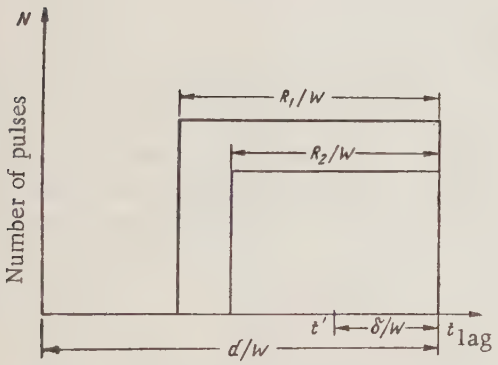

Fig. 3. Distribution (theoretical) of pulses with respect to time lag for two groups of α particles of different energies and intensities.

Let us determine the variation of the ratio of the line strength as a result of the introduction of collimation. The degree of collimation can be conveniently characterized by the value f, determined from the ratio

$$\frac{f}{w} = t_{max} - t'. \tag{2}$$

Hence, it is evident that the proportion ρ of recorded pulses of α particles of a given line is determined by the relationship

$$\rho = \frac{N}{N_0} = 1 - \frac{f}{R}, \tag{3}$$

where N_0 is the line strength before the introduction of collimation; N is the strength of the same line after the introduction of collimation.

From equation (3) it is seen that the variation of the line strength depends on the path (and, therefore, on the energy) of the α particles.

Let there be two lines with strengths N_1^0 and N_2^0. In the experiment with collimation, the ratio $Q = N_1/N_2$ is measured, but it is necessary to measure the value $Q^0 = N_1^0/N_2^0$.

Employing equation (3) we obtain

$$Q^0 = \frac{N_1^0}{N_2^0} = \frac{N_1}{N_2}\frac{1-\frac{f}{R_2}}{1-\frac{f}{R_1}} = Q\frac{1-\frac{f}{R_2}}{1-\frac{f}{R_1}} = QA, \tag{4}$$

where A is the correction factor.

If the degree of collimation (i.e., the value f) is known, the true ratio of the line strengths Q^0 with respect to the observed Q can be found by means of equation (4). In consequence, the whole problem amounts to the accuracy with which the degree of collimation can be determined.

During the investigation of the isotopic composition of uranium ores, the following method of determining the correction factor was found to be simple and reliable. In the given case there are three lines in the spectrum, two of these (U^{234} and U^{238}) being fairly strong, and therefore suitable for measurements. Subsequently, all the values relating to U^{234}, U^{235}, and U^{238} were given the indices 234, 235, and 238, respectively, and, in addition, the following symbols were used for the ratio of the line strengths:

$$Q_{234}^0 = \frac{N_{238}^0}{N_{234}^0}, \quad Q_{234} = \frac{N_{238}}{N_{234}}, \quad Q_{235}^0 = \frac{N_{238}}{N_{235}^0}, \quad Q_{235} = \frac{N_{238}}{N_{235}}.$$

For the investigated ratio of the line strengths of U^{238} and U^{235}, equation (4) is converted as follows:

$$Q_{235}^0 = Q_{235}A_{235} = Q_{235}\frac{Q_{235}}{Q_{238}} = Q_{235}\left(1 + \frac{Q_{235}-Q_{238}}{Q_{238}}\right) = Q_{235}(1+P_{235}), \tag{5}$$

where

$$P_{235} = \frac{Q_{235} - Q_{238}}{Q_{238}} = \frac{f}{1 - \frac{f}{R_{238}}} \left(\frac{1}{R_{238}} - \frac{1}{R_{235}} \right). \tag{5a}$$

Similarly, for the U^{234} and U^{238} lines we have

$$Q^0_{234} = Q_{234} A_{234} = Q_{234} (1 + P_{234}), \tag{6}$$

where

$$P_{234} = \frac{f}{1 - \frac{f}{R_{238}}} \left(\frac{1}{R_{238}} - \frac{1}{R_{234}} \right). \tag{6a}$$

The values of Q^0_{234} and Q_{234} are determined by experiment, which makes it possible to determine A_{234} and, therefore, P_{234}. Further, by employing equations (5a) and (6a),it is easy to establish the relation between the P_{235} and P_{234}:

$$P_{235} = \frac{\frac{1}{R_{238}} - \frac{1}{R_{235}}}{\frac{1}{R_{238}} - \frac{1}{R_{234}}} P_{234} = \frac{R_{235} - R_{238}}{R_{234} - R_{238}} \frac{R_{234}}{R_{235}} P_{234} = bP_{234}, \tag{7}$$

where

$$b = \frac{R_{235} - R_{238}}{R_{234} - R_{238}} \frac{R_{234}}{R_{235}}, \tag{8}$$

Since the paths are only present in equation (8) in the form of ratios, the coefficient is determined only by the energy of the α particles, and is independent of such values as pressure, temperature, etc. During the determination of the numerical value of the coefficient,the differences of the paths can be replaced by the difference of the energies. The ratio R_{234}/R_{235}, determined by the path – energy curve [7], is equal to 1.135. The following values are adopted for the energies of the α particles: E_{238} = 4.195 Mev, E_{234} = 4.767 Mev, E_{235} = 4.390 Mev. Substituting these values in equation (8), we obtain b = 0.39.

TABLE 1

Results of Measurements without Collimation

Sample	Amount of uranium, mg	Measurement time , hours	N^0_{234}	N^0_{238}	Q^0_{234}
Standard, urnayl nitrate	1,50	4,0	118 200	118 750	1,005
No. 1, orthite.	0,65	4,5	42 280	41 800	0,989
No. 2, xenotime	0,42	8,0	47 030	47 510	1,010
No. 3, gadolinite.	0,18	14,0	40 150	37 800	0,941

Instead of the ratios of the energy differences, the ratio of the distances between the lines in the spectrum in Fig. 1 may be used. The same value is obtained for the coefficient b in this case.

By means of equations (6) and (7) we determine the correction factor for A_{235}:

$$A_{235} = (1 + bP_{234}) = [1 + b(A_{234} - 1)] = [1 + 0{,}39(A_{234} - 1)]. \tag{9}$$

Thus,for the investigated ratio Q^0_{235} we obtain the final equation

$$Q^0_{235} = Q_{235} [1 + 0{,}39(A_{234} - 1)]. \tag{10}$$

It can easily be shown that the relative error δA_{235} is related to δb by the following equation:

$$\delta A_{235} = \frac{\delta b\,[b\,(A_{234}-1)] + \delta A_{234} A_{234} b}{1 + b\,(A_{234}-1)}. \qquad (11)$$

For the degree of collimation, $A_{234} \approx 1.20$, actually employed,

$$\delta A_{235} \approx 0{,}1\delta b + 0{,}5\delta A_{234}.$$

The coefficient b is determined with an accuracy up to 5%. This means that the part of the error δA_{235}, due to the inaccuracy of the determination of b, does not exceed 0.5%. It may be noted that this error is systematic and occurs only during absolute measurements. In the case where the source investigated is compared with the standard and they are both investigated under approximately equal collimation, this error is still further reduced and may be neglected. Hence,

$$\delta A_{235} \approx 05\delta A_{234}.$$

The value of δA_{234}, determined only by statistics, can amount to a fairly small value (0.5-1%), depending on the accuracy required.

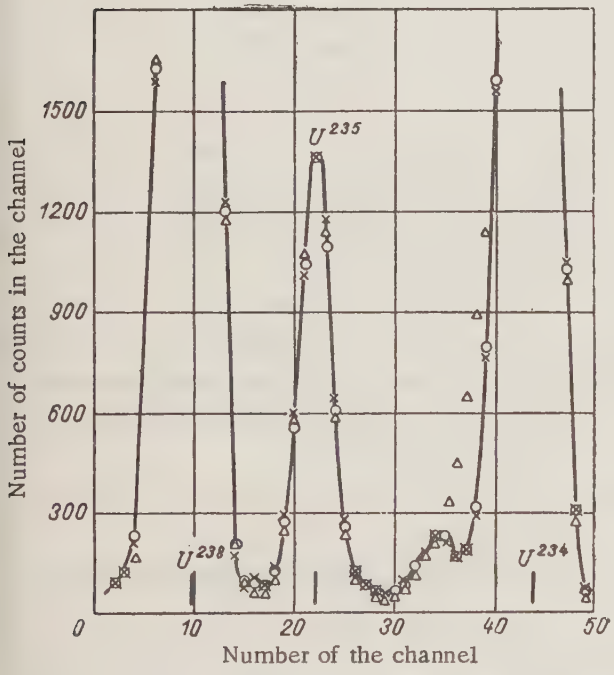

Fig. 4. Alpha spectrum of the investigated samples of uranium: ——) standard sample; (×) sample No. 1; ○) sample No. 2; △) sample No. 3.

From the above it follows that to determine the correction factor A_{235}, it is sufficient to know the ratio of the line intensities of U^{235} and U^{238} before and after the introduction of collimation; i.e., the values Q^0_{234} and Q_{234}.

To determine the value of the ratio Q_{234}, it is necessary to carry out a further experiment; it is obtained directly from the experiment with collimation for the determination of the U^{235} content. Only the experiment without collimation for the determination of the value of the ratio Q^0_{234} is an additional experiment, the time spent on this being roughly five times more than for the principal measurement. The fact that the correction factor A_{235} is determined directly from the principal experiment is all the more useful because, in this way, possible variations in the degree of collimation during the measurement period are unimportant.

Thus, the alteration in the ratio of the line intensities, caused by the introduction of electron collimation, may easily be allowed for by an error not exceeding 0.2-0.5%.

Results of the Measurements

To check the method and the agreement of the measurement results, the U^{235}/U^{238} ratio was determined for uranium samples obtained from commercial uranyl nitrate and uranium minerals. The measurements showed close agreement of the results. The mean ratio ~ 1/138 was taken as the unit. Subsequently, all measurements were carried out with respect to one sample, taken as the standard. The value $q = Q^0_{235\,\text{standard}}/Q^0_{235\,\text{sample}}$ was determined.

The value of q was determined as follows. The ratio Q^0_{234} was first obtained. To increase accuracy, this measurement was carried out with a mechanical collimator with a low degree of collimation (aluminum disc, 2 mm thick, with an orifice of diameter 4 mm). The main measurement was then carried out with electron collimation. The degree of collimation was established in such a way that the counting rate was reduced by roughly 100%. The ratios Q_{234} and Q_{235} were determined from this experiment; then Q_{235} was calculated by means of equation (10).

The measurement obtained for the background showed that it could be neglected. The low value of the background was obtained because the pulses from the high-voltage and collecting electrodes, coincident in time, were recorded. The results of the measurements and calculations for the standard and the three investigated samples are given in Tables 1 and 2. Figure 4 shows the α spectrum of the investigated uranium samples. The spectra have a common height in the maximum of the U^{235} line. As may be seen from Fig. 4, although the tail of the U^{234} line was markedly reduced as a result of the introduction of collimation, it is nevertheless 2-3% N_{235}. The complete similarity of the investigated spectra (samples No. 1 and 2 and the standard) makes it possible to affirm that, in the present case, this proportion is equivalent to an error of not more than 0.5%. Bearing this in mind, we conclude that the U^{235} content in samples No. 1 and 2 was determined with an error of less than 2%. As regards sample No. 3, the measurement error may be expected to be somewhat impaired by the presence of a small amount (traces) of Th^{230}. But in this case the separation of the uranium isotopes was, to some extent, even better, which is explained by the more careful processing as a result of the deficiency of the mineral of the laminated sample. In this case, too, the measurement error of the U^{235}/U^{238} ratio is, therefore, ~2%.

As may be seen from Table 2, a somewhat higher isotopic U^{235}/U^{238} ratio ($q \approx 1.046 \pm 0.02$) is observed in gadolinite. This indicates that the uranium of the given rare-earth mineral contains an excess of U^{235} and equals ~ 0.03% of the total uranium. As already indicated, a possible explanation of the anomaly discovered in the isotopic composition of uranium may be the existence of curium in nature.

TABLE 2

Results of Measurements with Collimation

Sample	Measurement time, hours	N_{234}	N_{238}	N_{235}	Q_{234}	A_{234}	Q_{235}	Q^0_{235}	q
Standard, uranyl nitrate	30	514 100	408 070	18 124	0,795	1,264	22,55	24,87	1
No. 1, orthite.	20	164 660	138 080	5 864	0,839	1,179	23,55	25,20	0,987
No. 2, xenotime . . .	30	157 880	130 590	5 706	0,827	1,221	22,89	24,86	1
No. 3, gadolinite. . .	70	148 310	117 670	5 310	0,793	1,187	22,16	23,78	1,046

If it is borne in mind that the age of the gadolinite investigated is ~ 2 billion years and the half life of Cm^{247} is $\gtrsim 4 \cdot 10^7$ years, then, neglecting the time required for conversion of all the curium to U^{235}, the amount of curium present in the investigated mineral at the period of its formation can be roughly assessed. The initial content of Cm^{247} in the given sample of gadolinite, with a mean uranium content of 0.06%, is $\gtrsim 10^{-3}$%.

In the near future, we plan to use the new method to improve the accuracy of the data obtained and carry out an investigation of other minerals.

In conclusion, the authors with to express their thanks to A. P. Komar and V. I. Baranov for the interest they have shown in this work.

LITERATURE CITED

1. H. Diamond et al., Phys. Rev. 105, 679 (1957).
2. V. V. Cherdyntsev et al., Geokhimiya 4, 373 (1960).
3. C. Ruffs, A. De, and P. Elving, J. Electrochem. Soc. 104, No. 2 (1957).
4. G. Valladas, These Institute du radium, (Paris, 1955).
5. B. A. Bochagov, A. A. Vorob'ev, and A. P. Komar, Izvestiya Akademii Nauk, SSSR, seriya fiz. 20, 1455 (1956).
6. Yu. I. Filimonov and G. A. Petrov, Izvestiya Akademii Nauk SSSR, seriya fiz. 20, 1434 (1956).
7. E. Segre, Experimental Nuclear Physics. 1 [Russian translation](Moscow, IL, 1955).

METHODS OF DIRECTIONAL DETECTION OF GAMMA RADIATION

V. P. Bovin

Translated from Atomnaya Énergiya, Vol. 9, No. 6, pp. 483-487,
December, 1960
Original article submitted February 22, 1960

An analysis is given of the principal characteristics and parameters of directional radiation detectors. Particular attention is paid to directional scintillation counters of the compensated type, and it is shown that they possess much better parameters than analogous instruments using gas-discharge counters. A description is given of various compensating systems which may be useful in connection with the detection and measurement of radioactive elements.

Directional recording of γ radiation is being increasingly used at the present time. This type of detection is employed whenever it is necessary to determine the position of the source of radiation or to measure the intensity in a given direction in the presence of other interfering radiation [7, 9, 10].

The distinctive features of a directional radiation counter are best shown by a polar diagram which gives for each direction (φ, θ) the ratio of the γ-ray sensitivity $q(\varphi, \theta)$ of the detector to the γ-ray sensitivity in the direction $\varphi = 0$, $\theta = 0$; i.e.,

$$\eta(\varphi, \theta) = \frac{q(\varphi, \theta)}{q(0, \theta)}, \quad (1)$$

where φ and θ are the two angles defining the direction of incidence of the γ rays.

The polar diagram is usually given either in the θ plane or in the φ plane. The angular resolution of such a system is usually described by the angular width of the polar diagram α (Fig. 1),which is defined as the angle between the two directions corresponding to one-half of the maximum sensitivity.

Directional radiation detectors can be used to measure weak signals against a strong background, owing to the improved signal-to-background ratio. In fact, the root-mean-square relative error in the counting rate n_0 in the presence of background $n_b \gg n_0$ is given by

$$\delta_{n_0} = \sqrt{\frac{n_0 + 2n_b/R_\varphi}{n_0^2 T}} \simeq \frac{1}{n_0}\sqrt{\frac{2n_b}{R_\varphi T}}, \quad (2)$$

where T is the time of measurement,and $R\varphi = n_0/n\varphi$ is the directivity.

The directional γ-ray sensitivity characteristics can be obtained in various ways. The main types of radiation detectors which have been used in this connection are special gas-discharge counters with bimetallic and ribbed cathodes and insulating beads on the anode [1, 2], composite radiation detectors incorporating coincidence and anticoincidence circuits [2, 3], radiation detectors with screens and collimators [4, 5], and compensated systems [6, 7, 10].

Special types of gas-discharge counters and composite radiation detectors have a rather low directivity and efficiency, and their characteristics are very dependent on the energy of the radiation. They have,therefore,not been used in practice.

The most widely used directional detectors are those of the screened type,because of their simplicity of construction and high directivity. The thickness of the screen, its form, and the dimensions of the aperture determine the angular resolution of the radiation detector. As a rule, the screens are made of lead and their thickness is sufficient for the virtually complete absorption of radiation incident upon them. Significant disadvantages of screened detectors are their large weight and the dependence of the directivity on the energy of the radiation. Thus, for example, the screen described by Takahashi et al. at the Second International Conference on the Peaceful Uses of Atomic

Energy in Geneva [7], had 4 cm thick walls, an angular resolution of 10°, and a weight of about 160 kg. Even with this screen thickness, radiations with energies in excess of 1 Mev were only partly absorbed.

The effect of unwanted radiation can be completely excluded in directional systems of the compensated type, in which the fraction of the unwanted radiation passing through the screen is compensated with the aid of an additional radiation detector. In this method, signals from both detectors are recorded in separate channels (Fig. 2a) and are fed into a differential counting device. With the radiation incident in a direction φ, the latter device produces the difference signal

$$\Delta n_\varphi = n_{1\varphi} - n_{2\varphi}, \tag{3}$$

where $n_{1\varphi} = mq_{1\varphi}N$, $n_{2\varphi} = mq_{2\varphi}N$; N is the number of γ rays of given energy reaching the radiation detector per unit time and m is a constant. The radiation detector having a large sensitivity in the direction $\varphi = 0$, for which Δn_0 is a maximum, will be referred to as the main detector. A directional sensitivity characteristic can be obtained with the aid of two types of compensating systems. In the first type (Fig. 2b) the main detector is screened, while in the second type (Fig. 2c) the compensating detector is screened. In order to compensate the fraction K of the unwanted radiation passing through the screen and recorded by the main detector, the sensitivity of the compensating detector in the system of the first type (Fig. 2b) should be of the form

$$q_2 = q_1 K. \tag{4}$$

In this case, a parallel beam of γ rays in the principal direction ($\varphi = 0$) gives rise to the difference signal

$$\Delta n_0 = n_{10} - n_{20} = n_{10}(1 - K^2). \tag{5}$$

In systems of the second type (Fig. 2c), the two channels are adjusted to the same sensitivity and hence the difference signal recorded for a parallel beam of γ rays incident along the principal direction is given by

$$\Delta n_0 = n_{10} - n_{20} = n_{10}(1 - K). \tag{6}$$

Comparison of Eq. (5) with Eq. (6) shows that the sensitivity of directional detectors of the first type is higher by a factor of 1 + K. The directional properties of a compensated system can be represented graphically as the difference between the directional characteristics of the main and the compensating detectors.

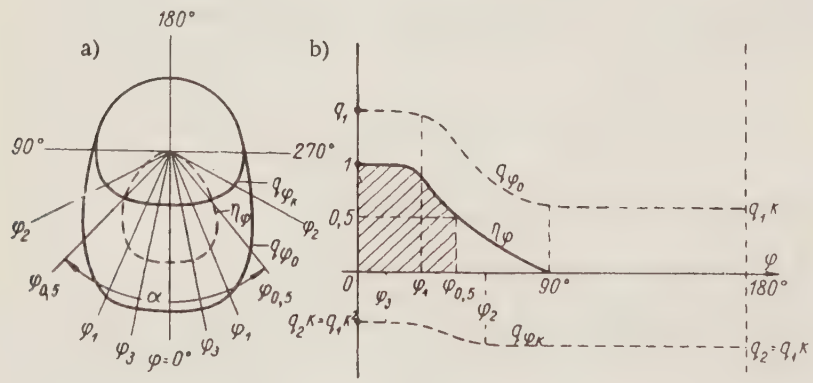

Fig. 1. The directional sensitivity of a compensated system of the first type in polar and Cartesian coordinates.

Figure 1 shows the directional characteristic for the compensated system of the first type (cf. Fig. 2b).

A disadvantage of both types of compensated systems is the increase in the statistical fluctuations at the differential counting unit, which are determined by the total error in both channels:

$$\sigma = \sqrt{\sigma_1^2 + \sigma_2^2}, \tag{7}$$

where σ_1 and σ_2 are the root-mean-square errors in the main and the compensating channels.

Let us consider the characteristics of the two types of compensated systems in an isotropic γ-radiation field. The number of pulses Δn recorded per unit time by the differential counting unit is given by

$$\Delta n = \int_{\Omega} n(\varphi, \theta)\, d\Omega, \tag{8}$$

where $d\Omega = \sin\theta\, d\theta\, d\varphi$ is an elementary solid angle, $n(\varphi, \theta)$ is the number of pulses recorded by the system in the direction (φ, θ) per unit time, and Ω is the solid angle within which $n(\varphi, \theta)$ differs from zero.

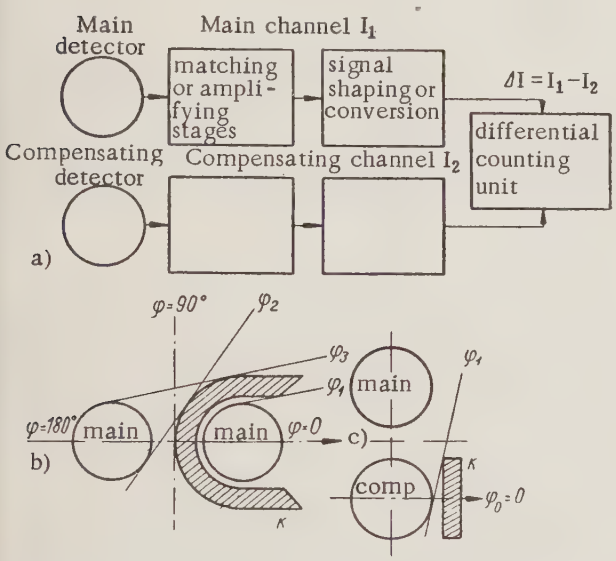

Fig. 2. Functional scheme and the two main types of compensated radiation detectors with directional properties.

The function $n(\varphi, \theta)$ can either be calculated or determined experimentally. When it is unknown, and only the total counting rate Δn and the counting rate Δn_0 for radiation incident in the principal direction only are given, it is convenient to use the effective solid angle Φ. This angle characterizes the directional properties of an equivalent system with a constant sensitivity within this angle and is defined by Δn; i.e.,

$$\Delta n = \Delta n_0 4\pi\Phi, \text{where } \Phi = \frac{\Delta n}{4\pi\Delta n_0} = \\ = \frac{1}{4\pi\Delta n_0}\int_{\Omega} n(\varphi, \theta)\, d\Omega. \tag{9}$$

The polar diagram for this case is in the form of a spherical sector with a radius equal to Δn_0 and a volume numerically equal to Δn.

Using the concept of the effective solid angle in the case of the compensated system of the first type, the number of γ rays recorded in the main channel per second is given by

$$n_1 = n\Phi + nK(1-\Phi),$$

where n is the number of γ rays recorded per second by the main detector with an isotropic sensitivity characteristic.

In the compensating channel, the number of counts per second is given by $n_2 = K[Kn\Phi + n(1-\Phi)]$. The root-mean-square error is then given by

$$\sigma_1 = \sqrt{\frac{n_1}{T} + \frac{n_2}{T}} = \sqrt{\frac{n}{T}[\Phi(1-K)^2 + 2K]}, \tag{10}$$

where T is the time of measurement in seconds.

The differential counting unit will record $\Delta n = n_1 - n_2 = n\Phi(1-K^2)$ pulses/sec. It follows that the relative root-mean-square error is given by

$$\delta_1 = \frac{\sigma_1}{\Delta n} = \frac{1}{K+1}\sqrt{\frac{1}{nT\Phi}\left[1 + \frac{2K}{\Phi(1-K)^2}\right]}. \tag{11}$$

A consideration of Eq. (11) shows that the error rapidly increases for screen transmission coefficients greater than 0.5 and for low effective solid angles. This is equivalent to a large unwanted radiation intensity, or a reduced fraction of radiation recorded by the compensated system (Fig. 3).

In the case of a narrow beam of γ rays incident along the principal direction, it may be assumed that $\Phi = 1$. In this case Eq. (11) is considerably simplified and the error is given by

$$\delta_1 = \frac{1}{1-K^2}\sqrt{\frac{1+K^2}{nT}}.$$

In the case of the compensated system of the second type, the fluctuations will be large, since the unwanted radiation is recorded by both detectors without attenuation and the sensitivity in the principal direction will be lower by a factor of 1 + K.

In fact, using the same notation as in the previous case, we find that

$$\sigma_2 = \sqrt{\frac{n_1}{T} + \frac{n_2}{T}} = \sqrt{\frac{n}{T} + \frac{nK\Phi + n(1-\Phi)}{T}} = \sqrt{\frac{2n - n\Phi(1-K)}{T}}\ ; \tag{12}$$

$$\delta_2 = \frac{\sigma_2}{\Delta n} = \frac{1}{1-K}\sqrt{\frac{1}{nT\Phi}\left(\frac{2}{\Phi} - 1 + K\right)}. \tag{13}$$

Even in the most favorable case, when $\Phi = 1$, the error due to statistical fluctuations in the compensated system of the second type will be greater by a factor of $[(1 + K)\sqrt{(K + 1)/(K^2 + 1)}]$.

In view of this, systems of the second type are recommended when it is necessary to reduce the weight of the detector to a minimum and in the case when it is necessary to record local sources against relatively low unwanted background. These systems are advantageous even in cases where the detectors have a large background n_b due to cosmic radiation and radioactive contamination. When the sensitivity of the main and the compensating channels are the same, this background has no effect on the differential count, while in systems of the first type there is a constant component equal to n_b (1-K).

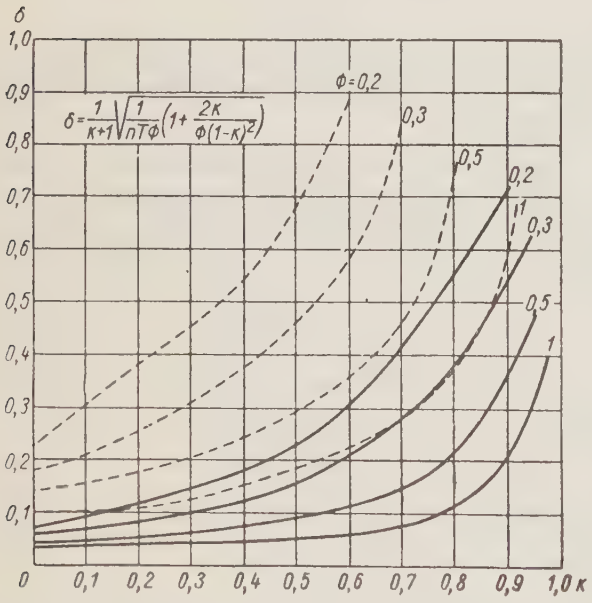

Fig. 3. Dependence of the relative root mean square error on the screen transmission coefficient and the effective solid angle for a compensated system: ---) nT = 100; ——) nT = 1000.

Gas-discharge counters or scintillation counters can be used in compensated directional detectors. Analysis shows that in the large majority of cases, scintillation counters have important advantages owing to their high efficiency, good time resolution, small phosphor dimensions, and the possibility of selection of spectral sensitivity characteristics.

In experimental studies of the efficiency of gas-discharge and scintillation counters incorporating various kinds of screens [8], it was found that in the case of the scintillation counters it is possible to select filters and working conditions so that Eq. (4) is satisfied in a sufficiently wide energy range.

Figure 4 shows a number of compensating systems and their directional characteristics. The scheme with two radiation detectors having equal sensitivities and a screen K_2 between them has a two-lobe characteristic (Fig. 4a). The sensitivity in the reverse direction ($\varphi = 180°$) can be reduced by an additional filter K_1. Without this filter the system can be used in the absence of radiation in the directions $90° < \varphi < 270°$.

The detector shown in Fig. 4b has a complex directional characteristic ensuring the same sensitivity in opposite directions along the x axis and one of the z directions. As a result, a zonal characteristic is obtained which is convenient in the location of moving local sources of radiation. The detectors shown in Figs. 4c, d, and e have single-lobe characteristics. The last detector can only be constructed with scintillation counters and belongs to the second type of compensated systems. It has a good geometrical symmetry since the main phosphor is located inside the compensating phosphor.

On the basis of the above principles, we developed, in 1956-58, portable directional scintillation monitors for γ-ray prospecting.*

*Instruments using gas-discharge counters (type RGN-1) were also developed in 1956 (design due to V. Nilov).

The detector in one of the instruments (type RND-58) is in the form of a scintillation counter [FÉU-31 and NaI(Tl)], arranged in a compensated system of the first type. The main phosphor is placed in a lead filter 12 mm thick. The recording circuit is transistorized and is based on miniaturized components. The total weight of the device is 3.5 kg, including a 1.5 kg probe. The instrument can be used to record γ radiation in the range 10-10^4 μr/hr against a background of unwanted radiation having an intensity which is higher than that to be measured by a factor

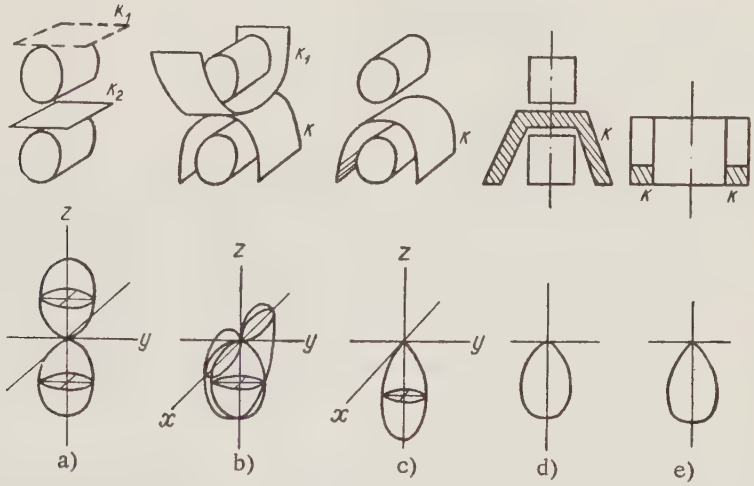

Fig. 4. Various designs of compensated radiation detectors and their directional properties.

of 5. The directivity is 100-110°, and the introduction of an additional collimator reduces it by a factor of 5 to 8. The indicator is in the form of a differential ratemeter with a time constant of 3 to 4 sec and a microammeter. The "decompensation" does not exceed ± (10-15)% when the spectral composition of the radiation changes by 100 kev. Total compensation can be obtained for any energy between 0.1 and 2 Mev. Satisfactory results have been obtained with this instrument under industrial conditions.

LITERATURE CITED

1. H. Stever, Phys. Rev. 59, 765 (1941).
2. S. Brown, Nucleonics 3, No. 2, 50 (1948).
3. D. Wilkinson, Rev. Scient. Instrum. 23, 414 (1952).
4. B. Corbett and A. Honour, Nucleonics 9, No. 5, 43 (1951).
5. G. Eicholz, G. Alexander, and A. Bettens, Nucleonics 15, No. 11, 90 (1957).
6. P. Hahn and E. Carothers, Nucleonics 6, No. 1, 54 (1950).
7. K. Takahashi et al., Proceedings of the Second International Conference on the Peaceful Uses of Atomic Energy (Geneva, 1958). Collected papers of foreign workers, Vol. 8 – Geology of Atomic Raw Materials, p. 465 (Moscow, Atomizdat, 1959) [in Russian].
8. V. P. Bovin, Atomnaya Énergiya 8, No. 2, 155 (1960).*
9. A. N. Svenson and V. P. Sigorskii, Avtom. i telemekh. 17, 828 (1956).
10. D. Veron, Phys. et radium 19, No. 12, 129 (1958).

*Original Russian pagination. See C. B. translation.

THE Li^6 (n, α)H^3 REACTION CROSS SECTION FOR 2.15 Mev NEUTRONS

V. P. Perelygin and K. V. Tolstov

Translated from Atomnaya Énergiya, Vol. 9, No. 6, pp. 488-489, December, 1960
Original article submitted March 3, 1960

The total and differential cross section for the Li^6 (n, α)H^3 reaction has been determined for neutrons from the D + D reaction having an average energy of 2.15 Mev. The reaction was studied in nuclear emulsion.

Ilford-E-1 emulsions impregnated with lithium (containing 92% of Li^6) were used. The lithium was introduced by soaking the plates in a 10% water solution of $LiC_2H_3O_2 \cdot 2H_2O$. The lithium concentration in the plates was approximately $(2.75 \pm 0.1) \times 10^{-4}$ g/cm^2 and was determined by spectral analysis. A beam of singly ionized deuterium molecules having an energy of 500 kev was incident on a heavy ice target. The diameter of the target was 2.5 cm. The total neutron yield was determined with the aid of a proportional counter which recorded protons emitted in a known solid angle from the D(d, p)H^3 reaction.

The emulsions were at a distance of 14.5 cm from the center of the target, and the neutrons were incident normally on the emulsion surface. Neutrons reaching the emulsions were at 145° to the deuterium ion beam, and their integral flux was $(6.5 \pm 0.2) \times 10^7$ neutron/cm^2. The effective neutron energy was 2.15 ± 0.1 Mev. At this energy the maximum range of the recoil protons in the emulsion was 45 μ, while the minimum total track length of the α particle and the triton was greater than 50μ. In addition to the recoil protons, protons having a range of the order of 65μ were observed. These were due to the N^{14} (n, p)C^{14} reaction which takes place with the liberation of 0.6 Mev of energy. These protons constituted about 10% of the number of protons due to the reaction under investigation, and could be easily identified by the lower ionization density and the absence of the α-particle track. The ranges and angles of the α particles and the tritons to the direction of the neutron beam were determined in addition to their total energy. In some cases, owing to errors in the precise location of the reaction site in the nuclear emulsion, the total energy differed by ± 0.5 Mev from the true value of 6.93 Mev. Only those events were selected for which there was a given relation between the range and the angle. The number of cases for which this relation was not satisfied was less than 20% of the total number of measured tracks. 311 cases of Li^6 (n, α)H^3 reaction were observed over an area of 1.05 cm^2.

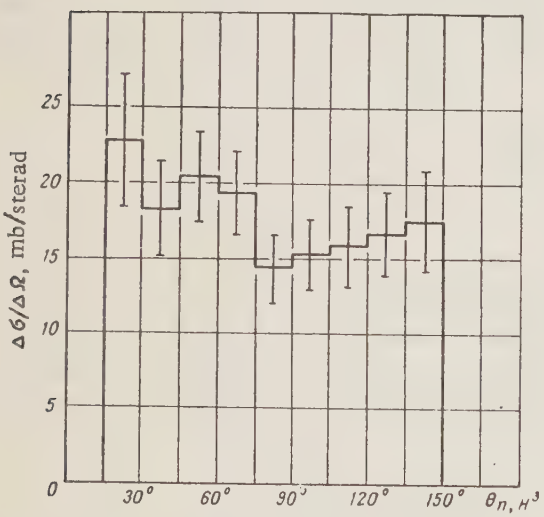

Differential cross section of the reaction Li^6(n, α)H^3 in the system with center of inertia Li^7*.

In the analysis of the results, corrections were introduced for the tracks leaving the emulsion, and the final calculation was carried out in the center of mass system of the compound nucleus Li^7. The reaction was not observed in the angle ranges 0-15° and 150-180°, owing to losses of tracks with large dip angles.

The differential cross section for the reaction is shown in the figure. The correction for the tracks having large dip angles was obtained by extrapolating the curve shown in the figure. The total reaction cross section, incorporating all the corrections, was found to be 215 ± 30 mb.* The root-mean-square error is made up of the following con-

*This result was referred to earlier in [1].

tributions: statistical – 6%, error in the number of nuclei – 4%, error in the determination of the neutron flux – 3%, geometrical corrections – 10%, spread in the values obtained in different series of experiments – 6%.

Our result agreed to within experimental error with that reported in [2], where the reaction cross section was found to be 215 ± 23 and 189 ± 22 mb for neutron energies of 1.86 and 2.39 Mev. It is also in agreement with the results reported in [1], where the reaction cross section at 2.5 Mev was found to be 170 ± 20 mb. The agreement is less satisfactory in the case of [3], where the reaction cross section for 1.5 and 2.0 Mev neutrons was found to be 320 ± ± 60 and 270 ± 40 mb, respectively.

In conclusion, the authors wish to thank O. I. Kozints, T. A. Romanova, and F. A. Tikhomirov for help in the present experiments.

LITERATURE CITED

1. A. V. Elpidinskii, F. L. Shapiro, and I. V. Shtranikh, Nuclear Reactions in Light Nuclei, supplement No. 5 to Atomnaya Énergiya [in Russian] (Atomizdat, 1957).
2. F. Ribe, Phys. Rev. 103, 741 (1956).
3. J. Weddell and J. Roberts, Phys. Rev. 95, 117 (1954).

PRODUCTION OF FAST NEUTRINO BEAMS

V. S. Barashenkov and Hsien Ting-ch'ang

Translated from Atomnaya Énergiya, Vol. 9, No. 6, pp. 489-490,
December, 1960
Original article submitted June 22, 1960

The attention of many physicists has recently been turned to experiments with high-energy neutrinos [1]. These experiments give considerable possibility for investigations of many important characteristics of weak interactions. In particular, it is possible to check whether weak interactions actually become strong at high energies [2].

An intense beam of high-energy neutrinos can be obtained from large proton accelerators, such as the proton synchrotron at Dubna and the 30-Bev accelerator at Geneva. In this case, the neutrino is produced as the result of the decay of charged π mesons generated in collisions of fast nucleons (Fig. 1). The energy spectrum and angular distribution of such neutrinos can be calculated if the spectrum and angular distribution of the π mesons produced in NN collisions are known. In the general case, this is a very complicated problem, especially if the finite size of the neutrino detector is taken into account [3]. However, the calculations are considerably simplified if only fast neutrinos emitted at small angles to the primary proton beam direction are considered. In this case, the angle of emission of the neutrino Θ_ν differs very little from the angle at which the decaying π meson moves: $\Theta_\nu \simeq \Theta$ (see Fig. 1).

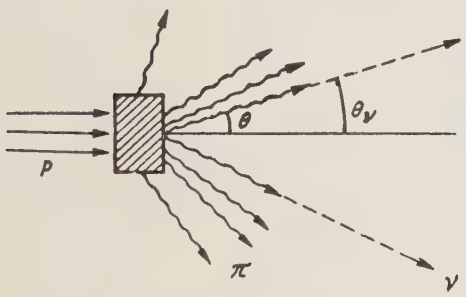

Fig. 1. Neutrino beam produced by the decay of $\pi^{\pm}$ mesons generated by fast protons.

Let us consider a neutrino of energy $E > 1$ Bev and angles Θ_ν of the order of a few degrees. Since in the planned experiments the neutrino detector with a transverse cross section $S_D \sim 1\ m^2$ is to be placed at distances of several tens of meters from the target,* such an approximation is quite satisfactory.

If $W_\pi(p; \Theta)$ is the momentum distribution of the charged π mesons emitted at an angle Θ to the primary proton beam, the corresponding energy spectrum of the neutrinos at a distance L from the target in which the π mesons are produced has the form

$$W_\nu(E; \Theta; L) = a \int\limits_{>aE/m} W_\pi(p; \Theta) \times \left[1 - \exp\left(-\frac{L}{l}\frac{m}{p}\right)\right] \frac{dp}{p}.$$

Here, $a = m^2/(m^2-\mu^2)$; $\underline{m}$ is the π-meson mass, and μ is the μ-meson mass. If L is given in meters, then $l = \tau c \cdot 10^{-2} = 7.68$ (τ is the lifetime of a charged π meson).

This expression differs from the corresponding expression for γ quanta produced in the decay of π^0 mesons [4, 5] only in the exponential term and the value of the coefficient $\underline{a}$.

Figure 2 shows the calculated neutrino spectra for the angle $\Theta = 0°$.

The calculations indicate that the spectra of neutrinos emitted at small angles depends very weakly on the angle. For example, the number of neutrinos of given energy emitted at an angle $\Theta = 3°$ is only 5% less than the number of neutrinos emitted at the same energy at an angle of $\Theta = 0°$. This is also illustrated in Fig. 3, in which the values of the entire neutrino flux of energy $E > 1$ Bev and $E > 2$ Bev are shown for the angles $\Theta = 0°$ and $\Theta = 3°$:

$$W_\nu^{(1)}(\Theta; L) = \int\limits_{E>1} W_\nu(E; \Theta; L)\, dE; \quad W_\nu^{(2)}(\Theta; L) = \int\limits_{E>2} W_\nu(E; \Theta; L)\, dE.$$

*We recall that, owing to the relativistic time dilatation, the π mesons decay only at large distances from the target.

The spectra W_ν (E) and the functions $W_\nu^{(i)}$ (L) shown in Figs. 2 and 3 are normalized to a single inelastic NN collision in the target and to a unit soild angle:

$$\int W_\nu (E; \Theta; L)\, d\Omega\, dE = n,$$

where n = 2, 3 is the mean number of charged π mesons produced in a single NN collision at an energy of 10 Bev [5, 6]. As in [5], the values of the function W_π (p; Θ) was calculated from the statistical theory of multiple production.

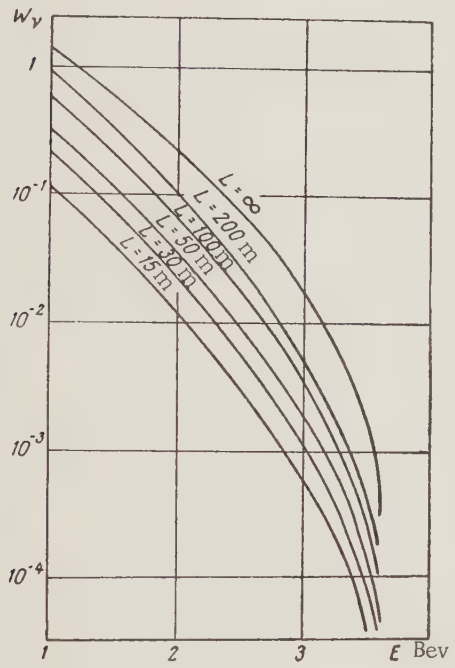

Fig. 2. Neutrino energy distribution at various distances from the target L at an angle $\Theta = 0°$ to the primary proton beam in the laboratory system.

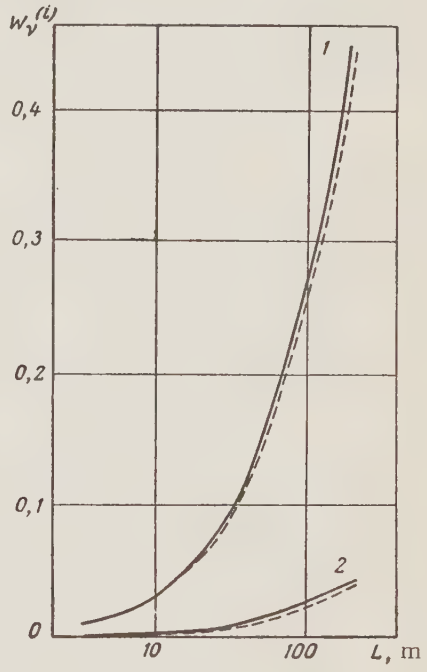

Fig. 3. Dependence of the neutrino flux of energy E > > 1 Bev (1) and E > 2 Bev (2) on the distance L to the target at neutrino angles of flight G = 0° (solid curve) and Θ = 3° (dotted curve) with respect to the primary proton beam in the laboratory system. The fluxes W_ν are normalized to a unit solid angle.

The neutrino flux per unit solid angle $W_\nu^{(1)}$ (Θ; L) increases rapidly with the distance from the target. The limiting values of the flux for L = ∞ are

Θ	$W_\nu^{(1)}(\Theta, \infty)$	$W_\nu^{(2)}(\Theta, \infty)$
0°	1,5	0,18
3°	1,4	0,16

With an increase in L, however, the solid angle of the neutrino $\Omega_D = S_D/L^2$ decreases rapidly; and, therefore, the number of neutrinos recorded by the detector decreases with an increase in the distance between the detector and the target. Thus, at a distance of L = 30 m, 1.1×10^{-8} neutrinos pass through 1 cm^2 of detector area (per single inelastic NN collision), and at distances of L equal to 50 and 100 m, the values are 0.6×10^{-8} and 0.27×10^{-8}, respectively. These values are very useful for various estimates in planning neutrino experiments.

In conclusion, the authors express their deep appreciation to M. A. Markov for many discussions and valuable advice, and to R. Asanov and I. Polubarinov for discussions and valuable critical remarks.

LITERATURE CITED

1. M. Markov, Hyperonen und K-mesonen (Berlin, Verlag der Wissenschaften, 1960); T. Lee and C. Yang, Theoretical Discussions on Possible High-Energy Neutrino Experiments, Preprint, 1960; N. Cabibbo and R. Gatto, Nuovo Cimento 15, 304 (1960); B. M. Pontecorvo, Report at the Ninth Annual Conference on High-Energy Physics, Kiev, 1959 [in Russian].
2. D. I. Blokhintsev, Zhur. Éksp. i Teor. Fiz. 35, 257 (1958); Uspekhi Fiz. Nauk 62, 381 (1957); H. Nagai and D. Ito, Anomalous Creation of μ Mesons Originating in the Weak Interactions, Preprint, Physics Institute, Hokkaido University, 1960.
3. I. V. Polubarinov, Interactions of Neutrinos Produced in a Parallel Monochromatic π-Meson Beam, Joint Institute for Nuclear Studies, Preprint D-577, 1960.
4. R. Sternheimer, Phys. Rev. 99, 277 (1955).
5. V. S. Barashenkov and Hsien Ting-ch'ang, Joint Institute for Nuclear Studies, Preprint D-577, 1960.
6. V. S. Barashenkov, Nuovo Cimento 14, 656 (1959).

A MODEL OF THE CIRCULAR SYNCHROCYCLOTRON

V. A. Petukhov, I. Gabanets, A. A. Zhuravlev,

M. Karmasin, V. I. Kotov, É. A. Myaé, Yu. L. Obukhov,

V. Zokhor, Yu. Tsirak, F. Benda, I. Dobiash, M. Marek,

T. Fukatko, and L. V. Svetov

Translated from Atomnaya Énergiya, Vol. 9, No. 6, pp. 491-492,
December, 1960
Original article submitted May 28, 1960

The idea of a circular synchrocyclotron, a strong-focusing accelerator with a time-independent magnetic field, was suggested in 1953 by A. A. Kolomenskii, V. A. Petukhov, and M. S. Rabinovich [1] and independently by Symon [2] in 1955. This type of accelerator would be very suitable from the point of view of increasing the intensity of the accelerated particle beam and the realization of the idea of colliding beams [3, 4, 5].

A model of the circular synchrocyclotron with radial sectors has been built at the Joint Institute for Nuclear Studies. The parameters of the model were chosen in such a way that it was possible to vary a number of its characteristics within a relatively wide range. In this way it was possible to carry out an exhaustive study of the behavior of the particle beam under various storage conditions.

Figure 1 shows a general view of the accelerator. The electromagnet consists of eight periodic elements, each of which has normal and reverse sectors, and also of two straight-line sections. The azimuthal dimensions of the normal sector, focusing the beam in the radial direction, are 22°, 30', while the dimensions of the reverse sector, which produces focusing in the vertical plane, and of the straight-line sections are 7° 30' each. The presence of the reverse sectors means that the orbit of the circular synchrocyclotron has a larger perimeter than that of an ordinary strong-focusing accelerator. This feacture of the circular synchrocyclotron is represented by a magnification coefficient which is equal to the ratio of the maximum radius of the orbit to the minimum radius of curvature. In the present case this coefficient was apporximately equal to 3.

The magnetic field in the sectors is produced by current coils wound on the surface of the poles along the radii of curvature of the instantaneous orbit. The coils are so distributed that the magnitude of the magnetic field increases with the radius R of the orbit in accordance with the law $H = H_0 (R/R_0)^4$. The magnitude of the magnetic field is 42 oe at R = 35 cm and 340 oe at R = 59 cm. In addition to the increase in the magnetic field with radius, the magnet gap increases in proportion to R, so that the vertical dimensions of the working region vary from 2 cm at the initial radius to 4 cm at the final radius. The increase in all the geometrical dimensions of the sectors in proportion to the radius ensures the geometrical similarity of the instantaneous orbits. This condition, together with the requirement that the average field index $\underline{k}$ should remain constant (in the model k = 4), leads to the dynamic similarity of orbits [6, 7], i.e., to a constancy of the frequencies of free oscillations during the acceleration process.

By changing the ratio of the fields in the normal and reverse sectors, it is possible to vary the number of betatron oscillations per revolution from 1 to 3 along the vertical, and from 2.5 to 3.5 along the radial direction. The fact that the frequencies of free oscillations could be varied in such a wide range means that it was possible to investigate the effect of various resonances on the free oscillations.

The model was designed for the acceleration of electrons. The injection of the electrons with energies between 20 and 40 kev can be carried out continuously and also in pulses. The acceleration is produced by an induced electric field (10-20 v per revolution) at a frequency of 450-500 cps. In order to improve the capture of the particles into the acceleration process, use is made of a forcing betatron core ensuring a voltage of 600 v per revolution over a time of about 1 μsec. Experiments carried out on the model show that electrons can be captured into the accelerating process without the inclusion of the forcing core but the intensity in the absence of the latter is considerably lower.

Figure 2 shows a photograph of the accelerated beam with (a) and without (b) forcing. In this figure (c) shows a beam accelerated up to 450 kev, i.e., to the energy which can be communicated to the particles by the induced electric field. By using a combination of the induced and high-frequency fields, the electron energy can be brought up to 2 Mev.

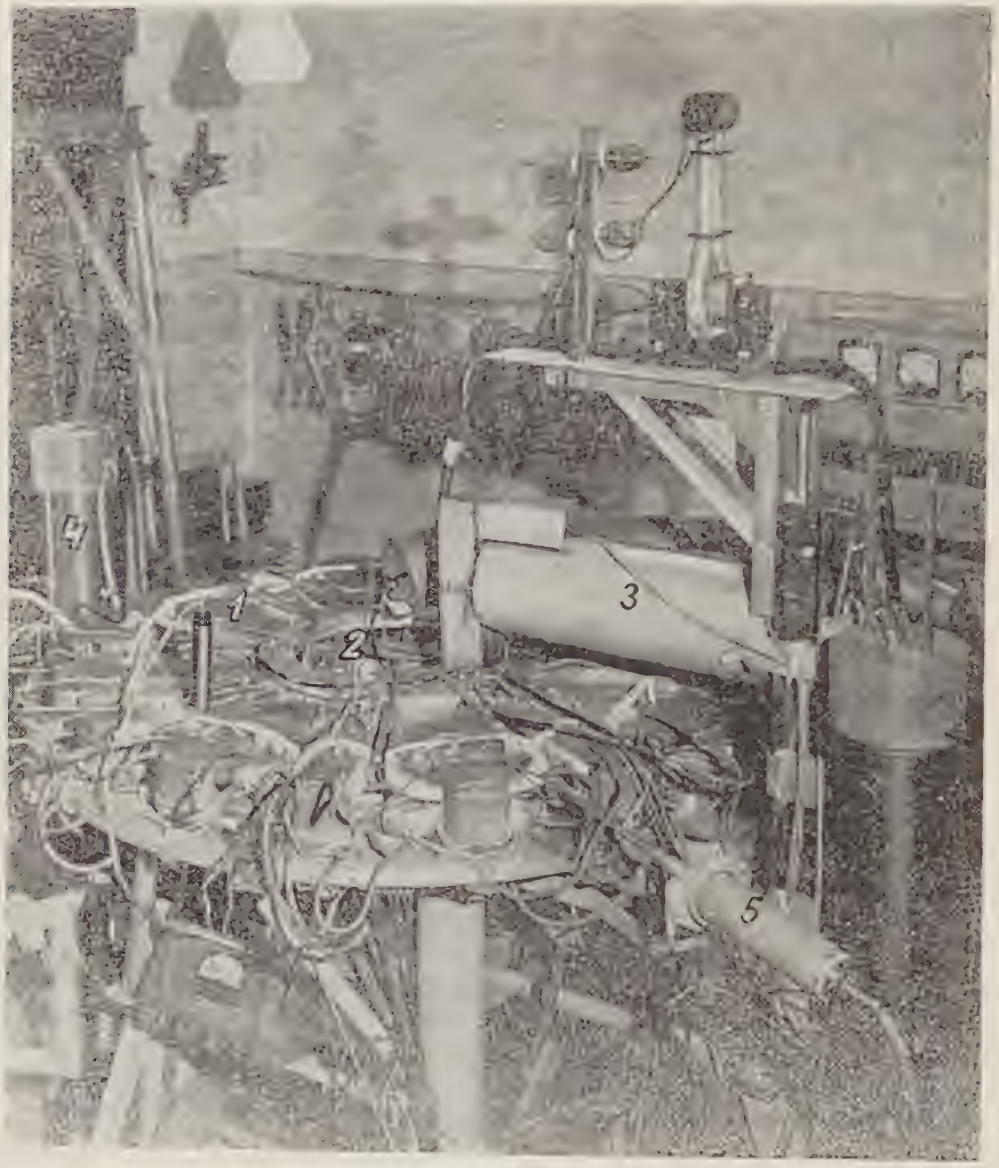

Fig. 1. General view of the model of the circular synchrocyclotron: 1) electromagnets; 2) electron injector; 3) induction acceleration core; 4) high-frequency oscillator; 5) photomultiplier.

Preliminary results obtained at the initial stages of the operation of the model showed that the accuracy of the assembly and the stability of the main magnetic characteristics is extremely important. Moreover, in accordance with theory, a large number of various resonances were observed. These resonances have an important effect on the intensity of the accelerated beam.

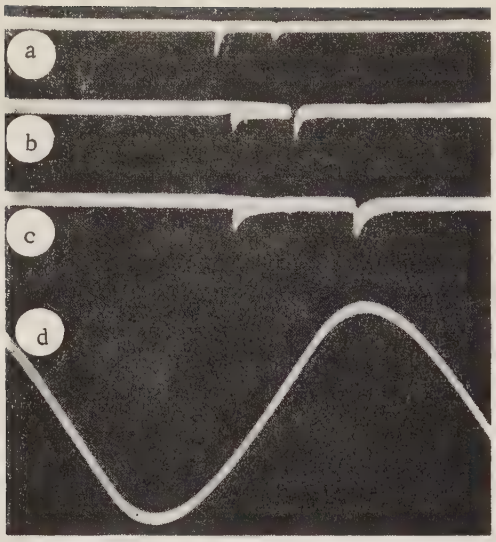

Fig. 2. Pulses of the accelerated beam. a) Without forcing; b) with forcing; c) beam accelerated to final energy; d) magnetic flux in the main core.

LITERATURE CITED

1. A. A. Kolomenskii, V. A. Petukhov, and M. S. Rabinovich, Some Problems in the Theory of Cyclic Accelerators, a collection of papers [in Russian] (Academy of Sciences Press, Moscow, 1955); Pribory i tekhnika éksperimenta No. 2, 26 (1956).
2. K. Symon, Phys. Rev. 98, 1152 (1955).
3. V. A. Petukhov, Zh. éksperim. i teor. fiz. 32, 379 (1957).
4. A. A. Kolomenskii, Zh. éksperim. i teor. fiz. 33, 298 (1957).
5. T. Ohkawa, Rev., Scient. Instrum. 29, 108 (1958).
6. K. Symon et al., Usp. fiz. nauk 61, 613 (1957).
7. A. A. Kolomenskii, Atomnaya Energiya 3, No. 12, 492 (1957).*

*Original Russian pagination. See C. B. translation.

APPLICATION OF THE SIMILARITY METHOD FOR SYSTEMATIZING EXPERIMENTAL DATA ON CRITICAL THERMAL FLUXES IN BOILING LIQUIDS

S. S. Kutateladze and G. I. Bobrovich

Translated from Atomnaya Énergiya, Vol. 9, No. 6, pp. 493-494,
December, 1960
Original article submitted May 27, 1960

Liquid-drop cooling is the most efficient method for cooling surfaces with intensive thermal fluxes. In this, the threshold of the maximum allowable thermal loads is determined by the value of the first critical thermal flux density for which film boiling occurs and the heat-transfer intensity sharply decreases (in any case, for a relative pressure p/p_{cr} which is not very close to unity and at flow rates which are not too high). The large number of the parameters influencing the value of the thermal-flux critical density makes the application of the similarity method highly desirable in this case. However, as is known, this method is effective only if the physical nature of the phenomenon under consideration is well understood [1].

At the present time, there are two hypotheses concerning the appearance of crisis under bubble-boiling conditions. One of them is most clearly formulated in papers by G. N. Kruzhilin [2 and 3]. According to this hypothesis, the first thermal-flux critical density is determined with respect to the same criteria which are used for the heat transfer processes in bubble boiling, namely: In the case of large-volume boiling in a liquid heated to the saturation temperature, the magnitude of the first thermal flux critical density is determined by the criterion function [3]

$$q_{cr}\frac{r\gamma''}{AT''(\gamma-\gamma'')\lambda}=f\left[\frac{\nu}{a};\frac{c\gamma AT''\sqrt{\sigma(\gamma-\gamma'')}}{(r\gamma'')^2};\frac{g\sigma}{\nu^2\gamma(\gamma-\gamma'')^{1/2}}\right]. \quad (1)$$

On the basis of many experimental data, represented in the form of products of the determining criteria in empirically chosen degrees, Kruzhilin proposed the following formula for calculations:

$$q_{cr}=4700\frac{T''^{0,32}\sigma^{0,21}(\gamma-\gamma'')^{0,48}(r\gamma'')^{0,36}\lambda^{0,40}}{\gamma^{0,31}c^{0,08}\mu^{0,14}}. \quad (2)$$

This hypothesis was not further developed. Nevertheless, Kruzhilin claims that it is valid from the physical point of view.

The second hypothesis, which was put forward by one of the authors of the present communication, is based on the assumption that the crisis in boiling represents a qualitatively particular phenomenon which is connected with disturbances in the hydrodynamic stability of the two-phase boundary layer when the critical vapor generation rate is attained [4]. This hypothesis made it possible, by using the similarity method, to derive a number of equations which are accurate to a constant coefficient. Some of these coefficients were subsequently calculated by using theoretical methods [5].

For the case of large-volume boiling of a nonviscous saturated liquid, the hydrodynamic theory yields the equation

$$\frac{q_{cr}}{r\sqrt{g\gamma''\left(1+\frac{\gamma''}{\gamma}\right)}\sqrt[4]{\sigma(\gamma-\gamma'')}}=K=\text{const}, \quad (3)$$

where K is of the order of 0.13-0.16.

Thus, the hypothesis under consideration yields equations which greatly differ among themselves with respect to the characteristics of the boiling liquid physical properties figuring in these equations. At the same time, Eqs. (2) and (3) are in satisfactory agreement with a vast amount of data obtained in identical experiments. However, it should

be borne in mind here that Eq. (3) has been derived theoretically, while Eq. (2) is empirical in structure and has four empirical coefficients (the proportionality factor and the three exponents of the criteria under the function sign in Eq. (1)). Therefore, the agreement between experimental data and calculations based on Eq. (3) provides a more convincing confirmation that the process physical interpretation forming the basis of the derivation of Eq. (3) is correct.

Complex k Values Calculated According to Eq. (4)

Substance	p/p_{cr}	k	Substance	p/p_{cr}	k
Water	0,005	0,132	Ethyl alcohol	0,017	0,123
	0,036	0,123		0,063	0,118
	0,086	0,121		0,133	0,128
	0,214	0,123		0,304	0,122
	0,340	0,121		0,590	0,133
	0,450	0,121		0,880	0,167
	0,580	0,122	Benzene	0,021	0,206
	0,850	0,132		0,073	0,181
Propane	0,270	0,183		0,170	0,182
	0,390	0,187		0,390	0,180
	0,470	0,196		0,670	0,214
	0,600	0,197			
	0,86	0,227			

If Eq. (2) is reduced to the form

$$k = \frac{0.415\, T^{*0.32}(\gamma - \gamma'')^{0.23}\lambda^{0.4}}{\gamma^{0.31}\gamma''^{0.14} r^{0.64} c^{0.08}\sigma^{0.04}\mu^{0.14}\left(1 + \frac{\gamma''}{\gamma}\right)^{0.5}} \quad (4)$$

we notice that it is a complex function of the saturation temperature and of a large number of the liquid physical parameters. The table provides the values of the complex, which was calculated for a number of substances by using Eq. (4). It is obvious that the redundant quantities (more accurately, the quantities which do not greatly affect the process under consideration), which appeared as a consequence of the incorrect physical hypothesis, were combined in processing the experimental data into a complex which is in complete agreement with the hydrodynamic principles and which remains a practically constant quantity.

Thus, Kruzhilin's unsuccessful approach in attempting to derive an equation for the critical thermal flux leads, even in the simplest case, to the introduction of a large number of factors which only slightly affect the process in question and, correspondingly, to an unnecessary complication of the equation. This was also the reason why Kruzhilin's method did not bring about any further advances in studying the effect of forced motion, underheating of the flow center, which makes it impossible to attain the saturation temperature, and other factors on the critical phenomena in boiling liquids.

LITERATURE CITED

1. L. I. Sedov, Similarity Methods and Dimensional Analysis in Mechanics [in Russian] (Gostekhizdat, Moscow, 1954).
2. G. N. Kruzhilin, Izvest. Akad. Nauk SSSR, Tech. Sci. Sect. 7, 967 (1948); ibid. 8, 701 (1949).
3. G. N. Kruzhilin and V. I. Subbotin, Transactions of the Second International Conference on the Peaceful Uses of Atomic Energy, Geneva, 1958. Reports by Soviet Scientists: Nuclear Reactors and Nuclear Power Engineering [in Russian] (Atomizdat, Moscow, 1959) Vol. 2, p. 134.
4. S. S. Kutateladze, Condensation and Boiling Heat Transfer [in Russian] (Mashgiz, Moscow, 1952).
5. N. Zuber, Hydrodynamic Aspects of Boiling Heat Transfer (thesis). AECU = 4439 (1959).

HEAT TRANSFER TO A MELT OF SODIUM AND POTASSIUM IN ANNULAR CLEARANCES

E. M. Khabakhpasheva and Yu. M. Il'in

Translated from Atomnaya Énergiya, Vol. 9, No. 6, pp. 494-496,
December, 1960
Original article submitted January 14, 1960

The majority of papers on heat transfer to liquid metals which were published in recent years in our country and abroad were devoted to the investigation of heat transfer in round pipes. Heat transfer in channels with more complicated sections has been studied to a much lesser extent. The theoretical solutions obtained in determining the heat-transfer coefficients in the case of flat and annular clearances [1 and 2] are based on a number of simplifying assumptions, and they must be checked experimentally.

In most cases, experiments on heat transfer in annular clearances were performed in different heat exchangers, and the values of the heat-transfer coefficients were determined by calculation on the basis of the measured heat-transfer coefficients [3]. This work involved the use of various assumptions concerning the relationship between the heat-transfer coefficients at the inside and the outside surfaces of the dividing pipe.

In the present paper, the heat-transfer coefficients in an annular clearance were determined on the basis of temperature measurements in a section sufficiently removed from the channel inlet. The experimental section consisted of a thick-walled copper tube with an inside diameter of 17 mm. Heaters (or flow restrictors) were installed along the pipe axis and were centered by means of special bushings at the experimental section inlet and outlet. The wall temperature along the copper pipe length was measured by means of eight thermocouples. In order to eliminate the heat leakage from the heater, a thermometer and a compensating heater were installed in the experimental section. For controlling the liquid-metal purity and the heat-transfer surface cleanliness, the heat-transfer coefficient was periodically measured in a pipe with a round cross section (without the internal heater). The heat-transfer coefficient values in the pipe were stable and were in good agreement with Lyon's equation [4] (Fig. 1):

$$Nu = 7 + 0{,}025\ Pe^{0{,}8}.$$

The experiments on heat transfer to a melt of sodium and potassium were performed for two-sided and single-sided heat supply in annular clearances of different widths (2.5, 3.5, and 4.5 mm). The experimental results are shown in the form of graphs in Figs. 2 and 3, where the Nusselt and Peclet numbers were obtained on the basis of the equivalent hydraulic diameter $d_e = d_1 - d_2$, which was used as the characteristic dimension. The diagrams also show curves representing the results of theoretical calculations [1 and 2].

It follows from Fig. 2 that, for one-sided heat supply, the Nusselt number values for narrow annular clearances ($d_1/d_2 \approx 1$) are lower by 25 to 30% than the Nusselt number values for round pipes for the same Peclet number values, and that they are in satisfactory agreement with theoretical data. The Nusselt number values for annular clearances and for two-sided heat supply (see Fig. 3) in cases where the Peclet number exceeds 500 also are in satisfactory agreement with theoretical data [1 and 5]; and they are 1.3 to 1.5 times as large as the corresponding Nusselt number values for round pipes.

Thus, the above results confirm the theoretical conclusion that, for coolants with small Prandtl number values, changes in the channel geometric shape or in the method of supplying heat considerably affect the heat-exchange intensity. The recommendation contained in manual [3], where it is suggested that the heat-transfer coefficients for liquid metal flow in flat and annular clearances be calculated in the first approximation by using heat-transfer equations for pipes with round cross sections on the basis of the equivalent hydraulic diameter, can be considered only as a very coarse approximation.

It should also be noted that the theoretical recommendations can be applied in heat-transfer calculations only if no thermal contact resistance is present. This condition is apparently satisfied in the case of heat transfer to alkali metals if they are thoroughly freed from oxides [6]. It is presently not yet possible to eliminate the thermal contact

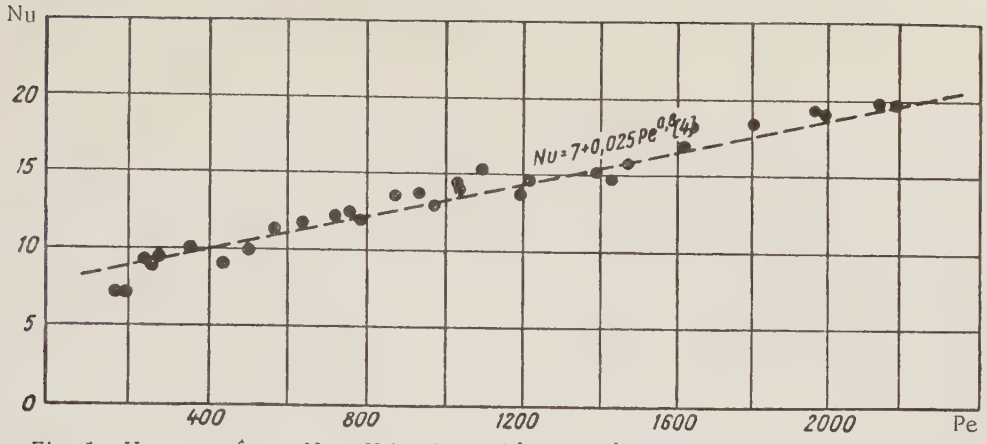

Fig. 1. Heat transfer to Na – K in pipes with a round cross section.

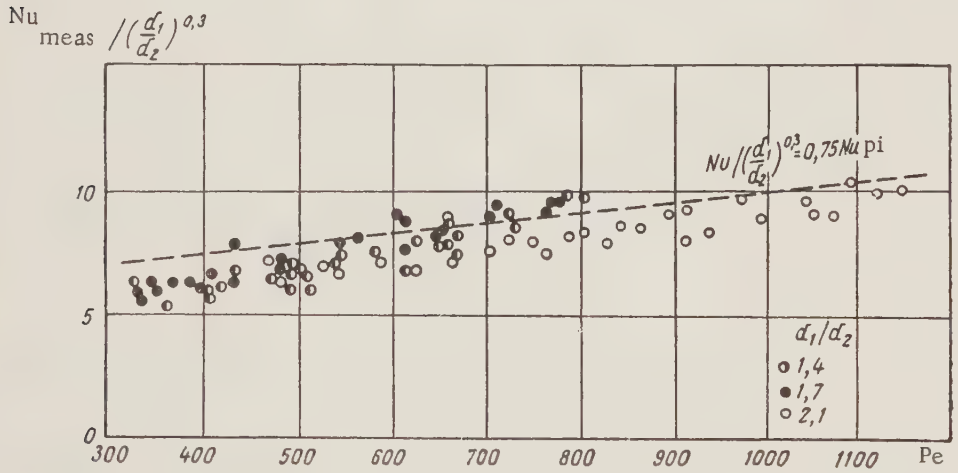

Fig. 2. Heat transfer to Na – K in annular clearances with different widths for one-sided heat supply (d_1 is the diameter of the heated surface). $Nu_{pi} = 7 + 0.025\,Pe^{0.8}$ [4] is the Nusselt number value for round pipes.

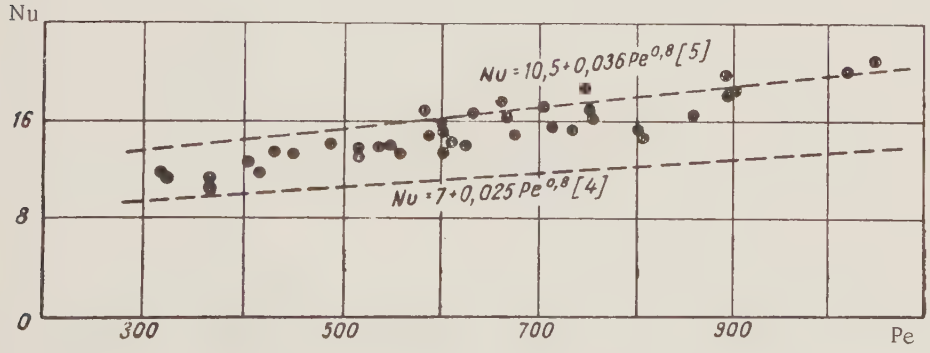

Fig. 3. Heat transfer to Na – K in an annular clearance for two-sided heat supply [$(d_1/d_2) = 1.4$; $(q_1 = q_2)$]. Here, q_1 and q_2 are the outside and inside thermal fluxes.

resistance in the case of heavy metal flow (mercury and the eutectic lead and bismuth alloy) in steel pipes [7]. In these cases, the effective transfer coefficient values for pipes with round cross sections and annular clearances depend on the thermal contact resistance value.

LITERATURE CITED

1. R. Seban, Trans. ASME 72, 759 (1960).
2. R. Baily, U. S. Atomic Energy Commiss., ORNL 521 (1955).
3. S. S. Kutateladze et al., Liquid-Metal Coolants [in Russian] (Atomizdat, Moscow, 1958).
4. R. Lyon, Chem. Engng Progr. 47, 75 (1951).
5. Nuclear Reactors. Nuclear Reactor Techniques [Russian translation] (IL, Moscow, 1958) Vol. 2.
6. P. L. Kirillov et al., Atomnaya Énergiya 6, 4, 382 (1959).*
7. M. Kh. Ibragimov, V. I. Subbotin, and P. A. Ushakov, Atomnaya Énergiya 8, 1, 54 (1960).*

*Original Russian pagination. See C. B. translation.

THERMAL CONTACT RESISTANCE

Yu. P. Shlykov and E. A. Ganin

Translated from Atomnaya Énergiya, Vol. 9, No. 6, pp. 496-498,
December, 1960
Original article submitted May 28, 1960

The thermal contact resistance must be taken into account in the case of large thermal flux values [1 and 2].

The actual contact area constitutes only an insignificant portion of the over-all area of the surfaces in contact (in most cases, it does not exceed 1-2% [3 and 4]). The heat transfer between surfaces in contact occurs mainly due to heat conduction through the medium filling the space between the burrs in the contact zone and through the points of direct contact.

The over-all thermal resistance can be expressed by the relation

$$\frac{1}{R_{oa}}=\frac{1}{R_{gas}}+\frac{1}{R_{act}}, \tag{1}$$

where R_{oa} is the over-all thermal contact resistance, R_{gas} is the gaseous layer thermal resistance, and R_{act} is the direct contact thermal resistance.

For R_{gas}, we can use the thermal resistance of a layer whose thickness is equal to the equivalent (with respect to the volume) clearance between the surfaces in contact:

$$\delta_{eq}=\frac{V_{gas}}{S_n}, \tag{2}$$

where V_{gas} is the volume enclosed between the projections in the contact zone, which is filled with a gas whose thermal conductivity is λ_{gas}, and S_n is the contact nominal area.

Since the absolute value of δ_{eg} is negligible for the classes of finish quality accepted in machine construction, the heat can be transferred through the layer only by pure heat conduction, i.e.,

$$R_{gas}=\frac{\delta_{eq}}{\lambda_{gas}}. \tag{3}$$

Let us use the concept of the relative drawing together of surfaces in contact when a load is applied [5]:

$$\varepsilon=\frac{a}{h_{av}}, \tag{4}$$

where a is the absolute value of the reduction in spacing (μ), and h_{av} is the microroughness height (μ).

By expressing V_{gas} and then δ_{eg} in terms of ε for the case where a rough and an "absolutely" smooth surface are brought into contact, the following relationship is obtained for R_{gas}:

$$R_{gas}=\frac{h_{av}}{2\lambda_{gas}}(1-\varepsilon)^2. \tag{5}$$

For determining R_{act}, we used the results obtained in an analytical investigation of contact spot thermal resistance, which was performed by Cetinkale and Fishenden [6], and the results obtained in Holm's work on electrical contact resistance [7].

When surfaces are compressed, the contact spot dimensions remain practically constant, and the increase in the actual contact surface area occurs mainly as a result of the greater number of contact points [1, 5, and 8]. If we denote by η the ratio of the actual contact area S_{act} to the nominal area S_n, we obtain the following dependence:

$$R_{act} = \frac{1}{2{,}1\eta\lambda_m} 10^{-4}, \tag{6}$$

where λ_m is the thermal conductivity of the material in contact, and 2.1×10^4 is a coefficient whose dimension is 1/m.

The relative magnitude of the actual contact area η and the relative reduction in spacing ε vary in relation to the load and the quality of the surface finish. These factors determine the thermal resistance variation.

On the basis of theoretical and experimental investigation of contacts between rough and absolutely smooth surfaces, the relations of ε and η to the load, the microroughness height (finish quality), and the physical properties of materials, were obtained in [5].

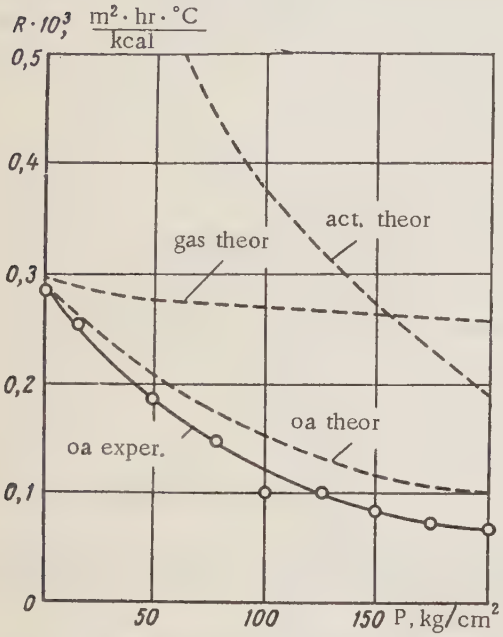

Fig. 1. Dependence of the thermal resistance and its components on loading.

By using expressions (5) and (6), the value of R_{oa} can be determined with respect to known values of ε and η.

Calculations show that the value of $(1-\varepsilon)^2$ and, consequently, of R_{gas} does not change by more than 15% (Fig. 1); and, therefore, for practical purposes, R_{gas} can be determined by using the simplified equation

$$R_{gas} = \frac{h_{av}}{2\lambda_{gas}}. \tag{7}$$

For surfaces whose finish quality is not better than class 9 or 10, the following calculation formula was obtained after some simplifications [9]:

$$R_{act} = \frac{S_n C \sigma_s}{2{,}1 \cdot 10^4 \lambda_m N}, \tag{8}$$

where N is the load (kg), σ_s is the yield point of the material after it has been subjected to the maximum amount of cold-working (it is assumed to be equal to the ultimate strength), and C is a coefficient which is assumed to be equal to 3.

Figure 1 shows the theoretical and experimental curves for the case where a smooth (▽ 12) surface is in contact with a rough (▽4) surface. The specimens were made of Steel 1Kh18N9T.

An analysis of the $R_{gas\ theor}$ and $R_{act\ theor}$ curves indicates that the over-all thermal resistance components are commensurable within a rather wide loading range. The decrease in the over-all thermal contact resistance when the specimens are compressed with a greater force is mainly due to an increase in the actual contact surface area.

The contact between two rough surfaces is usually encountered in practice. In this case, R_{gas} is calculated by using the equation

$$R_{gas} = \frac{h_{av}}{\lambda_{gas}}, \tag{9}$$

where R_{act} is determined from expression (8).

The results obtained in analytical calculations of thermal contact resistance according to Eqs. (8) and (9)* are in good agreement with experimental data. Some of these data are shown in Fig. 2.

$$\lambda_m = \frac{2\lambda_{m1}\lambda_{m2}}{\lambda_{m1} + \lambda_{m2}}.$$

*If different metals are in contact, the σ_s value for the less plastic material is used, and λ_m is determined from the expression shown above.

Thus, the thermal resistance of the contact between rough surfaces for different compressive forces can be determined analytically with a sufficient degree of accuracy.

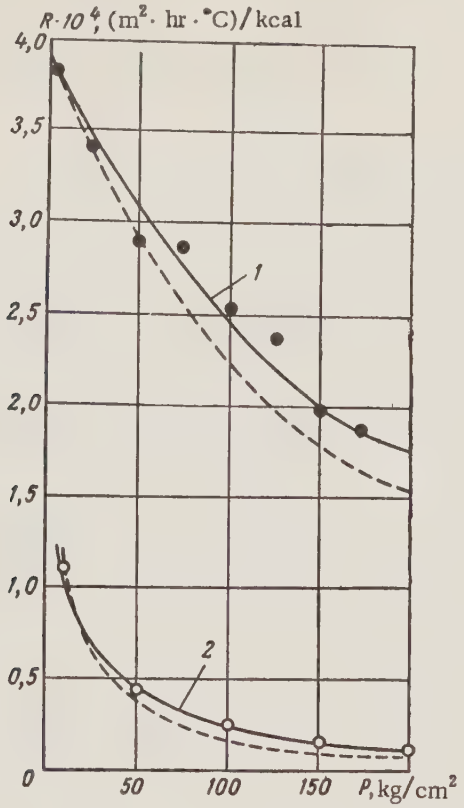

Fig. 2. Thermal contact resistance. 1) Steel 1Kh18N9T, finish: ∇5; 2) duralumin D-16, finish: ∇4; ----) theoretical data.

LITERATURE CITED

1. F. Boeschoten and E. Van Der Held, The thermal Conductance of Contacts between Aluminum and other Metals. Physics 23, No. 1, 37 (1957).
2. R. Skipper and K. Wootton, Thermal Resistance between Uranium and Can. Report submitted to the Second International Conference on the Peaceful Uses of Atomic Energy (Geneva, 1958).
3. F. Bowden and D. Tabor, Friction and Lubrication of Solids (1950).
4. I. V. Kragel'skii, Zhurnal Tekhnicheskoi Fiziki 12, 11 – 12, 1, 91 (1942).
5. N. B. Demkin, Tr. Instituta Mashinovedeniya AN SSSR 1, 131 (1959).
6. T. Cetinkale and M. Fishenden, Thermal Conductance of Metal Surfaces in Contact. General Discussion on Heat Transfer. The Institution of Mechanical Engineers (1951).
7. R. Holm, Electric Contacts (Stockholm, 1946).
8. E. M. Shvetsova, "Determination of the actual contact areas of surfaces by means of transparent models," Sbornik: Trenie i Iznos v Mashinakh (Collection: Friction and Wear in Machines) 7, 12 – 33 (1953).
9. Yu. P. Shlykov, E. A. Ganin, and N. B. Demkin, "Investigation of contact heat exchange," Teploénergetika 6 (1960).

EFFECT OF RADIOACTIVE RADIATION ON THE DIELECTRIC PROPERTIES OF ELECTRICAL INSULATORS

K. A. Vodop'yanov, B. I. Borozhtsov, M. D. Lavrov,

E. S. Nesmelova, and G. I. Potakhova

Translated from Atomnaya Énergiya, Vol. 9, No. 6, pp. 498-500,
December, 1960
Original article submitted December 1, 1959

The investigation of the effect of γ radiation on the dielectric properties of solid plastic dielectrics is of great importance for the selection of electrical insulators for electrical and electronic devices which are exposed to radiation.

In dependence on the physicochemical properties of the material and its structure, radiation can cause ionization, displacement of atoms, or dissociation of molecules. In this, the electrophysical properties of solid dielectric changes considerably.

We investigated the frequency and the temperature characteristics of the permittivity and the dielectric loss angle for polyethylene, "Kel-F," and "product 10" (a mixture of polystyrene with vinylnaphthalene) before and after they were irradiated by γ rays; the dose rate was from 400 to 1200 r/min, and the irradiation dose was from 2000 to 100,000 r. A betatron with 15-Mev particles served as the γ-radiation source. The specimens consisted of disks which were 1-2 mm thick.

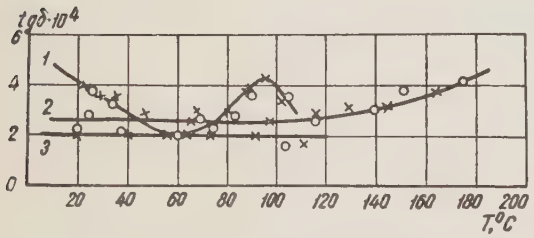

Fig. 1. Dependence of the loss angle on temperature at the 10 cps frequency for an irradiation dose of 50,000 r. 1) Polyethylene; 2) "Kel-F"; 3) "product 10"; O) unirradiated; ×) irradiated.

The frequency dependences of the loss angle and the permittivity of the organic dielectrics under investigation remain almost unchanged after irradiation with a dose of 50,000 r. For a frequency of 10^7 cps and an irradiation dose in excess of 1000, 000 r, the loss angle slightly increases only in "Kel-F"; for polyethylene and the "product 10," the loss angle variation remains within the measurement error limits. The fact that the loss angle is independent of the radiation effects in all of the three dielectrics is also observed at different temperatures (Fig. 1).

The permittivity of polyethylene, "Kel-F," and "product 10" changes little after they are exposed to temperature action and radiation. On the basis of an analysis of the frequency and the temperature dependences of the loss angle and permittivity of organic dielectrics before and after irradiation, it can be assumed that, in polyethylene, the frequency and the temperature maxima of the loss angle are determined by directional polarization of the polar radicals (c = 0) in molecules. With respect to its properties and molecular structure, "Kel-F" is close to polyethylene, with the difference, however, that "Kel-F" contains fluorine, which is characterized by stable bonds, instead of hydrogen with unstable bonds. "Kel-F" is a weakly polar dielectric, and, therefore, the observed increase in the loss angle with an increase in frequency is apparently also due to the orientation of polar groups entering the "Kel-F" composition. In comparison with polyethylene and "Kel-F," the loss angle in "product 10" depends to a much lesser degree on frequency and temperature, which indicates that dielectric dipole losses are not present in the measured frequency and temperature intervals.

Figure 2 shows the dependences of the loss angle and the permittivity of glass textolite SKM-1 on frequency before and after irradiation. In order to determine the causes of the increase in the loss angle of glass textolite SKM-1 after irradiation in the low-frequency region, we measured the temperature dependence of the specific volume resistance (Fig. 3) and the loss angle of glass textolite SKM-1 at different frequencies (Fig. 4). On the basis of the obtained data, it can be assumed that the effect of radioactive irradiation on glass textolite SKM-1 is manifested in an increase in the loss angle and a decrease in volume resistivity in that frequency region where dielectric losses of ohmic character are observed.

Similar characteristics were obtained for the AG 4, K-211-3, K-114-35, and FKIM-25 plastics, which are based on various modifications of phenolformaldehyde resins. In dependence on external conditions (temperature and frequency), the dielectric loss angle in these plastics will be determined by relaxation processes and by conductivity (Fig. 5). Loss angle measurements, performed at a temperature of -60°C, indicate the absence of conductivity losses and the presence of relaxation losses.

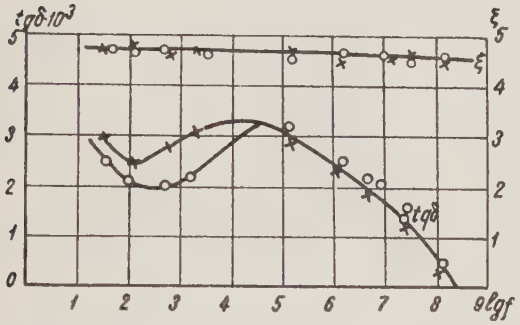

Fig. 2. Dependence of the loss angle and the permittivity of glass textolite SKM-1 [(O) unirradiated; x) irradiated)] on frequency at room temperature for an irradiation dose of 100,000 r.

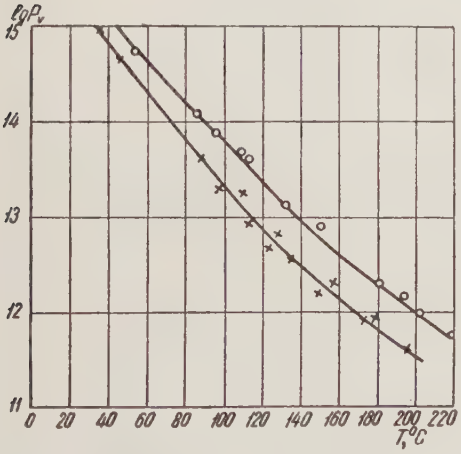

Fig. 3. Dependence of volume resistivity of glass textolite SKM-1 [(O) unirradiated; x) irradiated)] on temperature for an irradiation dose of 100,000 r.

The temperature dependences of the loss angle in polyamide-68 at different frequencies are shown in Fig. 6. These dependences can be used as an example for explaining the manner in which irradiation affects the various losses. The decrease in the angle loss, which is determined by and is observed at frequencies from 50 to 10 cps, is probably connected with an increase in the polymerization of polyamide-68 under the action of radiation. The fact that dipole losses did not change after irradiation is connected with the prevalence of the orientation effect of polar groups in polyamide-68 over those changes in the dynamics of elementary particles or molecules which are caused by irradiation. Similar phenomena are observed in other polar plastic dielectrics, such as polyvinyl chloride, lavsan, and FKPM-25.

We also investigated two varieties of organic silicon rubber: rubber 14r-2, which is based on synthetic organic silicon rubber, titanium dioxide, and benzoyl peroxide, and rubber 14r-6, which differed from rubber 14r-2 by the fact that it contained powdered silica gel and zinc white instead of titanium dioxide. In comparison with rubber 14r-6, rubber 14r-2 had a lower electrical conductivity and a smaller dielectric loss angle.

The results of loss angle vs frequency measurements before and after irradiation indicate (Fig. 7) that a decrease in the loss angle with an increase in frequency is characteristic of both rubbers. The effect of radiation on rubber 14r-6 depends on the state of the specimen under investigation. If the specimen has not passed through the second vulcanization stage, as was the case in our experiments, irradiation leads to a sharp decrease in the loss angle, which diminishes with an increase in frequency. It is obvious that irradiation leads to further vulcanization of rubber 14r-6. A different situation is encountered in the case of completely vulcanized specimens: After such specimens are irradiated, the dielectric loss angle and permittivity increase, while the effect of irradiation is similar to that observed in rubber 14r-2.

The presence of ohmic dielectric losses in rubber apparently also causes a noticeable change in the dielectric loss angle in the low-frequency range after irradiation.

Thus, for the majority of solid plastic dielectrics, the change in the loss angle as a result of irradiation is the greater, the lower the frequency. With an increase in frequency, this change diminishes and becomes hardly noticeable at high frequencies.

We are of the opinion that the loss angle variation in solid plastic dielectrics as a result of radioactive irradiation is determined by the dielectric loss mechanism. It was shown experimentally that, in cases where ohmic losses are observed, also a considerable change in the loss angle occurs; in the presence of dielectric dipole losses, noticeable changes in the loss angle do not take place.

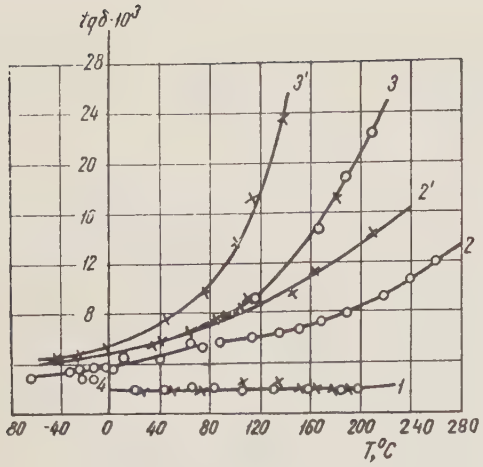

Fig. 4. Dependence of the loss angle in glass textolite SKM-1 [(O) unirradiated; ×) irradiated)] on temperature for an irradiation dose of 100,000 r at the following frequencies: 1) 106 cps; 2 and 2') 10^4 cps; 3 and 3') 50 cps.

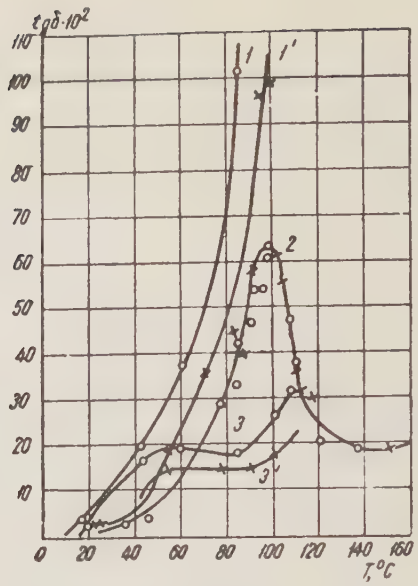

Fig. 6. Dependence of the loss angle in polyamide-68 [(O) unirradiated; ×) irradiated)] on temperature for an irradiation dose of 50,000 r at the following frequencies: 1 and 1') 50 cps; 2) 106 cps; 3 and 3') $5 \cdot 10^3$ cps.

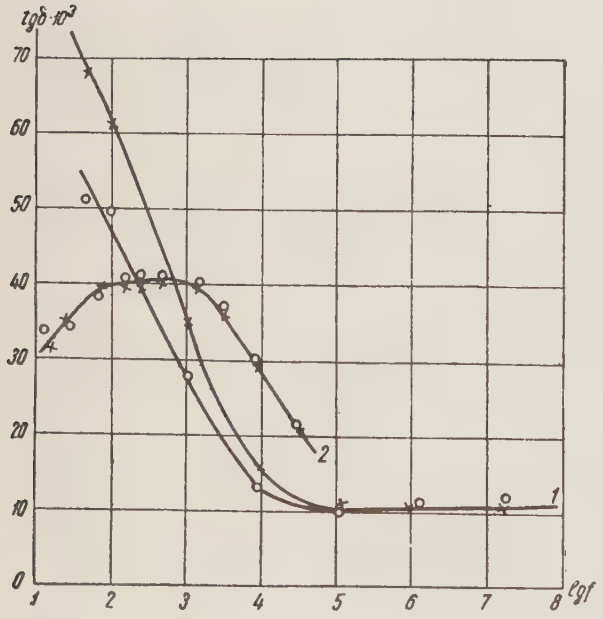

Fig. 5. Dependence of the loss angle in plastic AG-4 [(O) unirradiated; ×) irradiated) on frequency for an irradiation dose of 48,000 r at the following temperatures: 1) + 20°C; 2) -60°C.

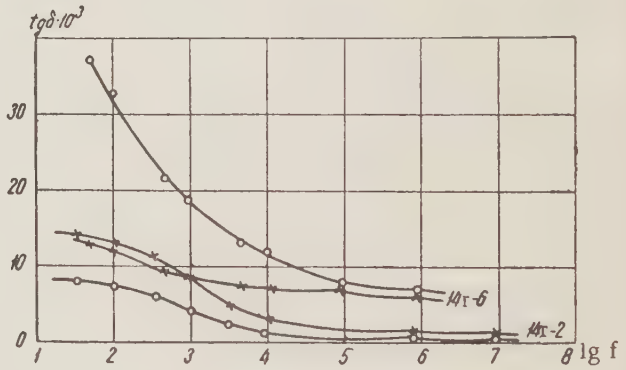

Fig. 7. Dependence of the loss angle in rubber [(O) unirradiated; ×) irradiated)] on frequency for an irradiation dose of 50,000 r.

Consequently, before any conclusions are drawn regarding the resistance of solid plastic dielectrics to the effect of a certain dose of γ-radiation of a given intensity, it is necessary to know the character of polarization and of dielectric losses in different temperature and frequency intervals.

The authors hereby express their gratitude to N. I. Ol'shanskaya, T. G. Mikhailova, L. T. Murashko, and A.I. Tovbina for their help in performing the experiments.

ISOTOPIC COMPOSITION OF RUTHENIUM

K. G. Ordzhonikdze and O. S. Akirtava

Translated from Atomnaya Énergiya, Vol. 9, No. 6, pp. 501-503,
December, 1960
Original article submitted May 4, 1960

The relative content of ruthenium isotopes has been determined on several occasions [1-3]; but the method employed did not have the simplicity which is desirable for series analyses, and in a number of cases did not make it possible to carry out precision measurements. The problem was therefore presented of developing a fairly accurate and simple method of measuring the isotopic composition of ruthenium, which does not require preliminary chemical treatment of the sample and permits direct measurement of the isotopic composition of enriched samples, taken from the pockets of an electromagnetic separating plant.

The experiments were carried out in an MS-3 type industrial mass spectrometer with recording of the ion currents by an external microammeter and a Speedomax Recorder automatic electronic potentiometer with magnetic-field linear time scanning. A standard source with focusing of the ion beam was used. Check measurements in neon and mercury (Hg^+ and Hg^{++}) showed that systematic errors do not occur if the apparatus is correctly adjusted [4, 5].

To obtain maximum accuracy of the measurement of the isotopic composition of ruthenium, the conditions for obtaining the most stable ion currents during the ionization of ruthenium vapor by an electron beam and by the thermionic emission method were investigated. In the first case, a directly heated evaporator, making it possible to avoid overheating of the components of the source, was used to obtain ruthenium vapor. The inverted U-shaped evaporator, made of 2 × 0.02 mm tungsten strip, was constructed to a width of 0.9 mm in the center and had a cavity, holding 1-2 mg of the substance investigated. This shape made it possible to obtain the temperatures necessary for the evaporation of ruthenium, with the minimum heating power (~ 30 watts). The evaporator was fixed in the holder installed opposite the corresponding slit in the ionization chamber of the ion source. The design of the holder makes it possible to change the evaporator rapidly. To increase the stability of evaporation, ruthenium powder was mixed with degassed tungsten powder in the optimum ratio of 1:3. When this mixture is sintered it becomes porous and evaporation of ruthenium from it takes place more uniformly; the process continues longer and the ruthenium evaporates completely, without leaving a residue. With ruthenium ion currents sufficient for measurements, this made it possible to reduce the weight of the investigated sample for analysis. Thus, to carry out an experiment 0.3-0.7 mg of ruthenium metal was placed in the evaporator.

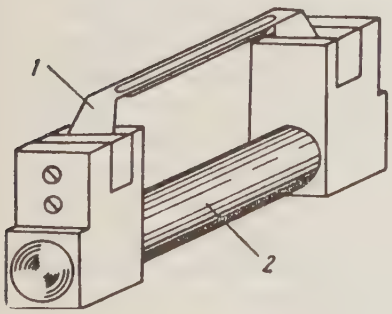

Fig. 1. Emitter with holder: 1) Emitter; 2) ceramic insulator of the holder.

Depending on the character of the source, two maxima of the Ru^+ ion current were observed with corresponding electron ionization energy value of 20 and 90-100 ev, respectively. In the latter case the line strength of the ruthenium isotopes was two-threefold more intense than with an electron energy of 20 ev. In addition to the monovalent ions, di- and trivalent ruthenium ions were observed in the spectrum of the masses. The value of the current of Ru^{++} ions was three- fivefold less intense than the current of Ru^+ ions, and the emission intensity of the Ru^{++} ions did not allow them to be measured in practice. Lines, corresponding to ruthenium compounds, were absent in the observed spectrum.

Measurements of the relative abundance of ruthenium isotopes were carried out in currents of univalent and divalent ions. To reduce the mercury background, a series of experiments with an electron ionization energy of 20 ev was carried out. The current of Hg^{++} ions was reduced 20-30-fold, so that the background was reduced to 0.1-0.5%, of the useful signal. Within the limits of such accuracy the background could be neglected.

Measurements in divalent ruthenium atoms were complicated by the presence of background lines with mass numbers of 50, 51, and 52 in the spectrum. The background was due to the material of the evaporator, and its intensity reached 5% of the value of the useful signal.

By means of the method of ionization by evaporation and subsequent bombardment by an electron beam, the relative content of ruthenium isotopes can be determined with an accuracy reaching 0.5-1%. Within the limits of such an error, it is best to carry out the measurements in Ru^+ ions with a minimum energy of the ionizing electrons (20 ev), when the mercury background becomes negligible.

To obtain a high accuracy of measurement of the isotopic composition of ruthenium, we investigated the possibility of its thermionic emission; for this purpose, an emitter (Fig. 1), which was previously employed for the isotopic analysis of alkali metals [4, 7], was used. This emitter was punched from tungsten foil of thickness 0.02 mm. The area of its central part (14 × 0.9 mm) corresponds to the dimensions of the slit of the first lens of the ion source. The U-shaped profile of the active part does not permit appreciable deformations of the emitter, which could influence the form of the lines of the mass-spectrum.

A mixture of ruthenium powder and degassed tungsten in a gravimetric ratio of 1:5 to 1:20 was wetted with alcohol, and about 6-8 mg was placed in the cavity of the emitter, forming an even layer.

An appreciable emission of ruthenium ions, of the order of 10^{-14} amp for Ru^{102} isotope, commenced at an emitter temperature of ~1950°C.

Measurements of the abundance of ruthenium isotopes were carried out with currents (at the collector) of the order of 10^{-12}-10^{-11} amp in the 2000-2250°C temperature range. The pressure on the source did not exceed $5 \cdot 10^{-7}$ mm Hg, and remained at $(1-2) \cdot 10^{-7}$ mm Hg on the analyzer side. Variations of intensity within the limits of sensitivity of the apparatus were not observed. The value of the current of ruthenium ions remained constant for a certain time after the commencement of emission, depending on the amount of sample used, and then decreased regularly as the material was exhausted. The intensity could be kept constant by gradually increasing the heater current.

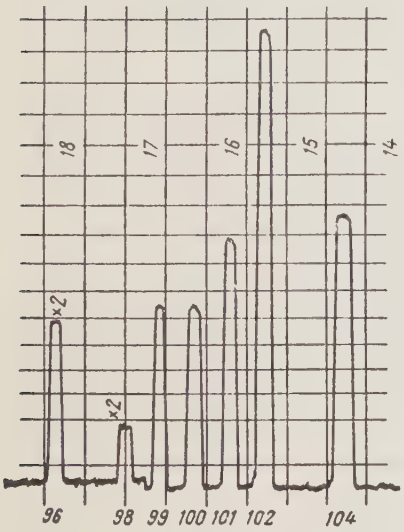

Fig. 2. Mass-spectrum of ruthenium isotopes.

Figure 2 gives the mass-spectrum of ruthenium isotopes obtained as a result of the observations (the sensitivity of the apparatus was increased 100% for recording the $^{96}Ru^+$ and $^{98}Ru^+$ peaks). To obtain the same measurement accuracy for all isotopes, the sensitivity of the recording circuit was increased during the recording of rare isotopes, so that the deviation of the potentiometer carriage was the same for all isotopes. The error of the determination of the relative abundance of each ruthenium isotope did not exceed 0.2%. To exclude the influence of the diminution of the intensity on the measurement results, scanning was carried out alternately in the direction of an increase in the masses and in the opposite direction. The abundance of the isotope was determined for one experiment as the mean of an even number of recorded spectra (in our case, 10). Table 1 gives the measurement results obtained in this way.

As is shown by the data of Table 1, the statistical errors in the determination of all isotopes, with the exception of ^{98}Ru, are within the limits of 0.06-0.15%. The value of the accuracy of the determination of the relative content of each isotope, given by the recording circuit, i.e., 0.2%, is given as the lower limit of errors for the values found for the relative abundance of ruthenium isotopes. ^{98}Ru isotope, for which the statistical error somewhat exceeds this value, forms an exception.

The values we obtained for the relative content of ruthenium isotopes are given, together with the results of other authors, in Table 2. As may be seen from this Table, the results of our experiment agree closely with the values given in [3]. The data of [1-2] are somewhat too high for the rare isotopes and correspondingly low for the more common isotopes.

In spite of the high ionization potential of ruthenium (7.3 ev), considerably exceeding the work function of pure tungsten (4.52 ev), a fairly high value is obtained for the emission intensity of the ruthenium ions (10^{-11}-10^{-12} at the collector of the apparatus), which is also stable, ensuring high accuracy (0.2%) of isotopic analysis. In all probability this can be explained by the fact that the work function of some parts of the sintered tungsten powder was increased as a result of the monoatomic layer of oxygen adsorbed on them. But the surface film of oxygen is very stable up to temperatures of 1700-2200°C [6]. The ionization of the ruthenium atoms in these parts of the emitter evidently also ensures a sufficient emission intensity for accurate measurements.

TABLE 1

Data of the Mass-Spectrometric Determination of the Content of Ruthenium Isotopes

Expt. No.	^{96}Ru	^{98}Ru	^{99}Ru	^{100}Ru	^{101}Ru	^{102}Ru	^{104}Ru
1	5,432	1,869	12,62	12,52	16,95	31,97	18,63
2	5,418	1,885	12,55	12,46	17,04	31,74	18,92
3	5,412	1,883	12,66	12,53	16,99	31,63	18,90
4	5,392	1,861	12,62	12,54	17,03	31,68	18,88
5	5,494	1,884	12,64	12,60	17,14	31,37	18,87
6	5,476	1,881	12,60	12,53	17,05	31,61	18,85
7	5,490	1,864	12,61	12,54	17,06	31,68	18,76
8	5,479	1,858	12,66	12,54	17,04	31,61	18,82
9	5,471	1,856	12,62	12,54	16,99	31,66	18,86
10	5,455	1,876	12,65	12,54	16,98	31,53	18,98
11	5,486	1,867	12,65	12,57	17,01	31,59	18,83
12	5,500	1,880	12,64	12,53	17,03	31,48	18,94
13	5,472	1,816	12,62	12,47	16,96	31,64	19,02
Mean . . .	5,460	1,868	12,63	12,53	17,02	31,63	18,87
Mean square error	0,008	0,005	0,008	0,010	0,014	0,039	0,027

TABLE 2

Results of Determination of the Isotopic Composition of Ruthenium from the Data of Various Authors

Ruthenium isotopes	[1]	[2]	[3]	Values obtained in the present work
^{96}Ru	5,68±0,17	5,50±0,02	5,47±0,03	5,46±0,01
^{98}Ru	2,22±0,09	1,91±0,01	1,84±0,02	1,868±0,005
^{99}Ru	12,81±0,09	12,70±0,01	12,77±0,05	12,63±0,02
^{100}Ru	12,70±0,19	12,69±0,05	12,56±0,05	12,53±0,02
^{101}Ru	16,98±0,25	17,01±0,03	17,10±0,06	17,02±0,03
^{102}Ru	31,34±0,47	31,52±0,06	31,70±0,06	31,63±0,06
^{104}Ru	18,27±0,27	18,67±0,06	18,56±0,05	18,87±0,04

In all probability, the use of a source with separate evaporator and ionizing filament [8] for ruthenium metal could not give an appreciable increase in the ionizing efficiency because the temperatures at which thermionic emission of ruthenium is observed are not markedly different from the maximum working temperature of the ionizing filament. Moreover, a sufficient vapor pressure of ruthenium metal is obtained only at high temperatures, close to the ionization temperature.

LITERATURE CITED

1. H. Ewald, Ber. Dtsch. Chem. Ges. 76A, 1 (1943); Z. Phys. 122, 487 (1944).
2. L. Friedman and A. Irsa, J. Amer. Chem. Soc. 75, 5741 (1953).
3. M. Smith, Electromagnetically Enriched Isotopes and Mass Spectrometry (London, 1956).
4. K. G. Ordzhonikidze, Cand. Thesis [in Russian] (FTI, Academy of Sciences, Georgian SSR, 1960).
5. K. G. Ordzhonikidze and G. N. Zubarev, Proc. All-Union Scientific-Technical Conference on the Uses of Radioactive and Stable Isotopes and Radiations in the National Economy and Science [in Russian] (Moscow, Acad. Sci. USSR Press, 1957) p. 78.
6. G. A. Morozov, Zhur. éksperim. i teor. fiz. 17, 1142 (1947); J. Langmuir and K. Kingdon, Phys. Rev. 34, 129 (1929); S. V. Starodubtsev and Yu. I. Tikhomirov, Symposium in honor of the 70th birthday of Academician A. F. Ioffe [in Russian] (Moscow, 1950) p. 117; W. Walcher, Z. Phys. 121, 604 (1943).
7. K. G. Ordzhinikidze and V. Shyuttse, Zhur. éksperim. i teor. fiz. 29, 479 (1955).
8. M. Inghram, Rev. Scient. Instrum. 24, 518 (1953).

THE HEAT OF FORMATION OF $PuBe_{13}$

V. V. Akhachinskii and L. M. Kopytin

Translated from Atomnaya Énergiya, Vol. 9, No. 6, pp. 504-505,
December, 1960
Original article submitted July 5, 1960

The literature contains no data on the heats of formation of intermetallic plutonium compounds.

We have determined the heat of formation of $PuBe_{13}$ by measuring the heat of solution of this intermetallide and its components in 19% hydrochloric acid, using an isothermally jacketed microcalorimeter (see figure). The calorimeter vessel consisted of an inner container welded from sheet tantalum and an outer container turned from copper. A manganin wire heater of 180 ohms resistance was placed in the space between these containers and the region filled with a layer of paraffin to hermetically seal the inner container. A copper resistance thermometer (40 m of wire, 0.05 mm in diameter) wound on the outer surface of the calorimeter was incorporated in a bridge circuit containing a lamp and scale galvanometer, the latter having a sensitivity of ~ 0.00003° per mm scale deflection. The thermal equivalent of the calorimeter was approximately 35 cal/deg and the cooling constant, $3 \cdot 10^{-4}$ sec^{-1}. The temperature of the jacket water (25°C) was held constant to within ± 0.001° by a special electrical device [1] which utilized a MMT-9 thermistor of ~ 1000 ohm resistance as a sensor. Distillation of the solvent was avoided by so choosing the temperature at the beginning of the principal period that the temperature at the final period would be somewhat below the jacket temperature. The calorimeter stirrer was lowered several millimeters at the beginning of the principal period to break the container on a special protuberance on the bottom of the calorimeter and bring the working material into reaction with the solvent. The hydrogen evolved during the experiment was collected in a gas burette. The calorimeter was cooled to 22° at the end of dissolution and its thermal equivalent determined by introducing a definite quantity of electrical energy. The results are expressed in 15° calories.

A heat-exchange correction was obtained from the formula:

$$\delta = k\left(\vartheta_c \sum_{i=1}^{n} \Delta t_i - \frac{\sum_{i=1}^{n} \vartheta_i \Delta t_i + \sum_{i=0}^{n-1} \vartheta_i \Delta t_{i+1}}{2}\right),$$

in which k represents the cooling constant for the calorimeter, ϑ_c is the convergent temperature, ϑ_0 is the temperature at the end of the initial period, ϑ_n is the temperature at the end of the principal period, and Δt_1 is the time interval between the last reading in the initial period and the first reading in the principal period.

Measurement of the amount of liberated hydrogen (with the requisite corrections) made it possible to determine the chemical composition and the phase composition for each charge of alloy from the well-known phase diagram for the Pu-Be system [2]. The phase composition was calculated from the equations

$$x + y = 1;$$
$$138{,}80x + 908{,}26y = v,$$

in which x and y are the amounts of Pu and $PuBe_{13}$, respectively, per 1 g of alloy; the coefficients 138.80 and 908.26 represent the amounts of hydrogen expressed in STP cm^3 evolved in the dissolution of 1 g of Pu and 1 g of $PuBe_{13}$, respectively (the latter figure was obtained from data on the component Pu and Be); and v is the volume of hydrogen evolved in the dissolution of 1 g of alloy.

The Be used in this work was 99.15% pure. The plutonium contained less than 0.2% total contaminants. The intermetallide $PuBe_{13}$ was prepared by fusing a mixture of metallic plutonium chunks and powdered beryllium in a high frequency electrical furnace. Fusion was carried out in a BeO crucible in an atmosphere of nitrogen. The lattice constant of the product compound (face-centered cubic) was a = 10.259 ± 0.001 kX* and its microhardness,

*The lattice constant of $PuBe_{13}$, a, is 10.26 kX according to [4].

Results on the Dissolutions of Beryllium, Plutonium, and the Alloy

Dissolved substances	Number of experiments	H_2 evolved per 1 g of substance, cm^3 (measured at STP)	Heat of solution, ΔH, kcal/mole
Be	6	2477.8 ± 0.67	89.38 ± 0.06
Pu	4	138.8 ± 0.13	141.02 ± 0.19*
Alloy	5	From 830 to 848	1267.2 ± 2.3

* The value of this quantity is given as 141.64 ± 0.2 kcal/(g·atom)

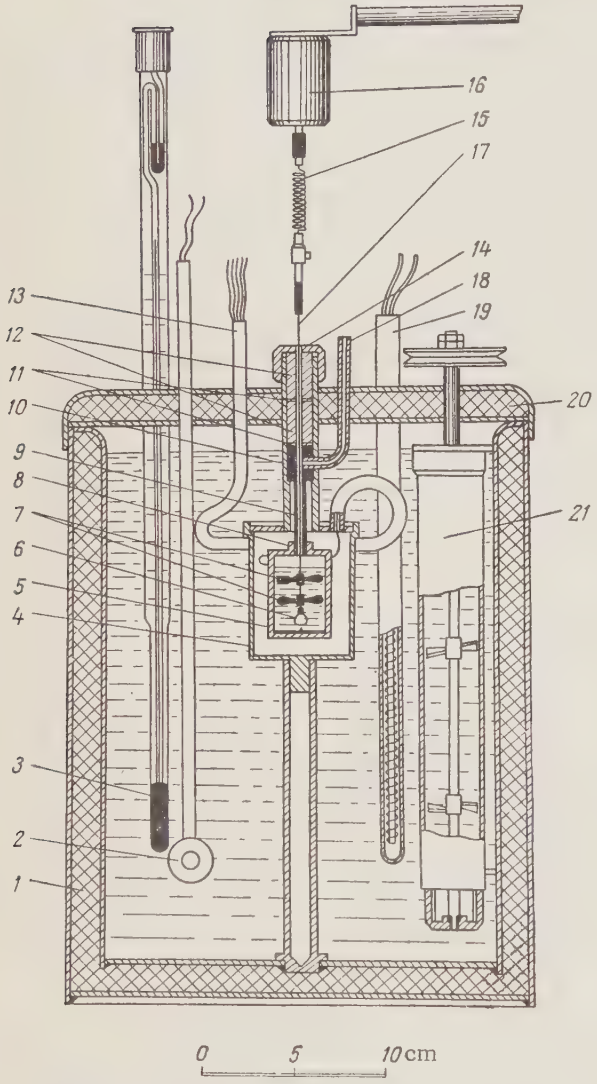

Construction of microcalorimeter: 1) Calorimeter jacket; 2) thermistor; 3) Beckmann thermometer; 4) housing; 5) calorimeter vessel; 6) container with working material; 7) impellers; 8) calorimeter cover; 9) ebony bushing; 10) tube; 11) felt packing; 12) copper bushings; 13) tube for escape of hydrogen; 14) packing nut; 15) spring; 16) Warren motor; 17) stirrer shaft; 18) tube connecting calorimeter with gas burette; 19) jacket heater; 2) jacket cover; 21) stirrer.

1045 kg/mm^2. Metallographic analysis showed small inclusions of free plutonium distributed on the grain boundaries of the intermetallide. Measurements on the amount of hydrogen evolved during alloy dissolution showed this plutonium to be distributed nonuniformly. The phase composition of the charge was determined from these same measurements and varied from 92.17 weight % $PuBe_{13}$ and 7.83 weight % Pu to 89.78 weight % $PuBe_{13}$ and 10.22 weight % Pu.

The heat of solution of $PuBe_{13}$ was calculated for each charge separately, account being taken of the phase composition in order to avoid effects from nonuniformity of the alloy.

Results on the dissolution of beryllium, plutonium, and the alloy are presented in the table. The values for the heat of solution contain a correction for the heat of vaporization of the hydrochloric acid required for saturating the liberated hydrogen (0.206 kcal/mole H).

The probable error is given as a measure of the accuracy of the results for Be and Pu. The maximum experimental error is given for $PuBe_{13}$, this quantity covering both accidental errors and possible systematic errors in the determination of the alloy composition. These latter errors arise from the fact that the quantity of gas evolved in the dissolution of unit mass of a mixture of the components is not the same as that evolved in dissolving the alloy obtained from this mixture. This, in turn, is due to such factors as the vaporization of the volatile contaminants and interaction of the contaminants with one another.

The data of the table were used for a Hess Law calculation of ΔH°_{298}, the heat of formation of $PuBe_{13}$, and led to the value of 35.7 ± 3.4 kcal/mole.

It was assumed in these calculations that the heat liberated in reaction of unit mass of contaminants during formation of the alloy is the same as the heat liberated in the reaction of unit mass of the component substances. The error resulting from this assumption was estimated to be 1 kcal/mole; this has been allowed for in determining the uncertainty in the heat of formation.

The authors conclude by expressing their thanks to E. S. Smotritska for preparing the alloy, to A. N. Elistratova for her aid in carrying out the measurements, and to M. I. Ivanov for valuable advice.

LITERATURE CITED

1. V. V. Akhachinskii and V. P. Mashirev, Pribory i Tekhnika Éksperimenta 5, 94 (1958).
2. S. T. Konobeevskii, Session of Acad. Sci. USSR on Peaceful Uses of Atomic Energy (Meeting of Chemistry Section) [in Russian] (Moscow, Acad. Sci. USSR Press, 1955) p. 362.
3. G. Seaborg, J. Katz, and W. Manning, The Transuranium Elements 14B, Part II, Paper, 6, 53.
4. O. Runnals, Canad. J. Chem. 34,No. 2, 133 (1956).

MEASUREMENT OF THE ABSOLUTE CONCENTRATION OF THORON IN THE AIR IN INDUSTRIAL ENCLOSURES

Yu. N. Burmistenko

Translated from Atomnaya Énergiya, Vol. 9, No. 6, pp. 505-506,
December, 1960
Original article submitted June 12, 1960

Owing to its small half-life (54.5 sec), the concentration of thoron is usually estimated by an air flow method. The magnitude of the ionization current due to the thoron in the ionization chamber is a function of the speed of the air passing through the ionization chamber; and hence in order to determine the thoron concentration, the relation between the ionization current and the air speed (for constant concentration of thoron in the air) must be known.

Let Q_0 be the concentration of Tn in air (disint /sec · l), V the volume of the ionization chamber (l), and ω the speed of air (l/sec). The number of thoron atoms in one liter of air is then given by $N_0 = Q_0/\lambda$ where λ is the decay constant of thoron.

The number of thoron atoms entering the chamber per second is $N_0\omega$, while the number of thoron atoms leaving the chamber per second is $N_0\omega e^{-\lambda(V/\omega)}$. It follows that the number of thoron atoms which disintegrate per second in the chamber is given by:

$$N = N_0\omega\left(1 - e^{-\lambda\frac{V}{\omega}}\right) = \frac{Q_0\omega}{\lambda}\left(1 - e^{-\lambda\frac{V}{\omega}}\right).$$

The ionization current is proportional to the number of disintegrations taking place in the chamber per second and the ionizing power of the α particles emitted during the disintegration of thoron. The current is given by:

$$I = a \cdot 3{,}74 \cdot 10^5 e\ N = 5{,}96 \cdot 10^{-14} a\ \frac{Q_0\omega}{\lambda}\left(1 - e^{-\lambda\frac{V}{\omega}}\right)\ [a], \qquad (1)$$

where a is a constant for the given chamber, 3.74×10^5 is the number of ion pairs produced by the α particles from Tn + ThA per disintegration, and e is the electronic charge.

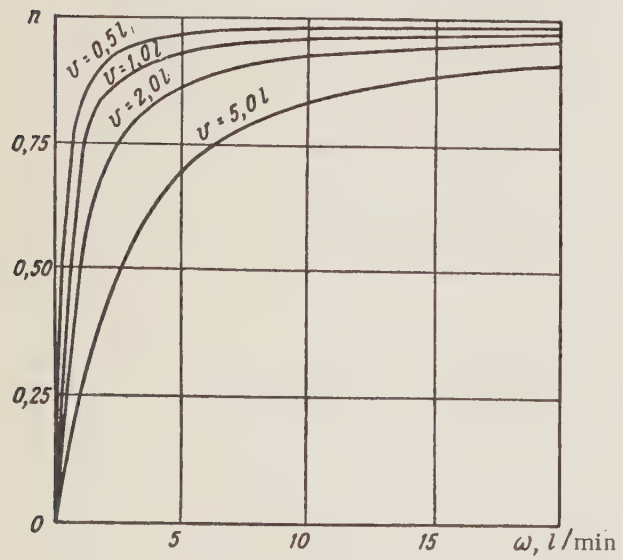

Ionization current due to thoron as a function of air speed.

It is clear from this formula that as air speed increases the ionization current tends to a limiting value which can be found with the aid of the l'Hospital rule for $\omega \to \infty$ and is given by

$$\lim I_{\omega\to\infty} = 5{,}96 \cdot 10^{-14} a Q_0 V = k Q_0 V, \qquad (2)$$

where $k = 5.96 \cdot 10^{-14} a$.

The figure shows the ionization current as a function of the air speed for different volumes of the ionization chamber. The curves were calculated using Eq. 1 for $\lim I_{\omega \to \infty} = 1$.

The apparatus used to measure the thoron concentration incorporates an ionization chamber, an electrometer, a flowmeter, and an airblower (vacuum main).

The instrument is conveniently calibrated with the aid of a liquid radium standard. A correction was introduced for the difference in the ionizing power of α particles from Rn and Tn (and their decay products).

The correction coefficient has been calculated by V. I. Baranov [1, 2] and is equal to 1.47. It follows that the conversion coefficient for the instrument is given by

$$i_{Tn}=\frac{Q_{Rn}}{I_{Rn}}\ 1{,}47\ \text{C/dw/min}, \tag{3}$$

where Q_{Rn} is the amount of radon in the standard and I_{Rn} is the standard ionization current.

A liquid thorium standard cannot be used to calibrate the instrument, since the rate of production of the emanation by the standard would depend on the air speed and the construction of the bubbler.

In order to determine the thoron concentration in air one must measure the ionization current for a constant speed of the air passing through the chamber. The thoron concentration can then be calculated from the formula

$$Q_0=\frac{i_{Tn}I_{Tn}}{V}\frac{1}{n}\ \text{C/liter}, \tag{4}$$

where I_{Tn} is the ionization current due to thoron, V is the volume of the ionization chamber, and $1/n$ is a correction which is determined from the curves given in the figure for a given air speed.

The measured concentration of thoron may be affected by external γ rays, or by the presence of radon in air. For this reason the ionization current due to thoron was determined as the difference between the ionization current measured while the air was passing through the chamber (I_0) and the ionization current measured with stationary air (I_1), the difference being given by

$$I_{Tn}=I_0-I_1. \tag{5}$$

An exposure of 5 to 6 minutes is necessary for a virtually complete disintegration of the thoron.

LITERATURE CITED

1. V. I. Baranov, Radiometry [in Russian] (Academy of Sciences USSR Press, 1956).
2. A. P. Kirikov et al., Radioactive Geophysical Methods and their Application to Geology [in Russian] (ONTI, Gorgeonefteizdat, 1934).

ON THE FORM OF THE ABSORPTION CURVE FOR BETA-RADIATION IN ALUMINUM

N. E. Tsvetaeva

Translated from Atomnaya Énergiya, Vol. 9, No. 6, pp. 507-508,
December, 1960
Original article submitted May 7, 1960

The absorption curve for β radiation is often qualitatively described by the exponential formula $I = I_0 e^{-\mu x}$ where the absorption coefficient μ is a function of the energy E_0 of the β radiation. However, this representation of the absorption curve is very approximate.* Experimental data indicate that the form of this curve depends on the geometrical conditions under which the measurements are carried out and differes appreciably from the exponential form [1, 2]. If the absorber is located next to the window of the counter, while the specimen is at a distance of several centimeters from it, then the absorption curve is very similar in form to the exponential. However, the initial part of the curve differs considerably from that predicted by the exponential formula. Some authors ascribe this to extraneous effects [2, 3]. This tendency to see an exponential curve where it does not really exist leads to considerable errors in the determination of the absolute activity of β radiation with end-window counters, and also in the analysis of complex β radiation by the absorption method.

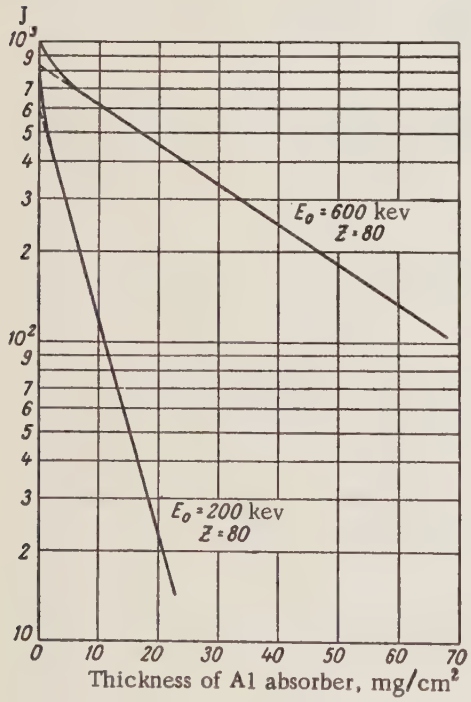

Fig. 1. Computed absorption curves for β radiation in Al.

Half-Layer Values of Absorption

E_0, kev	Z	$d_{1/2i}$, mg/cm²	$d_{1/2m}$, mg/cm²	Data of [6]
200	4	2,80	4,5	3,9
	20	2,05	4,5	
	80	1,75	4,5	
600	4	19	26	24
	20	13	25	
	80	8	23	

We have computed by graphical integration the absorption curves for simple β spectra with energies E_0 = 200 and 600 kev, and β emitters with atomic numbers Z = 4, 20, and 80. The computation was based on the data obtained by Seliger [4] for the absorption of monochromatic electrons, and the theoretical allowed β spectra given by Marshall in [5]. The computed curves correspond to the case where the absorber is located next to the window of the counter and a narrow beam of β particles is employed.

Figure 1 shows that the computed absorption curves differ from the exponential for small values of the absorber thickness.

The table gives half-layer values obtained from the computed curves for the initial $(d_{\frac{1}{2}})_i$ and middle $(d_{\frac{1}{2}})_m$ parts of the absorption curve. As can be seen from the table the values of $(d_{\frac{1}{2}})_i$ and $(d_{\frac{1}{2}})_m$ are very different. Moreover, $(d_{\frac{1}{2}})_i$ depends on the atomic number Z of the β emitter.

*The original absorption curves were based on ionization chamber data. These were closer to the exponential form than the geiger counter data.

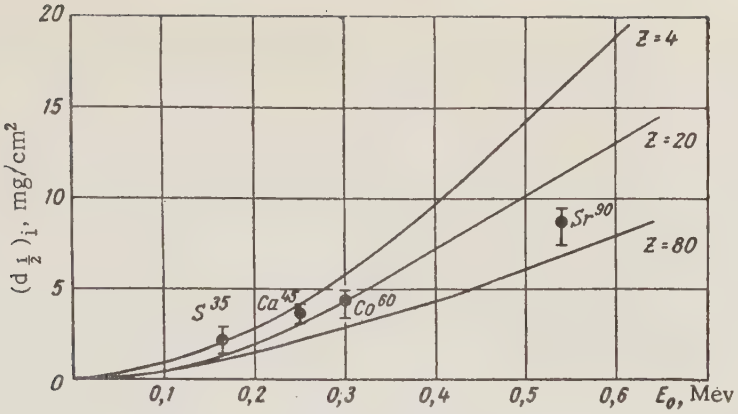

Fig. 2. Computed $(d\frac{1}{2})_i = f(E_0)$ for β emitters with Z = 4, 20 and 80. The points represent the values of $(d\frac{1}{2})_i$ obtained experimentally [7].

Even in the case of the thin window, the use of $(d\frac{1}{2})_m$ in correcting for the absorption of β radiation will lead to a large error in the absolute β activity. Thus, with a window thickness of 2mg/cm² the error is of the order of 30%. In such cases one should use the function $(d\frac{1}{2})_i = f(E_0)$ and take into account the atomic number of the β emitter (Fig. 2). Figure 2 also shows some experimental points representing half-value layers for S^{35}, Ca^{45}, Co^{60}, and Sr^{90} [7]. As can be seen these points agree with the calculations to within experimental error, except for S^{35}. In the latter case the low value of the energy of the β radiation (E_0 = 0.167 Mev) made it difficult to determine $(d\frac{1}{2})_i$.

LITERATURE CITED

1. F. Johnston and J. Willard, Science 7, 11 (1949).
2. T. Novey and N. Elliott, National Nuclear Energy Series Manhetten Project Technical Section, div. IV. PPR, 9, 44 (1951).
3. I. B. Kerim – Markus and M. A. L'vova, paper in the collection Studies in the Dosimetry of Ionizing Radiations [in Russian] (Academy of Sciences USSR Press, 1957).
4. H. Seliger, Phys. Rev. 100, No. 4, 1029 (1955).
5. J. Marshall, Nucleonics 13, No. 8 (1955).
6. N. G. Gusev, Radioactive Radiations and Shielding Handbook [in Russian] (Medgiz, 1956).
7. N. E. Tsvetaeva and M. N. Brusentsova, Atomnaya Énergiya 4, No. 6, 583 (1958).*

*Original Russian pagination. See C. B. translation.

SECOND ALL-UNION CONFERENCE ON NUCLEAR REACTIONS AT LOW AND MEDIUM ENERGIES

A. A. Ogloblin and V. I. Chuev

Translated from Atomnaya Énergiya, Vol. 9, No. 6, pp. 509-529, December, 1960

The Second All-Union Conference on Nuclear Reactions at Low and Medium Energies convened in Moscow July 21-28, 1960. Approximately 600 colleagues from nuclear research laboratories throughout the Soviet Union and scientists from 16 different countries were in attendance. The agenda of the Conference dealt with the most pressing problems in nuclear physics. 20 review papers were presented by Soviet scientists, outlining findings from over 100 research projects. Reports by foreign delegates were also heard.

The first day's sessions were devoted to research on few-nucleon systems. The lighter nuclei are of particular interest for research on nuclear phenomena. The study of the lightest nuclei may shed important light on such aspects of nuclear forces as are not manifested in nucleon-nucleon collisions (presence of multiple forces, etc.). Furthermore, data on nuclear reactions between the lightest nuclei are essential in the study of thermonuclear processes.

A review of experimental research on few-nucleon systems was offered in a paper by N. A. Vlasov. Particularly detailed attention was given by the reported to an analysis of the spectra of neutrons and protons formed in reactions between H^1, H^2, H^3, He^3, and He^4 nuclei. These reactions are three-particle reactions, as a rule, and the character of the spectra of recorded particles depends strongly on interactions in the final state. Information on nuclear interactions produced in such experiments is not obtainable in many cases by scattering experiments. The reporter also gave an account of experiments on measurement of neutron polarization in the T (p, n) He^3 and T (d, n) He^4 reactions, and presented a vivid picture of the problem, now under heated discussion, of the possible existence of superheavy isotopes of hydrogen and helium (H^5, He^8) and of the tetraneutron.

Theoretical questions related to the structure of light nuclei were dealt with in the report by A. I. Baz'. One of the chief defects in the shell model is the incorrect description of the periphery of the nucleus, failing to take into account formation of groupings of three and four nucleons, which have a high probability of appearing at the surface of the nucleus. The reporter dwelt in detailed fashion on the role of the nuclear surface in explaining the existence of levels with large reduced widths. He also considered the influence of surface effects on the breakdown of charge invariance, observed in some individual cases, manifested in the nonconservation of isotopic spin in some reactions and in the appearance, in some nuclei, of levels bearing no analogy to the mirror nucleus (e.g., Li^8 and B^8, Be^9 and B^9, etc).

H. Tyren (Sweden) told of experiments which he conducted in research on scattering of 450-Mev protons on D^2, He^4, Li^7, and C^{12} nuclei. At this energy, quasi-elastic scattering of the incident protons on protons composing the target nucleus takes place. An analysis of the experimental findings supports certain inferences as to the character of the momentum distribution of the protons in the nuclides studied. These findings are in harmony with shell-model predictions. I. S. Shapiro told of information obtainable on the structure of light nuclei through studying muon capture by those nuclei.

A host of data has been accumulated in recent years on the properties of nuclei by means of direct nuclear reactions going to completion without any compound nucleus forming in the interim. Studies of direct reactions, particularly the stripping and pick-up reactions, have turned out to be highly valuable in nuclear spectrometry, since this research reveals information not only on spins and parities, but also on configurations of nuclear levels. Direct processes were discussed in review papers by A. A. Ogloblin, who surveyed the experimental work, and V. G. Neudachnik who discussed related theoretical problems. In the papers presented to the Conference, primary attention focused on a study of the structure of the nucleus in pick-up reactions, which at yet have received insufficient study. The (d, t) pick-up reaction on several nuclei ranging from Li to Al and several medium and heavy nuclei was treated in papers by N. A. Vlasov, S. P. Kalinin, A. A. Ogloblin, and V. I. Chuev. It was shown that excitation of hold levels is the predominant mechanism in pick-up reactions, leading to the determination of single-particle states inside the nucleus and determination of binding energy of the nucleon in those states. This sort of data was obtained for O^{18}, F^{19}, and Zr nuclides. Mixing of the s- and d-states of the neutron in nuclei with A = 18 to A = 27 was also studied, as well as

the rotational structure of the Mg^{24} nucleus. The other pick-up reaction (n, d) was studied by G. E. Velyukhov and A. N. Prokof'ev on F^{19}, Ne^{20}, P^{31}, S^{32}, and by Laura Colli (Italy) and colleagues on nuclei from Se^{45} to Ni^{66}. Findings on states of the proton in these nuclei were also obtained.

In both review papers, emphasis was laid on the fact that subsequent application of the method of distorted waves with the use of optical potentials to stripping and pick-up reactions brought about remarkable agreement between experimental data and theoretical predictions. For a correct choice of potential parameters, great importance is attached to the data on polarization of particles as measured in the C^{12} (d, n) N^{13} reaction by I. I. Levintov et al., and by J. Nurzynskii and associates (Poland). E. Almqvist (Canada) told of studies on the mechanism involved in the Si^{28} (d, p) Si^{29} reaction with the aid of experiments in which the angular p-γ correlations were measured and the variation in angular distributions of protons with energy was studied.

Several papers were devoted to studies of the mechanism of (α, p), (p, α), (d, α), (α, t), etc. reactions. The nature of the angular distribution showed that these reactions proceed as a direct process of rather complex character. In particular, N. A. Vlasov and associates showed in their work that the (α, t) reaction is not equivalent to the (d, n) stripping reaction. The angular distributions in the (d, α) reaction, as demonstrated in a paper by P. Cerineo (Yugoslavia), evidence somewhat better agreement with the assumption that the reaction proceeds by a pick-up mechanism rather than by a knock-out process.

An investigation of several direct processes occurring in response to bombardment of the C^{12} nucleus by protons at 150 Mev was discovered in a detailed paper submitted by P. Radvan (France).

An investigation of scattering of nucleons on nuclei played a substantial role in creating the cloudy crystal ball model of the nucleus. A survey of research work on elastic scattering of protons was made by A. P. Klyucharev. This research encompassed study of proton scattering on targets of separated nuclides in the range extending from Z = 20 to Z = 30 at proton energies below the potential barrier top. It was demonstrated that the angular distributions differ substantially for nuclei of even and odd A, if the number of nucleons is close to a magic number. This is apparently related to the fact that an odd nucleon opens up the nuclear surface and appreciably increases the probability of absorption of an impinging particle. With increased energy, the pattern of elastic scattering approximates to a diffraction pattern and the isotope effect evokes a milder response from the shape of the angular distributions. A similar paper dealing with Cr, Co, Ni, Cu, and Zn nuclei was submitted by Chou Teh-Ming and associates (China).

The present state of the cloudy crystal ball model of the nucleus was discussed in a paper by P. É. Nemirovskii, who reviewed work on inelastic scattering of nucleons. The reporter laid emphasis on the fact that the current intensive search for improved parameters for each separate nuclide is in contradiction to the fundamental concept of this model. Most of the papers also fail to provide any justification for the assertion that concentration of absorption at the surface of the nucleus leads to better agreement with experiment than a potential with an imaginary part distributed over the nuclear volume. N. Hintz (USA) adduced some empirical data at variance with this belief. Nemirovskii devoted much attention to various applications of the cloudy crystal ball model to the theory of radiative capture, inelastic scattering, and polarization.

J. Peterson (USA) gave an account of a new interpretation of giant resonances in total neutron cross sections, similar to the interpretation of the Ramsauer effect with reference to electrons. E. Almqvist gave a report on a study of giant resonances in total neutron sections, for nuclei from Mg to Zn. A resonance of this type was discovered for Ni^{58}.

A. Strzałkowski (Poland) delivered a report on elastic scattering of deuterons by some light nuclei. P. Heugelouw (Netherlands) reported on the results of an investigation of elastic scattering of deuterons by Ag and Au. An analysis of inelastic proton scattering data and (n, p), (n, 2n), (n, pn) reactions was made, in his report, by U. Facchini (Italy). He pointed out that statistical theory is capable of explaining most of the efffects observed in such reactions, for the energy range 13-18 Mev.

One of the sessions of the Conference was devoted to a study of nuclei with the aid of multiply charged ions. A review of work on Coulomb excitations of nuclei was made by I. Kh. Lemberg. He noted that the investigation of Coulombic excitation has been extended to cover light and medium nuclei, for which it is possible to obtain data on the lifetimes of excited states. It is interesting that data on the lifetime of Ne levels were obtained as a result of excitation of states in the bombarding nucleus, rather than in the target nucleus.

A. Zucker gave a report on heavy-ion research in the USA. He noted that one of the most characteristic features of reactions with heavy ions at 10 Mev/nucleon energy is the important role of large angular moments. Formation of a compound nucleus is therefore not a basic process, and a neutron transfer reaction of the (N^{14}, N^{13}) type has a high probability of occurrence.

E. Almqvist reported on heavy-ion experiments conducted in Canada. Scattering cross sections and reaction cross sections in the case of interaction between two carbon nuclei have disclosed some sharp resonances with an anomalous high probability of decay of the compound nucleus Mg^{24} into two C^{12} nuclei. An analysis of the findings leads to the conclusion that separate molecular states exist in Mg^{24} with lifetimes of 10^{-20} to 10^{-21} sec, which may be represented as two oscillating C^{12} nuclei.

A problem of enormous interest in modern physics is the effect of resonant absorption of gamma rays without recoil, dicovered by R. Mossbauer in 1958. The essence of the Mossbauer effect is that the recoil momentum of a gamma photon emitted by a nucleus under certain conditions is imparted to the surrounding crystal as a whole, rather than to the nucleus alone. The gamma photon thereby carries off all the energy of decay and may be resonantly absorbed by a nucleus similar to the original one. This phenomenon and its numerous applications were discussed in a report by R. Mossbauer (West Germany), heard with intense interest. This report laid the foundations of the theory underlying this effect, and described experiments in which the effect was observed. Extremely narrow line widths (as narrow as 10^{-16} of the nuclear transition energy for Zn^{67}) have been brought within range of measurement by the Mossbauer effect.

The Mossbauer effect opens up extensive opportunities for studying the nature of intraatomic magnetic and electric fields, the magnetic and electric moments of excited states of nuclei, the effect of the detailed structure of electronic shells on the position of nuclear levels. R. Pound (USA) reported on a novel utilization of the Mossbauer effect for testing the general theory of relativity. He observed a change in the frequency of photons under terrestrial conditions as the photons progressed in a gravitational field. The measured frequency difference of upward and downward moving photons agrees with predictions of relativity theory to within 4%.

A report by F. L. Shapiro discussed the classical interpretation of the Mossbauer effect. This reporter also surveyed experimental research performed in the USSR on the study of this interesting phenomenon.

In the area of photonuclear reactions, primary attention was devoted to research on the shape of the giant resonance curve. A review of experimental work in this direction was made by L. E. Lazareva. The study of the resonance curve was made for oxygen. Measurements in the 21-23 Mev range of energies were carried out with high resolution, and the position of the narrow maximum detected in absorption cross sections was found to be in excellent agreement with theory. Some interesting data on the mechanism responsible for photodisintegration of nuclei were reported in papers by R. M. Osokina and associates. They showed that protons and neutrons are emitted as a result of direct interaction. In a paper by O. Bogdankevich and associates, the inelastic scattering cross section for gamma photons was measured and some features near the threshold of the (γ, n) reaction were revealed.

A detailed report on the shape of the giant resonance curve for nuclei with large deformations was delivered by E. Fuller (USA). The giant resonance peak splits into two humps in the case of deformed nuclei. The deformations and quadrupole moments of the nuclei may be found from the energy relations of both resonance peaks, and turn out to concur closely with the values arrived at in other experiments. Data on elastic scattering of gamma quanta by Ta, Ho, and Er indicate the existence of nuclear combination scattering.

A review of theoretical research on the mechanism responsible for photonuclear reactions was presented by A. M. Baldin.

The general regularities evident in the spectra of gamma photons produced in radiative capture of slow neutrons were discussed in a paper submitted by L. V. Groshev. At the present time, spectra for most elements have been derived, and it has been found that the shape of the spectrum is in large measure determined by the distribution of level densities. The development of new gamma-ray spectrometers with high resolving powers has in some cases enabled observation of excitation of single-particle and collective states. This was illustrated by the example of the nuclide Cd^{114}, whose spectrum was measured in the paper presented by L. V. Groshev and associates.

S. P. Tsytko presented a paper on radiative capture of protons.

Models of the nucleus were discussed at the last two sessions. A report on the shell model was presented by V. V. Balashov. The reporter emphasized that the shell model is in its present state (where residual interactions,

etc. are taken into account) capable of accounting for a host of experimental facts, particularly in the field of light nuclei.

A. S. Davydov laid great stress, in his report, on the model of a deformed nucleus lacking axial symmetry, a concept developed by himself and co-workers. The presently available empirical data on positions of nuclear levels, moments, and transition probabilities are not at variance with this model. D. P. Grechukhin told of one possibility for making a choice between the axial and nonaxial symmetry models of the nucleus.

Yu. T. Grin' presented a paper devoted to the application of the recently developed superconductivity theory to the nucleus. The reporter gave an account of the theoretical work carried out in the recent period by A. B. Migdal, S. T. Belyaev, S. I. Drozdov, D. F. Zaretskii, Yu. T. Grin', and others in which the effect of paired correlation on the various properties of the nucleus comes to the fore. L. A. Sliv took the floor on the same problem.

F. Villars (USA) dwelt upon several problems related to the theory of strongly deformed nuclei, particularly on quadrupole oscillations. G. Brown (United Kingdom) told of the results of calculations of nuclear-shell wave functions, with interactions between a nucleon and a hole taken into account.

This Conference on nuclear reactions undertook a much wider range and scope of problems than its name would indicate. The addition of several new problems to the Conference agenda made it possible to outline the basic trends evident in the development of low-energy and medium-energy nuclear physics, and to shed light on the most interesting results arrived at in recent work.

The materials of the Conference will be published by the Academy of Sciences of the USSR as a separate symposium, during the second quarter of 1961.

INTERNATIONAL CONFERENCE ON PLUTONIUM METALLURGY

Translated from Atomnaya Énergiya, Vol. 9, No. 6, pp. 509-529,
December, 1960

The International Conference on Plutonium Metallurgy, organized by the Commissariat de l'Energie Atomique and the French Metallurgical Society, convened at Grenoble (France), April 19 to 22, 1960. 200 persons from 20 countries were in attendance at the conference, to hear over 40 papers submitted prior to the conference.

The first session was devoted to the physical properties and the metallurgy of plutonium. It may be said that six allotropic modifications of plutonium and their properties are known at the present time (properties such as electrical conductivity, emf, specific heat, heat of transformation, magnetic behavior) to some significant degree. The anomaly of electrical resistance at 100°K is yet to be explained, the crystalline structure of the α and β phases is still obscure, and the problem of the negative coefficient of expansion of the δ phase has not been fully resolved.

In a report by Kerjean (France), a description was given of the technology of fabrication of 200 g plutonium ingots via reduction of calcium tetrafluoride. 40% excess of calcium is taken (the British prefer a somewhat smaller excess); the burden is compacted into pellets. Twelve pellets are charged semiautomatically into a calcium fluoride crucible, which is high-frequency heated in an argon atmosphere under the conditions: heating to 600-800°C for 1 min 30 sec, leaving to stand for 45 sec, 97.3% metal yield. All of the steps are carried out in a line of argon-filled glove boxes. Since plutonium tetrafluoride is an intense source of fast neutrons, extreme precautions must be observed when handling it (keeping a distance of 80 cm from the source, avoiding handling of the substance more than 2 to 3 hours daily).

A variety of methods for producing pure plutonium received some measure of attention, in particular electrolysis with careful prior purification of the original plutonium nitrate. Calcium thermal reduction in crucibles of magnesium oxide resulted in 99.8% pure metal at Los Alamos.

The second session was devoted to plutonium alloys. Phase diagrams of the Pu – Nb, Pu – Cu, Pu – C systems were reported on, and results were presented for research on ternary systems, especially the Pu – U – Mo system, which has received detailed study with respect to the kinetics of phase transformations.

The third session heard reports of findings on the ceramics technology of oxides of plutonium and PuO_2-UO_2 systems, in connection with the great interest manifested in the use of these materials as nuclear fuel. Several variants of the sintering process for PuO_2 were examined, and it was shown that sintering of PuO_2 follows a path similar to that for UO_2. Work on sintering studies, behavior under irradiation, and results of measurements of the thermal expansion coefficient for PuO_2 and PuO_2-UO_2 solid solutions were reported on by representatives of the USA.

At the concluding session, problems involving applications for plutonium in thermal reactors (fuel elements incorporating Pu – Al alloys) and in fast breeder reactors (the LAMPRE reactor with a liquid eutectic for Pu – Fe melting at 410°C, and the Rhapsodie reactor with fuel elements of Pu – U – Mo alloy) were discussed. The mechanical properties of plutonium and problems involving the compatibility of plutonium alloys and cladding materials (stainless steel, niobium, etc.) were examined.

The results of current investigations of plutonium-base nuclear fuel may be summarized as follows.

Pure plutonium is unsuitable as nuclear fuel because of the presence of allotropic transformations and other unfavorable properties.

Liquid plutonium-base fuels are quite expensive.

Plutonium carbides have not been investigated to any great extent, and it is still not proved that their thermal conductivities and irradiation behavior are the same as those of uranium carbide.

Ternary alloys have excellent properties, but are difficult to clad.

The most favorable results have been obtained with plutonium oxides and $PuO_2 - UO_2$ solid solutions, despite some unresolved problems which are still plaguing the researchers.

AT THE LATVIAN INSTITUTE OF PHYSICS

Yu. Koryakin

Translated from Atomnaya Énergiya, Vol. 9, No. 6, pp. 512-514,
December, 1960

At Salaspils, 20 km from Riga, construction work is being completed on the first nuclear research reactor in the Baltic republics, the IRT reactor of the Institute of Physics of the Academy of Sciences of the Latvian SSR (Fig. 1). This reactor, IRT-type, is rated at 2000 kw(th). Similar reactors are being built at various points throughout the Soviet Union.

At the present time, finish-up work and assembling is going on in the reactor hall (Fig. 2). Some of the administrative quarters are already completed, and work has been started in them on immediate preparation of research work to be carried out on the reactor. The control and measuring instruments, reactor control system, shielding, and dosimetry laboratory will soon be operational. The reactor tank has been mounted in place and the heavy concrete biological shielding is nearing completion. The reactor assembling job and placing of instrumentations were carried out under the supervision and with the direct participation of workers attached to the Institute's reactor laboratory. Colleagues of the I. V. Kurchatov Order of Lenin Institute of Atomic Energy and other institutions were also of great assistance to them in this tank.

Many of the contracts and operations involved in erection of the reactor were carried out through the efforts of the Institute of Physics and enterprises under the jurisdiction of the Latvian Council of the National Economy. For example, the reactor control desk was designed under the supervision of colleagues of the reactor laboratory of the Institute, and was fabricated in Latvian plants.

Builders performed a number of construction tasks which were new to their experience, in the course of erecting the reactor plant. For example, a method for preparing and pouring heavy concrete was put into practice. In the zone of highest radiation, heavy concrete of 6.5 g/cm^3 density was used, while concrete of 5.2 g/cm^3 density was used in other shielding sections.

In line with research schedules projected in advance, some modifications were introduced into the standard reference design. For example, the single hot cell originally envisaged was extended to two hot cells before plans were frozen.

The progress of work on the reactor project was a constant concern to the government of the Latvian SSR, particularly to J. V. Peive, Chairman of the Council of Ministers, who is a frequent visitor to the reactor site.

The start-up of the reactor will mean a significant boost to the activities of the Institute of Physics in nuclear physics problems, and will encourage penetration of the achievements of nuclear energy uses into the national economy of the Baltic republics. Scientists from Lithuania and Estonia will also participate in research work associated with the reactor.

The following trends were outlined for the work of the Institute at the August 1960 session of the Presidium of the Academy of Sciences of the Latvian SSR: physics of the nucleus and uses of isotopes, solid state physics, and magnetic phenomena.

The avenues of research involved in the first category are, with particular emphasis, the following:

1) nuclear spectroscopy of short-lived nuclides and capture gammas. Properties of radioactive nuclides (emission spectrum, lifetime, etc.) with half-lives in the second and minute range will be investigated;

2) investigation of radiations by means of magnetic spectrometers. Methods will be developed for research on circular polarization of gamma quanta in response to capture of polarized neutrons, and the quantum characteristics of the energy levels of compound nuclei will be determined. Magnetic spectrometers will be relied upon for studying the spectra of internal-conversion electrons of radioactive nuclides with half-lives ranging from several seconds up to two to five days. An electromagnetic dispatching system will be built for delivery of irradiated specimens from the reactor to the spectrometer for similar research on radioactive nuclides with half-lives in the second and minute range.

3) studies of neutron fluxes in the core and experimental channels of the reactor;

4) theoretical research on ionization and excitation of atoms and ions by slow electrons. This research is dictated by the needs of applied spectroscopy, astrophysics, and other branches of physics and chemistry with regard to derivation of the fundamental characteristics of atoms and molecules, particularly and in the first instance for data on the effective excitation and ionization cross sections of atoms and molecules. In particular, a research project is in the hopper for computing the excitation functions of various atoms by programming them into an electronic computer;

5) the study of transient response in relay-type radioactive sensors. These investigations are called for by the fact that the fundamental parameters of relay-action instruments (sensitivity, speed of response, reliability, performance stability) are sensibly dependent on the radiation detectors used and on the circuitry of the relay recorders. The interrelatedness of these parameters is felt particularly where transients are involved; the transients are determined by the changes in radiation intensity in the various recording processes.

Fig. 1. General view of the reactor building under construction at the Salaspils reactor site.

Another of the laboratories attached to the Institute of Physics, one engaged in studies of radioative automation techniques, has already started work on its program for developing techniques for utilizing radioactive isotopes in science and technology. This program includes a study of the effect of random statistical processes on basic instrument constants in radioactivity measuring instruments, investigation of the yield and energy spectrum of bremsstrahlung and characteristic radiation from beta sources, evolving efficient recording techniques, developing new sources of soft gamma rays and new beta preparations, a scientific development of fundamentals of standardization and normalization of process control instrumentation using nuclear radiations.

The topics included in the second category of research mentioned above are:

1) the study of problems of radiation effects on the magnetic and electrical properties of metals and alloys;

2) investigation of nuclear radiation effects on semiconductors and dielectrics;

3) semiconductor diffusion studies;

4) nuclear magnetic resonance studies of the structure of matter;

5) investigation of magnetohydrodynamic phenomena in flows of liquid metals at low Reynolds numbers;

6) study of techniques of electromagnetic transport of liquid metals.

The Latvian Institute of Physics has been engaged for the last five years in research on developing the foundations of electromagnetic pump theory. During that time, an approximate theory and calculation procedure has been arrived at applying to the basic variants of electromagnetic pumps, induction-type and conduction-type pumps. Several experimental pump designs have been worked out, with excellent performance characteristics. In 1960, work was started under contract with the Leningrad Council of the National Economy on building electromagnetic metering pumps for feeding pressure casting machines. The savings realizable from putting such metering pump units into production practice run into tens of millions of rubles annually.

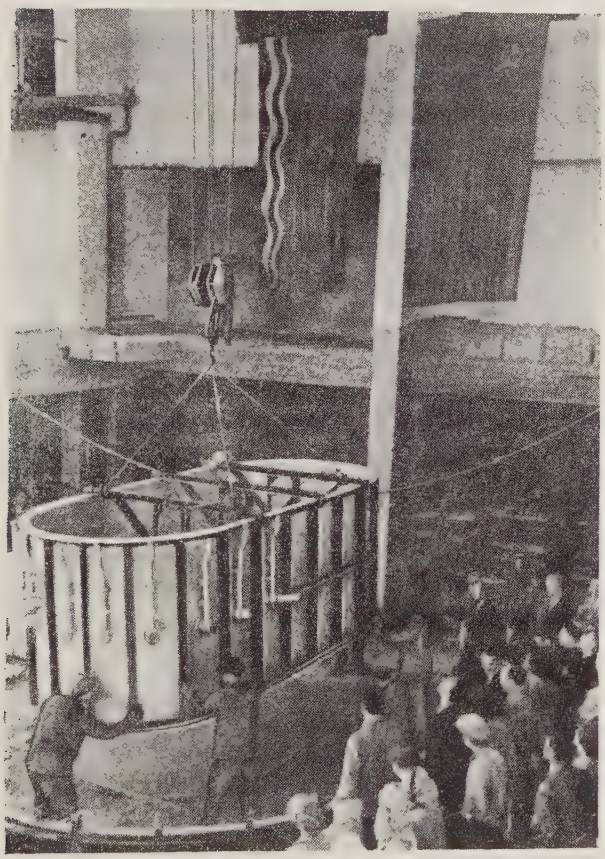

Fig. 2. Laying the bottom of the reactor pressure vessel in place.

It would be no exaggeration to state that a whole school of specialists on electromagnetic pumps, a line of equipment with widespread applications in nuclear industry and research, has been trained under the Latvian Institute of Physics.

The scope of the problems facing the Institute is thus a true reflection of the enormous gains registered by Latvian physicists and scientists in the field of peaceful uses of nuclear energy.

The building of the Salaspils research reactor marks only the first stage in the expansion of nuclear energy applications in Latvia. The Salaspils reactor will provide the basis around which a nuclear research center is projected for the coming years.

A building for physics and engineering work on radioactive materials and radiations and advanced techniques for use in the national economy is one goal. Another is the construction of a radiochemical building for the production, processing, and shaping of pile-produced radioisotopes.

A building with cryogenic equipment for the production of liquid helium and liquid hydrogen will be built on the premises of the coming research centers, as well as a radiation circuit with high gamma radiation level required for work in radiological physics, radiochemistry, and radiobiology.

Plans now being drawn up for this center include a building housing a linear accelerator and another for a 25 Mev proton accelerator. It will be used to investigate between charged particles and nuclei, and to produce some radioactive isotopes which are difficult to obtain from reactors. Finally, living quarters for the research workers attached to the center will be set up in the environs of the center.

After completion of a whole complex of nuclear research buildings at Salaspils, the Latvian Institute of Physics will place the most advanced equipment at the disposition of the center, which will be capable of resolving problems of first-ranking interest to the national economy in the area of peaceful uses of atomic energy.

THE HUNGARIAN INDUSTRIAL EXHIBIT AT MOSCOW

Yu. Mityaev

Translated from Atomnaya Energiya, Vol. 9, No. 6, pp. 515-516, December, 1960

The Gorky Central Park of Culture and Recreations was host during August and September, 1960 to the Hungarian Industrial Exhibit. Instruments reflecting the most highly developed branch on nuclear industry in Hungary, that of instrument design, figured prominently among the exhibits. The exhibits attested to the great gains achieved by Hungary in peaceful uses of atomic energy (Fig. 1). Instruments fabricated in the Republic several years back were placed on exhibit for comparison purposes, illustrating in sharp contrast what great strides forward Hungary has made in the field of nuclear instrument design.

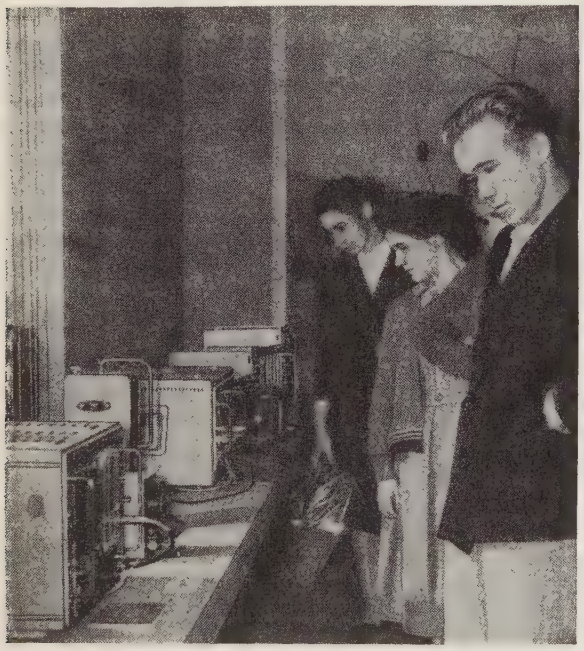

Fig. 1. At the Hungarian Industrial Exhibit. Photo by S. Blinov.

A clinical device of original design, a gamma-ray scintillation isotope scanner (Fig. 2) designed to detect and map cancerous and other tumors with the aid of radioactive isotopes, appeared on exhibit. A harmless dose of a radioactive preparation is introduced into the organism of the patient, in a form such that it will be deposited in the site of the supposed tumor (e.g., a preparation containing I^{131} would be administered to locate a thyroid tumor). Then the isotope scanner automatically maps the radioactivity of the patient's body. Radiation maps taken with two different body orientations reveal not only the location but the size as well of the tumor. The gamma-ray isotope scanner operates with a scintillation-counter head, and is completely automatic. Different modes of performance may be resorted to in order to obtain low-definition or high-definition radioactivity maps. About 80 such instruments are available at present. All of them are being employed successfully in clinics and hospitals throughout the Hungarian Peoples Republic.

A variety of instruments designed to measure radiation intensities under laboratory, plant, and field conditions alike were given prominent display at the exhibit. These are portable transistorized devices, with low weight and little bulk; they can be employed to great advantage in agriculture, biology, and uranium prospecting. Most of the instruments are designed to work from either a scintillation counter of a halide gas-discharge counter. Some of the portable instruments have a small built-in Co^{60} source for determining radiation levels by the comparison method.

Reliable pocket dosimeters (together with charging device) designed for dosimetric monitoring of personnel working under exposure to x-rays and gamma rays were also in display. Among the other dosimetric instruments, there was an acoustic threshold indicator for signaling an alarm whenever a predetermined radiation level is surpassed.

A set of instruments for precision measurement of radioactive speed specimens was put on display. The set consists of an original-design lead castle (Fig. 3) housing the test preparation, a broadband 70 Mc amplifier for a pulse-height analyzer with resolving time of 5 sec, and a power supplies unit. The design of the lead castl facilitates the study of both solid and liquid specimens.

In addition, a varied display of radio engineering equipment was available: Scalers with wide bandwidht, high-voltage stabilized power supplied, timers and clocks for remote control of various physics instruments, standard modular units for synthesizing measurements circuits, etc. Scintillation crystal of vinyltoluene produced in Hungary can

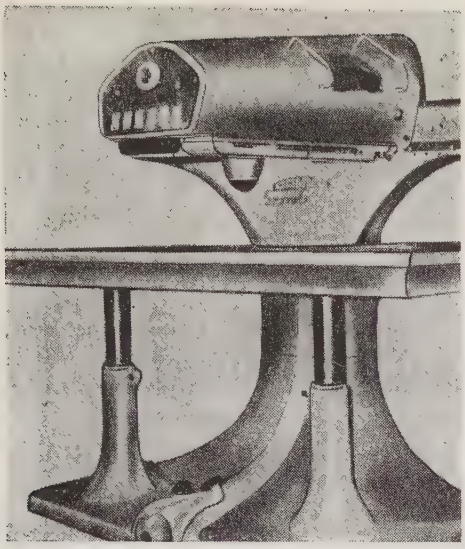

Fig. 2. Gamma-ray scintillation isotope scanner.

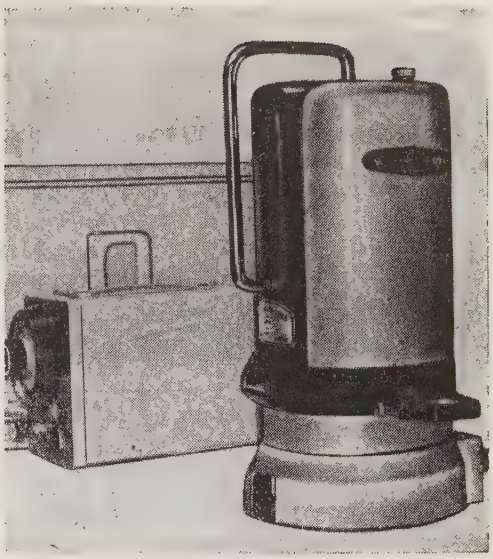

Fig. 3. General-purpose lead column.

be fabricated with ease into wafers of any shape, forming a substrate for deposition of a layer of some other scintillator, e.g., NaI.

A characteristic feature of the exposition was the fact that the overwhelming majority of the instruments exhibited are being mass-produced by Hungarian industry and are being used in many applications not only in scientific research, but also in the various branches of industry, medicine, and agriculture.

AT THE JAPANESE INDUSTRIAL EXHIBIT IN MOSCOW

Yu. Koryakin

Translated from Atomnaya Énergiya, Vol. 9, No. 6, pp. 516-517, December, 1960

The Sokol'niki Park of Culture and Recreation was host, during August and September, 1960, to the Japanese Industrial Exhibit. On display was a broad variety of electronic equipment produced by Japanese firms. Of particular interest were several types of electron microscopes of various magnifications (Fig. 1) and a large number of electronic devices by Yokogawa Ltd. Yokogawa instruments are primarily for process control and enjoy a broad range of application.

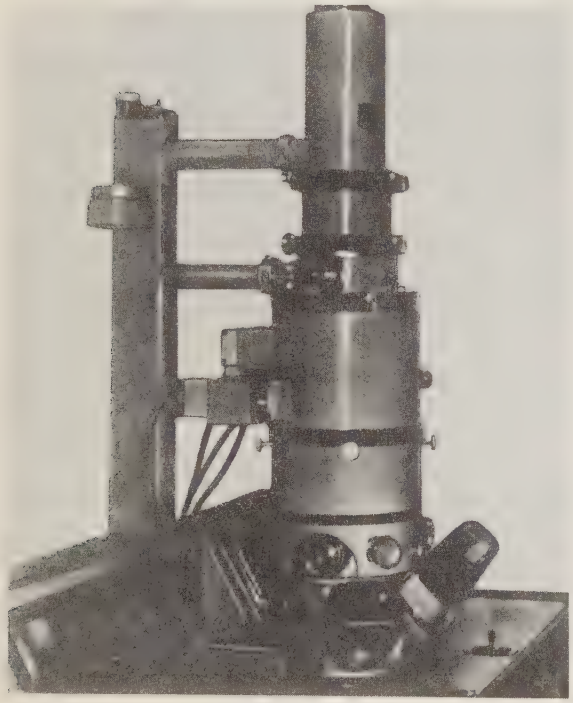

Fig. 1. Japanese manufactured electron microscope.

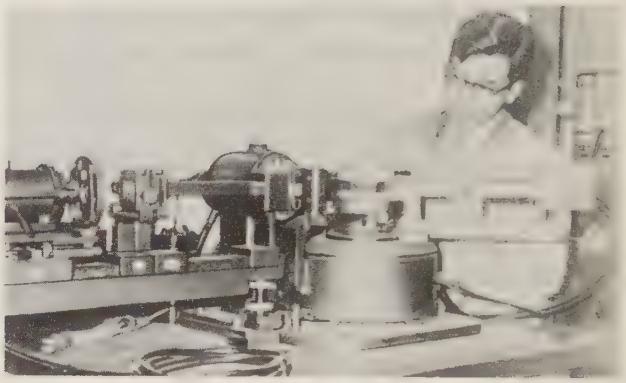

Fig. 2. Yokogaw [a complete electronic control system].

Fig. 3. Setup for x-ray analysis of specimens and composition of materials.

An arrangement of compressed size for quantitative and qualitative x-ray analysis of samples and the composition of test materials attracted some attention (see Fig. 3). The facility is designed for metallurgical, chemical, textile, ceramic, and other branches of industry.

NEW REGULATIONS GOVERNING HANDLING OF RADIOACTIVE MATERIALS AND SOURCES OF IONIZING RADIATIONS

L. Lazareva, N. Leshchinskii, P. Moiseitsev,

V. Sinitsyn, and A. Shtan'

Translated from Atomnaya Énergiya, Vol. 9, No. 6, pp. 525-529, December, 1960

The State Committee on the Uses of Atomic Energy under the jurisdiction of the Council of Ministers of the USSR and the State Health Inspection Commission of the Ministry of Public Health of the USSR have evolved, and promulgated on June 23, 1960, a new set of "Health and Safety Regulations Governing Handling of Radioactive Materials and Sources of Ionizing Radiations," No. 333-60 [1], which now replace the previous "Health and Safety Regulations Governing the Transportation, Storage, and Handling of Radioactive Materials," No. 233-57 [2] promulgated in 1957.

The regulations will be communicated to all institutions, enterprises, laboratories, and other organizations under all ministries and local authorities engaged in transporting and storing radioactive materials and sources of ionizing radiations. They are obligatory regulations governing the design, construction, reequipping, and operation of enterprises, institutions, laboratories, and other buildings and facilities intended for work with radioactive materials and sources of ionizing radiations.

The new regulations take due account of experience gained in using radioactive materials and ionizing radiations in the Soviet Union during the recent period, as well as recent data on their effects of living organisms and on materials, and the basic recommendations of international bodies relevant to these questions [3, 4].

New critical tolerance levels for ionizing radiations and new critical tolerance concentrations for radioactive substances in water and air were put into effect at the same time as the regulations referred to. Other new standards include a unique radiation hazard symbol for proper marking of objects, rooms, equipment, instruments, materials, etc., inside or outside of which a radiation hazard is present, nameplates for enterprises, institutions, laboratories, etc. authorized to handle radioactive materials, and several other regulations, requirements, statutes and forms.

The regulations are based on the need to ensure safety in handling of radioactive materials, and incorporate the latest critical tolerance dosage. These regulations stipulate 5 rem annually as the permissible dosage for any workers exposed to radioactive materials or sources of ionizing radiations, with reference to all forms of external irradiation. This form corresponds to 0.1 rem weekly for personnel continually exposed. For personnel working with a radius of exposure to the radiations, but not directly engaged in handling radioactive materials or sources, the yearly dosage is set at 0.5 rem.

The regulations are careful to strictly delineate requirements governing handling of radioactive materials in properly closed containers, i.e., in such a state or packed such that the radiations do not propagate to the surrounding medium, so that they can act only as external radiation sources, distinguishing them from radioactive substances present in open form whereby the radiations are not hindered from propagating into the surrounding medium and affecting the organism both from outside and by penetration into the organism. To provide safety in handling of radioactive materials present in closed form and in handling and using other sources of ionizing radiations (x-ray tubes, accelerators, etc.), only biological shielding need be specified; i.e., attenuation of the radiations is required at those points where personnel may suffer exposure, to keep the dosage well below critical levels.

The regulations spell out concrete measures to be fulfilled in building and using high-level isotope facilities, x-ray diagnostic equipment, radiotherapeutic equipment, nondestructive radiography facilities, and other equipment and instruments involving the use of radioactive substances. In observance of these requirements, instruments may be employed without special restrictions in workshops, installations, laboratories, and other work places, thereby significantly broadening the field of possible applications without incurring a hazard of radiation injury.

Requirements and recommendations governing work with radioactive materials present in open form are spelled out painstakingly in the regulations. All radioactive materials are classified according to their radiation toxicity (radiation effects when radiation enters the organism) into four groups: Group A includes radioactive materials of particularly high radiation toxicity (Sr^{90}, Po^{210}, Ra^{226}, etc.), group B includes radioactive materials of high radiotoxicity level (Ca^{45}, Co^{60}, I^{131}, etc.), group C includes materials of average radiotoxicity (Na^{24}, P^{32}, Fe^{59}, I^{132}, etc.), and group D embraces low-toxicity isotopes (H^3, C^{14}, Cr^{51}, etc.). Assigned to group A are, primarily, those radioactive substances whose critical concentrations in the air of rooms occupied by personnel is not more than $1 \cdot 10^{-13}$ curie/liter. Group B has assigned to it substances whose critical concentrations range from $1 \cdot 10^{-13}$ to $1 \cdot 10^{-11}$ curie/liter, and group D includes substances for which concentrations greater than $1 \cdot 10^{-9}$ curie/liter in air are permitted.

Depending on the degree of radiotoxicity and the activity of the radioactive substances at the working site (starting at 0.1 microcurie for the most highly radiotoxic substances), three classes of operations involving exposure to radiation have been singled out. Work operations assigned to class III may involve the use of ordinary, nonshielded working places equipped in compliance with the regulations applying to chemical laboratories, and in some cases work with nonradioactive substances may be authorized for the same places. Work operations assigned to class II must be carried out in rooms specially set apart and,furthermore,equipped with specialized or adapted equipment, depending on the nature of the work. Work operations assigned to class I must be restricted to separate work places with special zonal planning, safety partitions, specialized ducting and hoods, specialized equipment for high-level work (glove boxes, junior caves, etc).

Institutions, enterprises, and laboratories are grouped into three categories depending on the annual needs for radioactive materials in open form, since the amount of hot wastes and contamination of air and drainage passages is largely dependent on the magnitude of those needs.

The pertinent class and category are governing factors for institutions, enterprises, and laboratories with respect to specifications for planning, isolation, and equipment of working places and rooms, the system specified for waste collection and disposal, drainage, ventilation, the use of various types of operating equipment, etc.

The regulations devote considerable space to problems concerning the correct organization of the production, transportation, inventorying, issuing, and storage of radioactive materials, since proper management is a deciding factor in the preservation, safe handling, and rational use of such substances.

The regulations forbid introduction of radioactive materials into foodstuffs. Applications for radioactive substances in the various branches of the national economy via introduction of those substances into the finished industrial product is permissible under conditions that the residual activity (in curies/kg) of the end product not exceed by more than 100 times the critical tolerance concentration (in curie/liter) for water in open reservoirs in the case of radioactive substances having half-lives up to 60 days. For substances with half-lives longer than 60 days, residual activity must not exceed 10 times the critical level for water in open reservoirs.

Requirements governing the collection, disposal, and burial of radioactive wastes, including regulations covering conveyances and burial sites, are listed in special subsections.

Particular attention is devoted in the regulations to measures for individual shielding, personal hygiene, and dosimetric monitoring. A list of recommended protective clothing, "Don't Do . . ." rules for working with radioactive substances and sources of ionizing radiations, techniques and means for decontamination, and other useful information are appended to the regulations.

An appendix of teminology and technical definitions is included to facilitate understanding of the regulations. Also appended are formulas and tables, an ample selection of examples illustrating radiation shielding calculations, of concentrations of hot substances, and other valuable information.

The introduction of these new regulations remove any existing ambiguities in realm of applications of radioactive substances and sources of ionizing radiations, and establish the requirements and specifications corresponding to the present advanced state of knowledge about the effects of radioactive substances and ionizing radiations on the organism, which will contribute to the safe use of these tools on a broader scale.

LITERATURE CITED

1. Sanitarnye pravila raboty s radioaktivnymi veshchestvami i istochnikami ioniziruyushchikh izluchenii [Health and safety regulations governing the handling of radioactive materials and sources of ionizing radiations]. Moscow, State Atom Press (Gosatomizdat, 1960).
2. Sanitarnye pravila perevozki, khraneniya, ucheta i raboty s radioaktivnymi veshchestvami [Health and safety regulations governing the conveying, storage, inventorization, and handling of radioactive substances]. Moscow, Maritime Industry (Minsudprom, 1957).
3. Bezopasnoe obrashchenie s radioioztopami [Safe handling of hot isotopes]. Vienna, Internat'l. Atomic Energy Agency, 1958.
4. Recommendations of the International Commission on Radiological Shielding. Munich, ICRS (1959).

BIBLIOGRAPHY

NEW LITERATURE

Books and Symposia

Accelerators. A symposium. Moscow, Gosatomizdat, 1960

124 pages, 3 rubles, 60 kopeks
Translated from Atomnaya Énergiya, Vol. 9, No. 6, pp. 530-531, December, 1960

This symposium is composed of original articles decoted to advanced linear and cyclic accelerators. The first three articles discuss linear electron accelerators: A 6 Mev linear with constant phase velocity, installined at the Ukrainian Physics and Engineering Institute, is described; some problems in particle dynamics are studied and the process of electron bunching in a linear electron accelerator is discussed. A new plan for particle extraction from a synchrocyclotron is proposed in the fourth chapter. The fifth chapter presents a technique for beam extraction from a betatron or synchrotron doughnut by unilateral displacement of the equilibrium electron orbit outside the operating region, a technique developed at Tomsk Polytechnic Institute. The sixth chapter describes a ferrite frequency translation device for shifting a cyclotron into the synchrocyclotron mode. The seventh chapter takes up such problems as shaping axisymmetric magnetic field configurations by positioning of annular shims. The eighth chapter deals with the generation of multiply charged ions in a cyclotron. The ninth chapter describes a periodic-field cyclotron for accelerating multiply charged ions. The last three chapters discuss the effect of multiple scattering and emission in beam stacking, a technique for measuring the duration of an ion cluster in a cyclotron, and the results of an experiment on annular electron beam scanning at 3 Mev.

N. D. Fedorov. The cyclotron. Moscow, Atomizdat, 1960
88 pages, 2 rubles, 30 kopeks

The brochure tells of the cyclotron's background, delving into the early days of the cyclic resonance in accelerators. The operating principle underlying the cyclotron is discussed, and the problem of enhancing ion energy and beam intensity is gone into. Systems for extracting ions from the accelerator chamber are described. Basic information is given on cyclotron design, and a description of a cyclotron with an azimuthally varying magnetic field appears. The major applications of cyclotrons are indicated.

The brochure is written for a broad public.

M. A. Bak and Yu. F. Romanov. The neutron. Moscow, Atomizdat, 1960
82 pages, 2 rubles 15 kopeks

This brochure describes the discovery of the neutron and explains its fundamental properties. An account is given of interactions between neutrons and matter, fission of heavy nuclei in response to neutron bombardment, neutron sources, production of monoenergetic neutron beams, discovery of the antineutron. Neutron dosimetry and neutron shielding techniques are touched upon.

D. N. Trifonov. Element 61, Its Past, Present, and Future. Moscow, Atomizdat, 1960.
56 pages, 84 kopeks.

This booklet is devoted to the element promethium, of atomic number 61. A popular-style account is given of the history of its discovery and methods of winning and purifying it, closely related to the history of the other rare-earth elements, one of the most interesting problems in modern inorganic chemistry.

The booklet is aimed at the general reading public.

G. F. Silina, Yu. I. Zarembo, and L. E. Bertina. Chemical Technology and Metallurgy of Beryllium. Edited by V. I. Spitsyn. Moscow, Atomizdat, 1960, 120 pages, 3 rubles, 60 kopeks.

The basic problems involved in beryllium production and applications are discussed in this book. Chemical and physical properties of beryllium metal and beryllium compounds of technological interest are described. In the chapter devoted to industrial techniques for producing beryllium compounds, methods are given for detecting beryllium and producing technical-grade beryllia, purifying beryllium hydroxide to nuclear-grade specifications, producing ammonium fluoroberyllate, beryllium chloride, and beryllium carbide. Of various techniques developed to produce beryllium metal, those having some industrial significance, such as thermal reduction of halides, and fused-salts electrolysis, are discussed.

Data published in the literature during the past 15 years are used in the book.

The book is written for specialists working in the field of beryllium production and applications, and for students in metallurgical schools.

V. V. Fomin. The Chemistry of Extractive Processes. Moscow, Gosatomizdat, 1960,168 pages, 6 rubles, 60 kopeks.

This book, on the basis of published findings, summarizes current concepts of the extraction mechanism. The dependence of distribution constant on extraction conditions is discussed, and methods for evaluating this dependence are compared. Detailed numerical calculations are absent from the book; some mathematical derivations are left to the appendix, in order to simplify the presentation. A reference bibliography names 236 titles.

The book is aimed at scientific workers and students interested in extraction problems.

Yu. V. Sivintsev. Background Radiation of the Human Organism. Moscow, Gosatomizdat, 1960. 96 pages, 3 rubles.

On the basis of experimental data published in the literature, the components of external and internal irradiation of the human organism are discussed and the dose rates of the background irradiation of different parts of the human body, such as the gonads, lungs, and skeleton are evaluated. A comparison is drawn between these doses and dangerous mutagenic and carcinogenic doses. Proof is presented that the background radiation dose may be accepted as a basis in judging maximum radiation tolerance levels. A list of the pertinent literature consulted appears at the end of the book, with over 200 titles mentioned.

The book is written for physicists and biologists working in the field of research on biological effects of physical radiations, and for other persons interested in this problem.

INDEX

THE SOVIET JOURNAL OF ATOMIC ENERGY

Volume 9, Numbers 1-6

THE SOVIET JOURNAL OF

ATOMIC ENERGY

A translation of ATOMNAYA ÉNERGIYA, a publication of the Academy of Sciences of the USSR

(Russian original dated July, 1960)

Vol. 9, No. 1 July, 1961

CONTENTS

Annual subscription $75.00
Single issue 20.00
Single article 12.50

CONTENTS (continued)

NOTE

The Table of Contents lists all material that appears in Atomnaya Énergiya. Those items that originated in the English language are not included in the translation and are shown enclosed in brackets. Whenever possible, the English-language source containing the omitted reports will be given.

Consultants Bureau Enterprises, Inc.

THE SOVIET JOURNAL OF

ATOMIC ENERGY

A translation of ATOMNAYA ÉNERGIYA,
a publication of the Academy of Sciences of the USSR

(Russian original dated August, 1960)

Vol. 9, No. 2 August, 1961

CONTENTS

Annual subscription $ 75.00
Single issue 20.00
Single article 12.50

CONTENTS (continued)

NOTE

The Table of Contents lists all material that appears in Atomnaya Énergiya. Those items that originated in the English language are not included in the translation and are shown enclosed in brackets. Whenever possible, the English-language source containing the omitted reports will be given.

Consultants Bureau Enterprises, Inc.

THE SOVIET JOURNAL OF

ATOMIC ENERGY

A translation of ATOMNAYA ÉNERGIYA,
a publication of the Academy of Sciences of the USSR

(Russian Original dated September, 1960)

Vol. 9, No. 3 September, 1961

CONTENTS

Annual subscription $75.00
Single issue 20.00
Single article 12.50

NOTE

The Table of Contents lists all material that appears in Atomnaya Énergiya. Those items that originated in the English language are not included in the translation and are shown enclosed in brackets. Whenever possible, the English-language source containing the omitted reports will be given.

Consultants Bureau Enterprises, Inc.

THE SOVIET JOURNAL OF

ATOMIC ENERGY

A translation of ATOMNAYA ÉNERGIYA,
a publication of the Academy of Sciences of the USSR

(Russian original dated October, 1960)

Vol. 9, No. 4 September, 1961

CONTENTS

Annual subscription $ 75.00
Single issue 20.00
Single article 12.50

CONTENTS (continued)

NOTE

The Table of Contents lists all material that appears in Atomnaya Énergiya. Those items that originated in the English language are not included in the translation and are shown enclosed in brackets. Whenever possible, the English-language source containing the omitted reports will be given.

Consultants Bureau Enterprises, Inc.

THE SOVIET JOURNAL OF

ATOMIC ENERGY

A translation of ATOMNAYA ÉNERGIYA, a publication of the Academy of Sciences of the USSR

(Russian original dated November, 1960)

Vol. 9, No. 5 September, 1961

CONTENTS

Annual subscription $75.00
Single issue 20.00
Single article 12.50

CONTENTS (continued)

Note. The Table of Contents lists all material that appears in Atomnaya Énergiya. Those items that originated in the English language are not included in the translation and are shown enclosed in brackets. Whenever possible, the English-language source containing the omitted reports will be given. Consultants Bureau Enterprises, Inc.

THE SOVIET JOURNAL OF

ATOMIC ENERGY

A translation of ATOMNAYA ÉNERGIYA,
a publication of the Academy of Sciences of the USSR

(Russian Original Dated December, 1960)

Vol. 9, No. 6 October, 1961

CONTENTS

Annual subscription $ 75.00
Single issue 20.00
Single article 12.50

CONTENTS (continued)

NOTE

The Table of Contents lists all material that appears in Atomnaya Énergiya. Those items that originated in the English language are not included in the translation and are shown enclosed in brackets. Whenever possible, the English-language source containing the omitted reports will be given.

Consultants Bureau Enterprises, Inc.

THE SOVIET JOURNAL OF ATOMIC ENERGY

Volume 9, Numbers 1-6

(A translation of Atomnaya Énergiya)